DEVELOPMENT OF ELECTROCHEMICAL IMMUNOSENSORS FOR DETECTION OF TAU PROTEIN: COMPUTATIONAL AND EXPERIMENTAL STUDIES

By

Calvin Carl Harilal

(Reg. No: 21011423)

Submitted in fulfilment of the requirements of the degree of Master of Applied Science: Chemistry in the Faculty of Applied Sciences at the Durban University of Technology

November 2019

DECLARATION

I **Calvin Carl Harilal** declare that the thesis submitted for the degree of Master of Applied Science (M.App.Sci.): Chemistry at the Durban University of Technology is a result of my own investigation and has not already been accepted in substance for any degree, and is not being concurrently submitted for any other degree. All the work was done by the author.

Student Name: Calvin Carl Harilal

Student Signature: **Date:**

Supervisor Name: Prof K Bisetty

Signature: **Date:**

Co-Supervisor Name: Dr S Kanchi

Signature: …… **Date:**

ACKNOWLEDGEMENTS

Firstly, I thank God for all the opportunities afforded to me. I also thank the innumerable Saints for their intercession.

I wish to express my sincere gratitude to my supervisor, Prof K Bisetty for allowing me to be part of his research team and for all his efforts and support that ensured the completion of this thesis. My special thanks goes to Dr S Kanchi, my co-supervisor for his guidance and encouragement throughout this work. In addition I thank the members of the research group (Computational Modelling and Bio-analytical Chemistry) and to all those who contributed to this work in some way, particularly Mrs. Mavis Xhakaza and Mr Benni Hloma for their assistance with the experimental aspect of my research.

Finally, I extend my utmost appreciation to my parents for their support and for all the opportunities they have afforded me.

ABSTRACT

Tau protein is a microtubule-associated protein (MAP) found in neuronal cells of the central nervous system. In recent years it has become an important biomarker for neurodegeneration and pathologies of the nervous system, thereby necessitating novel approaches for its detection.

This study involves the development of two immunosensors for the detection of tau protein. The study makes use of nanomaterials and antibody transducers as signal enhancing strategies. Both sensors rely on indirect detection of tau protein as a copper(II) complex using a Cu(II)/Cu (I) redox probe. The electrochemical immunoassay is based on the immobilisation of anti-tau antibodies onto a gold working electrode that has been modified with nanomaterials using N-Hydroxysuccinimide (NHS) binder. The first sensor makes use of gold nanoparticles (AuNPs) and the second utilises a nanocomposite of graphene oxide (GO) decorated with silver nanoparticles (AgNPs). Cyclic voltammetry (CV) was used to optimise the electrochemical signal of the tau protein, while quantitative analyses were achieved by differential pulse voltammetry (DPV) and square wave voltammetry (SWV) under the established optimised conditions.

Results for the quantitative experimental studies revealed relatively low detection limits for both sensors. The lowest of these detection limits were obtained for DPV analysis of using sensor 1 which produced an LOD of 3.31 nM and an LOQ of 11.04 nM. For sensor 2 the SWV analysis produced the lowest LOD and LOQ of 1.73 nM and 5.76 nM respectively.

Computational chemistry methods implemented at the DFT level were used to support the developed electrochemical sensor. The molecular docking results showed relatively good binding affinity of -4.72 kcal/mol between the NHS and the antibody. A 100 ns MD simulation showed a good free binding energy value of -20.51 kcal/mol at pH 7, in accordance with the optimum pH implemented in the experimental work. Furthermore, adsorption studies were performed between the citrate coated nanoparticles on the Au electrode and NHS/anti-tau antibody/tau complex. The energy adsorption simulations revealed the energy favoured interaction between the designed layers with the stabilizing energy changes from --23.74 to -142.96 kcal/mol for sensor 1 and for sensor 2 it changed from -7.6 to -127.82 kcal/mol. Overall the computational data correlated well with experimental work.

The two novel immunosensors developed in this work, give new insights into electrochemical and computational methods for the detection of proteins, and could lead to the fabrication of a device for point-of-applications in early diagnosis of neurodegenerative disorders.

LIST OF PUBLICATIONS

Manuscript submitted to ACS Nano:

Fabrication of an electrochemical biosensor for tau protein detection using a nanocomposite of multifunctional nanoparticles and graphene oxide, Calvin Harilal, Suvardhan Kanchi, Mohd Shahbaaz and Krishna Bisetty.

TABLE OF CONTENTS

LIST OF FIGURES

LIST OF TABLES

LIST OF ACRONYMS AND SYMBOLS

Ab	Antibodies
AD	Alzheimer's disease
AE	Auxiliary electrode
AGNPs	Silver nanoparticles
AuE	Gold Electrode
AuNPs	Gold nanoparticles
BSA	Bovine serum albumin
C-terminal	Carboxy-terminal
CNS	Central nervous system
CSF	Cerebrospinal fluid
CV	Cyclic voltammetry
DFT	Density functional theory
DPV	Differential pulse voltammetry
EDC	1-Ethyl-3-(3-dimethylaminopropyl)carbodiimide
ELISA	Enzyme-linked immunosorbent assay
FFF	Field-flow fractionation
GO	Graphene oxide
HR-TEM	High resolution transmission electron *microscopy*
LOD	Limit of detection
LOQ	Limit of quantification
MALS	Multi-Angle Light Scattering Detector
MAP	Microtubule-associated protein

MPA	3-mercaptopropionic acid
MD	Molecular dynamic simulations
NHS	N-Hydroxysuccinimide
NPs	Nanoparticles
NDDs	Neurodegenerative diseases
NFTs	Neurofibrillary tangles
nTau	Normal tau
N-terminal	Amino-terminal
PBS	Phosphate-buffered saline
PHF	Paired helical filament
pTau	Phosphorylated tau
PTM	Post-translational modifications
RE	Reference electrode
ROS	Reactive oxygen species
SPE	Screen-printed electrode
SWV	Square wave voltammetry
TEM	Transmission electron microscopy
WE	Working electrode

CHAPTER ONE

INTRODUCTION

This chapter gives an overview of neurodegenerative diseases and describes the basic functions, properties, pathologies of tau protein and the current analytical methods employed for tau protein detection. In addition the properties of biosensors as having application for tau protein analysis are discussed. This is followed by the aims, objectives and a chapter summaries for this thesis.

1.1. BACKGROUND

Neurodegenerative diseases (NDDs) are associated with loss or dysfunction of neuronal cells. The world health organisation (WHO) indicate that, worldwide around 47 million people have dementia and there are 9.9 million new cases every year. In addition WHO also predicts that by 2040, neurodegenerative diseases such as Alzheimer's and other causes of dementia will overtake cancer to become the second leading cause of death after cardiovascular disease. Alzheimer's disease (AD) is the most common form of dementia and possibly contributes to 60-70 % of cases (Duthey, 2013). AD is a progressive neurodegenerative disorder that causes dementia, a general term for memory loss and other cognitive abilities serious enough to interfere with daily life, in approximately 10 % of individuals older than 65 years (Blennow et al., 2006). Studies of the human brain of patients affected by NDDs have displayed a trend of proteins with altered physicochemical properties (Kovacs and Budka, 2010). One such protein is microtubule associated protein, Tau. Tau protein occurs as six isoforms in the human brain ranging from 352 to 441 amino acids, each differentiated by their binding domains. It is considered an intrinsically disordered protein, adopting many distinct conformations under physiological conditions. Tau is also a phosphoprotein and in a normal adult human brain, tau contains 2–3 moles phosphate per mole of tau protein. Its primary function is to stabilise microtubules which are a major component of neuronal cell process involved in maintaining the cell shape and axonal transport in the cytoskeleton (Robert and Mathuranath, 2007). In NDDs, tau protein is abnormally hyper-phosphorylated and aggregated into paired helical filament (PHF), a principal ultrastructural component of NFT (Kosik, 1990, Iqbal et al., 2010).

Tau protein levels in cerebrospinal fluid (CSF) are said to increase with age. The typical levels of tau protein in age group 21-50 years are 136± 89 pg/ml, age group 51-70 years are 243± 127 pg/ml and 341± 171 for the age group >71 years. The levels of tau in CSF from patients with AD are above 450 pg/ml for the age group 51-70 years and as high as 600 pg/ml for the age group > 71 years. Levels of phosphorylated tau are also elevated in AD. (Humpel, 2011).

Current clinical quantification techniques for tau protein in CSF is performed using an enzyme-linked immunosorbent assay (ELISA) kit (Blennow, 2004). A quantitative LC-MS/MS method to measure tau in CSF using antibodies has also been reported (McAvoy et al., 2014). In recent years, other methods such as tau detection by localised surface plasmon resonance (LSPR)-based immune-chips and Immuno-magnetic reduction (IMR) have also been reported (Vestergaard et al., 2008, Yang et al., 2017).

Analytical detection of tau protein has become essential due to its implication in AD and other NDDs. Been able to quantify tau protein in CSF or other biological fluids will prove helpful in signalling the early signs and monitoring the progress of NDDs, as elevated levels of tau are indicative of NDDs. Costs, simplicity and analysis time are three important factors when considering a method for analytical detection. The methods currently employed for tau protein analysis often lack in one or more of the above mentioned factors.

The field of electrochemical biosensors have become a popular trend in developing methods of analysis for a variety of analytes, in which an electrical signal produced by an analyte is proportional to the concentration of the analyte. Electrochemical biosensors are advantageous in multiple aspects. They are relatively simple, financially viable and can be miniaturised into easy-to-use portable devices. In addition signal amplification strategies such as the use of nanomaterials and functionalisation with analyte specific biomolecules can be incorporated into these sensors in order to achieve high sensitivity and low detection limits. Such a device is ideal for point-of-care applications as they require small sample volumes and are able to produce results within minutes. (Hammond et al., 2016)

1.2. AIMS AND OBJECTIVES

Aims

This study is aimed at developing and evaluating the performance of two electrochemical nano-immunosensors for the detection of tau protein by experimental and computational methods.

Objectives

- To synthesise gold nanoparticles using a chemical reduction of the gold precursor salt.
- To synthesis silver nanoparticles by a chemical reduction of the silver precursor salt using vegetable extract.
- To perform structural characterisation studies of the synthesised nanoparticles by UV-Vis spectroscopy, transmission electron microscopy (TEM), Field-flow fractionation (FFF) and Thermogravimetric analysis (TGA).
- To fabricate each immunosensor for tau protein detection by;
    - firstly, conducting a stepwise modification of bare Au electrode with AuNPs then immobilising anti tau antibodies onto the AuNPs/Au electrode surface using a covalent linker, and
    - secondly, to conduct a stepwise modification of the bare Au electrode with Ag/GO nanocomposite followed by the immobilisation with anti tau antibodies onto the Ag/GO/Au electrode surface using covalent linker.
- To optimise the electrochemical signal for detection of tau protein for each sensor in terms of pH, scan rate and deposition time using CV.
- To perform electrochemical characterisation studies of tau protein for both sensors using cyclic voltammetry (CV).
- To conduct quantitative measurements of tau protein for each sensor by square wave voltammetry (SWV) and differential pulse voltammetry (DPV).
- To establish LODs and LOQs for each immunosensor.
- To validate the experimental studies by constructing computer models of the immunosensors and performing interaction studies at the density functional theory (DFT) level.

1.3. THESIS OUTLINE

This thesis is divided into six chapters. Following the introduction, further chapters in this thesis are divided as follows:

Chapter two: Literature review

This chapter gives an insight into tau protein in the context of neurodegeneration and reviews electrochemical studies pertaining to tau protein mechanisms, interactions and detection. A further discussion involves an overview of biosensing and the use of nanoparticles and other signal enhancement strategies.

Chapter three: Theoretical principles

This chapter provide details regarding the working principles and mechanisms pertaining to the analytical techniques employed in the experimental aspect of the study. The principles of the different techniques of computational modelling are also discussed here.

Chapter four: Materials and methods

Presented in this chapter are the methodologies employed in this study and the materials used to carry out the necessary work. For experimental work, this involves outlining the synthesis and characterisation of nanoparticles together with the fabrication of the immunosensors. An outline of computational techniques such as DFT and MD used for complementary studies will also be highlighted here.

Chapter five: Results and discussion

This chapter presents the findings of the study and deals with the chemical and statistical interpretation of all data. A comparative analysis between experimental and computational results are also presented here for validation and complementary purposes. The discussion further focuses on biosensors, nanoparticles and antibodies and their contributions to achieving the aims set out for the study.

Chapter six: Concluding remarks

This chapter summarises the achievements and limitations of the study, also indicating the contribution made to literature and recommendations for future work.

CHAPTER TWO

LITERATURE REVIEW

This chapter highlights the mechanism of the neuro-pathologies with emphasis on protein aggregates as potential biomarkers. A historical overview of tau protein relating to its discovery and eventual implication in neurodegeneration, together with important functional mechanisms relating to tau protein aggregation is also discussed. A review of electrochemical studies of tau protein is also reported. In addition, this chapter provides an overview of biosensor types and applications. Finally a review on nanomaterials and their properties and potential use as signal amplifiers for biosensors is provided.

2.1. NEURODEGENERATIVE DISEASES (NDDS)

2.1.1. Neurons

Neurons are cells that forms both the structural and functional components of the nervous system. They are generally classified according to function: sensory neurons, which response to stimulus; motor neurons, controlling muscular activity and interneurons neurons, involved in reflex function. Neuronal structure consists of a cell body, an axon, dendrites and synaptic terminals. An Axon transmit signals to interconnected target neurons, which is received by the dendrites via synapses. Neuronal activity is both chemical and electrical in nature. The human body contains networks of neurons that serve as pathways that allow information in the nervous system to be transmitted and processed, thereby controlling bodily function. Neurons are formed from stem cells by a process called, neurogenesis. The lifespan of neurons is the longest of all biological cells however they do not undergo mitosis like other cells, this has major ramifications once neurons are damaged, dysfunction or die. (Morris and Fillenz, 2003, Squire et al., 2008).

2.1.2. Neurodegeneration

Neurodegenerative diseases (NDDs) are traditionally defined as disorders characterized by progressive loss of neurons associated with deposition of proteins showing altered physicochemical properties in the brain and in peripheral organs (Kovacs, 2018). NDDs are incurable and statistics according to the World Health Organisation (WHO) reveal, that hundreds of millions of people worldwide are affected by neurological disorders with approximately 50 million people having epilepsy and 47 million been affected by dementia globally. They also indicate that there are approximately 9.9 million new cases every year.

There are varying types of NDDs, each defined by their clinical manifestations and details of neuropathology. NDDs, however feature some common mechanisms such; oxidative stress, neuro-inflammation, genetic factors and most commonly, protein deposits that have altered physicochemical properties and conformational changes (Yacoubian, 2017).

2.1.3. Mechanisms of NDDs

(I) Oxidative stress and mitochondrial dysfunction

Reactive oxygen species (ROS), such as free radicals have a function in cell signalling. Excess ROS may lead to damage of cells due to their ability to oxidise major biomolecules such as DNA, RNA, proteins and lipids (Wang et al., 2014). Oxidative stress results from an imbalance in the body caused by the production of ROS and the body's ability to detoxify their effects. Oxidative stress has been implicated as source of mitochondrial dysfunction, which is a prominent feature in both; Alzheimer's disease (AD) and Parkinson's disease. Oxidation of mitochondrial DNA, may lead to mutations, impairing its components and function which leads to neuronal cell death and production of more ROS, therefore continuing the cycle (Facecchia et al., 2011).

(II) Neuro-inflammation

Neuro-inflammation is as an inflammatory response within the brain or spinal cord to; injury, infection or neurodegenerative diseases, thus triggering an immune defence to potential harm. These responses are triggered to defend against potential harm. Such inflammatory response, considered acute, play a positive role in ensuring recovery. This

however becomes problematic if there is a prolonged inflammatory response that yields no positive results. The inflammatory response becomes chronic in nature and can lead to neuron damage (Bazan et al., 2012). Microglia are immune cells of the central nervous system (CNS) are activated during inflammation, they function as phagocytes and recognizing and scavenge dead cells, pathogens and several endogenous, and exogenous compounds (von Bernhardi et al., 2016, DiSabato et al., 2016). Microglia also release inflammatory mediators such as cytokines and chemokines, free radicals and ROS. These features of microglia play an important neuroprotective role but excess function can lead to neurotoxicity (Milatovic et al., 2017).

2.1.4. Biomarkers

Biomarkers are objective, quantifiable characteristics of biological processes or medical signs (Rachakonda et al., 2004). In NDDs, biomarkers are used to; indicate the presence or onset of neurodegeneration, monitor progression of the disease and also monitor the effects of treatment. There are varying types of biomarkers, such as; genetic, DNA, RNA and biochemical molecules. The common analysing medium for biomarkers are blood and Cerebrospinal fluid (CSF). CSF is considered the more favourable biological fluid for measurements of brain mechanisms and disease as it surrounds the brain and spinal cord. However obtaining CSF involves invasive techniques such as a lumbar puncture. Although blood samples are easier to obtain, the blood matrix is more complex and less specific to neurological concerns than compared to CSF. Blood samples may however identify peripheral biomarkers that reflect damage to the brain and central nervous system. (Jeromin and Bowser, 2017).

Protein deposits and aggregates, often misfolded or in higher concentrations than normal are key biomarkers in NDDs. Study of these proteins, their distribution and genetic alterations aid are important in evaluating mechanism of NDDs. Each NDDs are normally associated with specific protein biomarkers. Some of the most frequent protein biomarkers involved in the pathogenesis of NDDS include:

Amyloid-β (Aβ), which aggregates to form extracellular senile plaques (SP) deposits. Tau protein that forms neurofibrillary tangles (NFTs) composed of paired helical filaments (PHF). Both Aβ and tau are hallmarks of Alzheimer's disease (AD). Alpha-synuclein (α-syn), a common feature in; Parkinson's disease (PD), dementia with Lewy bodies (DLB) and multiple

system atrophy (MSA). It is a major constituent of Lewy bodies and Lewy neurites (LN) and protein clumps that are present in these diseases. (Giacomelli et al., 2017, Mattsson, 2011, Beach, 2017, Chen-Plotkin, 2014).

2.2. Tau Protein

Weingarten and co-workers study involved isolating a protein factor from tubulin, which polymerize into microtubules, a major component of the cytoskeleton. They found this protein factor to be heat stable and in its absence, tubulin is unable to polymerize into microtubules. They denoted this protein factor tau (τ), and concluded that tau is a major regulator of microtubule formation in cells (Weingarten et al., 1975).Tau protein is present in almost constant stoichiometry with tubulin through its polymerisation and de-polymerisation cycles (Cleveland et al., 1977b). Cleveland and co-workers, in their study of tau protein structure, indicates that tau structure is asymmetric, thus allowing a single tau molecule to interact with multiple tubulin dimers. They also suggest that tau is elongated and has a slight α-helical structure (Cleveland et al., 1977a). Goedert and colleagues provided insight into the amino acid sequences and isoforms of tau protein, stating the existence of six isoforms of human tau protein ranging from 352-441 lengths of amino acid chains (Goedert et al., 1989). The human tau gene is located on chromosome 17 at band position 17q21, containing 16 exons. All exons except 4A, 6 and 8 are present in the human brain. The six isoforms of tau with molecular weight ranging from 45 to 65 kDa, are produced from the alternative splicing of exons 2, 3 and 10. The isomers can be differentiated by absence or presence of repeat-regions in either the) amino-terminal (N-terminal) or carboxy-terminal (C-terminal) part of the tau molecule. These isomers are also expressed at different stages of human development, giving rise to the idea of different functions and roles it might play in the human body. Distribution of tau isomers are not proportional to each other and differ in their quantity present in neuronal cells. Tau protein is also found to be phosphorylated in the cytoplasm (Buee et al., 2000).

Alois Alzheimer in the year 1906 discovered what we know today as plaques and neurofibrillary tangles. He made this discovery during a brain autopsy of a psychiatric patient. Emil Kraepelin, senior colleague of Alois Alzheimer had published the discovery in his textbook ‘Psychiatrie’ and introduced the diagnostic term Alzheimer’s disease (Hippius and Neundörfer, 2003, Tagarelli et al., 2006). The NFT described by Alois Alzheimer was later determined to be composed of mainly PHF (Kidd, 1963). In 1986, Grundke-Iqbal and their

team made an important finding that would lead to numerous advancements in understanding neurological pathologies. They found that tau protein was a major protein component of PHF (Grundke-Iqbal et al., 1986). The same group of scientists also found tau protein in PHF to be abnormally hyper-phosphorylated (Iqbal and Grundke-Iqbal, 2006).

2.2.1. Post-translational modifications of Tau protein

Tau protein undergoes several post-translational modifications (PTMs), these modifications play an important regulatory role in tau physiology. Irregularities however, contributes to protein dysfunction. The types of PTMs in tau protein, include: hyper-phosphorylation, glycosylation, ubiquitination, glycation, poly-amination, nitration, and proteolysis. It is still, however not known which PTM contributes the most in pathologies of tau. Most scientific work focuses on phosphorylation and whilst it is an important contributor of tau aggregation, other less investigated PTMs may also play a role in either supporting or preventing aggregation. (Gong et al., 2005, Martin et al., 2011)

(I) Tau phosphorylation

Phosphorylation is process by which a phosphate group is added to a protein at its serine, threonine and tyrosine amino acid residues by enzymatic action. Phosphorylation plays a role in regulating protein function by inducing conformational changes in its structure. Phosphorylation also has a significant role in several cellular processes. The enzymes involved in phosphorylation are; protein kinases and phosphatases. Kinases facilitate phosphate group transfer to substrates from Adenosine Triphosphate (ATP) or Guanosine Triphosphate (GTP) whereas phosphatases facilitates the transfer of phosphate from a phosphorylated protein to a water molecule (Cheng et al., 2011). The balance in the activity of these enzymes is therefore key and any imbalances could lead to hyper-phosphorylation and contribute to tau dysfunction. Some kinases involved in tau phosphorylation include; glycogen synthase kinase 3β (GSK3β), cyclin-dependent kinase 5 (Cdk5), adenosine monophosphate-activated protein kinase (AMPK), casein kinase 1 (CK1), microtubule affinity-regulating kinases (MARKs), cyclic AMP-dependent protein kinase A (PKA) and dual specificity tyrosine-phosphorylation-regulated kinase 1A (DYRK-1A). Phosphatases include; protein phosphatase-1, -2A, and -5 (PP1, PP2A, and PP5) (Noble et al., 2013). The

longest isoform of tau in an adult human brain tau 441, has 80 Serine/ threonine and 5 tyrosine phosphorylation sites (Johnson and Stoothoff, 2004). An important tau function is to promote microtubule assembly, which in part is regulated by its degree of phosphorylation. In a normal adult human brain, tau contains 2–3 moles phosphate per mole of tau protein. Hyper-phosphorylated tau has been detected in several neurodegenerative disorders. In an AD brain is phosphate/tau ratio is significantly higher than a normal brain. The hyper-phosphorylated state of tau allows for its aggregation into PHF (Wang et al., 2013). Hyper-phosphorylation can alter tau interaction with DNA effecting possible changes at the chromatin and transcriptional level, thus altering its physiological role. The interaction between hyper-phosphorylated tau and actin leads to the destabilization of microfilaments, which in turn causes protrusion of the cell membrane (Alonso et al., 2018). Tau phosphorylation at threonine residue 231 allows for cis/trans isomerization. The cis conformation is considered neurotoxic and has a prion-like nature, spreading its pathology from a neuron to another (Albayram et al., 2018).

(II) Other PTMs

Tau glycosylation involves the attachment of glycans to proteins by enzymatic process. Two main types of glycosylation are: N-glycosylation, which involves covalent attachment of branched sugars on asparagine residues and O-glycosylation, entailing monosaccharide attachment on either serine or threonine residues the protein (Lisowska and Jaskiewicz, 2012, Jaeken, 2016). Glycosylation serves to regulate; folding, stability and solubility of proteins. In addition it also is involved in cell processes such as; cellular signalling, immune recognition, and inter-cell interaction (Frenkel-Pinter et al., 2017). Due to the importance of these processes in protein regulation, any irregularities may contribute to a chain of dysfunction of the protein. Wang and co-workers discovered that hyper-phosphorylated tau protein in AD brain is glycosylated as opposed to normal tau protein. They found that the glycan groups aided in maintaining the shape of PHF structure, noting that when glycan groups were removed by de-glycosylation, PHF tangles were converted into bundles of straight filaments, thus restoring their accessibility to microtubule function (Wang et al., 1996). Liu and co-workers further supported these findings, indicating that tau in AD brain was glycosylated mainly through N-linkage and that glycosylation of tau is an early

abnormality that could lead to its hyper-phosphorylation (Liu et al., 2002). In contrast, Robertson and co-workers investigated the role of O-glycosylation of tau in AD, their observations indicated an inverse relationship between O-linked N-acetylglucosamine (O-GlcNAc) sugar residues and tau phosphorylation, indicating that O-GlcNAc compete with phosphate groups for amino acid acceptor sites on the protein, thus protecting it from abnormal phosphorylation (Robertson et al., 2004).

Tau glycation is the non-enzymatic process of covalently bonding reducing sugars to a protein, resulting in advanced glycation end products (AGEs). PHF tau has shown form AGEs due to its high lysine content and the high intra-neuronal concentrations of aldose/aldose phosphate which renders it vulnerable to glycation. Yan and co-workers demonstrated that AGEs of PHF tau generates ROIs that lead to oxidative stress, hence contributing to pathologies of NDDs (Yan et al., 1994). Glycation of tau also advances levels of phosphorylation that lead to aggregate formation (Liu et al., 2016).

Tau truncation is the removal of the N- or C- terminal portion of a protein by proteolysis. Tau protein is found to be truncated in AD. Truncation and hyper-phosphorylation are the only two PTM of tau that are able to directly influence NFT formation. It is also thought that truncation induces tau hyper-phosphorylation (Kovacech and Novak, 2010, Zhou et al., 2018).

Tau prolyl isomerization's involves the use of prolyl isomerase enzyme that catalyse the interconversion of cis/trans isomers of amino acid proline, which plays a role in protein folding and protein function (Schmidpeter and Schmid, 2015). Pin 1 (peptidyl-prolyl cis/trans isomerase), is an enzyme that catalyses' prolyl isomerization of specific phosphoserine/threonine-binding domains in tau. Pin 1 is said to regulate tau hyper-phosphorylation by stimulating its de-phosphorylation (Zhou et al., 2000). Pin 1 is deficiency is also a probable contributing factor of tau hyper-phosphorylation in AD (Kimura et al., 2013).

2.2.2. Tauopathy

Tauopathy is a group of neurodegenerative disorders, characterized by abnormal hyper-phosphorylated tau protein. Tauopathies are sub divided into two categories namely, primary tauopathies, in which tau deposits are the prevalent feature and secondary tauopathies, in which tau is present but includes and other elements that are hallmark features. Primary tauopathies include; Pick's disease, Progressive supranuclear palsy, Corticobasal degeneration, Globular glial tauopathy, Argyrophilic grain disease, Age-related tau astrogliopathy, Fronto-temporal dementia with parkinsonism linked to chromosome 17" [FTDP-17], Aging-related tau astrogliopathy, Parkinsonism-dementia complex of Guam, Postencephalitic parkinsonism, Atypical parkinsonism of Guadeloupe, Diffuse neurofilament tangles with calcification. Secondary tauopathies include; Alzheimer's disease, Chronic traumatic encephalopathy, Down syndrome, Prion diseases, Familial British and Danish dementia, Subacute sclerosing panencephalitis and Lewy body disorders (Kovacs, 2015, Arendt et al., 2016, Irwin, 2016, Josephs, 2017, Kovacs, 2017, Lebouvier et al., 2017).

2.3. SENSORS

2.3.1. Electrochemical biosensors

A biosensor is an analytical device in which a biological response is converted into a measurable signal (Grieshaber et al., 2008). Biological recognition and sensing are two fundamental operating principles of a biosensor, which contain three basic components i.e. a bio-receptor, a transducer and microelectronics. There are different types of biosensors, each differentiated by type of bio-receptors and transducers involved are shown in Figure 2.1 (Karunakaran et al., 2015b).

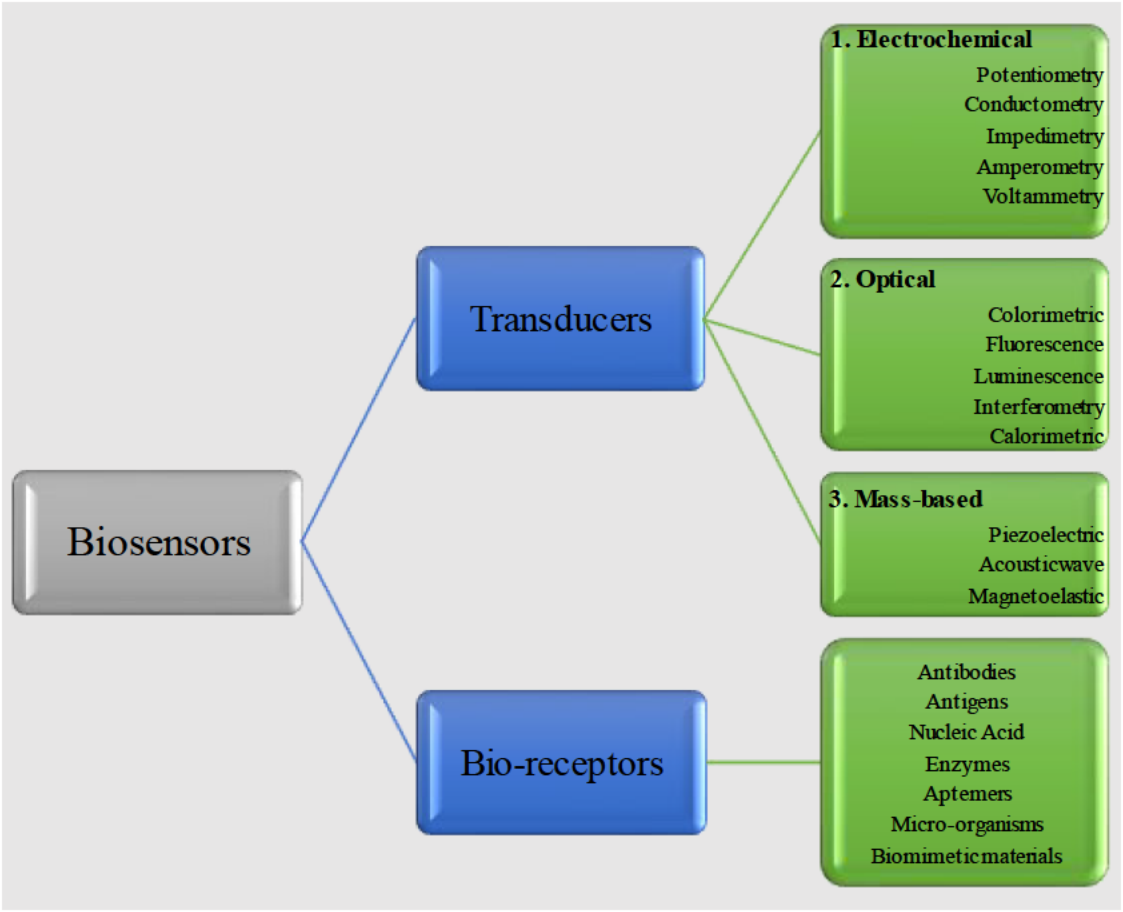

Figure 2. 1. Outline of biosensing types

Biosensors find application in numerous fields such as; monitoring and diagnosing medical conditions, environmental monitoring, the food/agriculture sector and various other industries. They are advantageous in terms of their simplicity compared to other analytical techniques,

they can be integrated with electronics to manufacture miniature portable devices, they are useful in point of care diagnostics as they provide results in a short time period and due to their ability to be selective to a specific analyte, analyte concentrations within a matrix can be determined with no or minimal sample preparation (Hammond et al., 2016).

2.3.2. Immunosensors

(I) Antibodies (Ab)

Antibodies are glycoproteins belonging to the immunoglobulin superfamily, are the body's natural defensive against pathogens by targeting pathogenic molecules called antigens. Antibodies are secreted by B cells of the adaptive immune system. B-cells are lymphocytes (subtype of white blood cell). B-cells differentiate to produce; memory B-cells which have the ability to recognise antigens after primary exposure and plasma cells, that secrete specific antibodies in response to specific antigens (Conroy et al., 2009).

Antibodies are Y-shaped, with each arm contain a light (25 kDa) and a heavy (50 kDa) chain connected by di-sulphide bonds as shown in Figure 2.2. The chains in turn contain constant (C) and variable (V) regions. The heavy chain has one variable (V_H) and three constant regions (C_{H1}, C_{H2} and C_{H3}), whereas the light chain contains only a single variable (V_L) and constant region (C_L). Heavy chains are used to distinguish the five immunoglobulin classes i.e. IgA, IgG, IgM, IgD and IgE. Antigen binding occurs at the variable region. The V_H and V_L regions make up an antibody's idiotype, which contain hypervariable complementary determining regions (CDRs). The amino acid groups from the CRDs interact with amino acid groups present in the antigen. The site on which an antibody is bound to the antigen is called an epitope (Zeng et al., 2012).

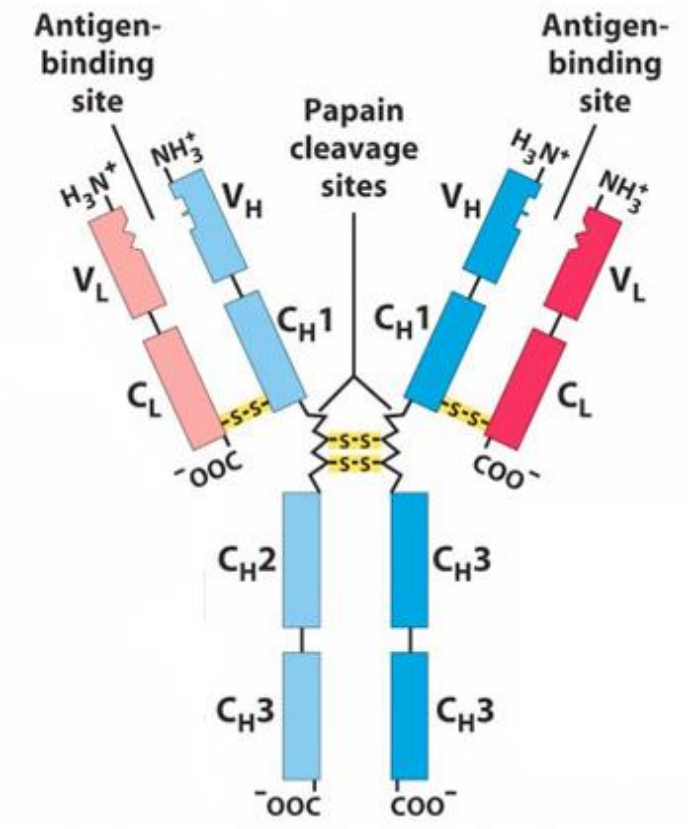

Figure 2. 2. Structure of an antibody (Gaurab, 2018)

(III) Production of antibodies

Technology allows for the production of antibodies by harnessing the bodies (human and animal) ability to naturally produce them. With current technology researchers are able to design and manufacture antibodies that aid in research, diagnostics and treatments of a various pathologies. Antibodies are produced in to basic forms; monoclonal antibodies (M_{Ab}) and polyclonal antibodies (P_{Ab}). M_{Ab} are produced from clones of a single B-cell, which only gives rise to one specific antibody molecule, they are therefore considered monovalent, binding to only one unique epitope on the antigen. P_{Ab} in contrast are produced from multiple B-cells which results in a collection of antibodies that have the ability to bind to multiple epitopes on the same antigen (Thermofisher Scientific, 2019). Antibodies can also be produced by synthetic means using recombinant DNA technology. Recombinant antibodies (R_{Ab}) as they are known, are antibody fragments consisting of V_L and V_H chains. Single-chain variable antibody fragment (scFv) is a common R_{Ab} format. Their production involves

using antibody DNA sequences obtained from a library developed from techniques such as phage display, then introducing these sequences into a host (bacteria, yeast, E-coli) to be expressed (Echko and Dozier, 2010, Ma and O'Kennedy, 2017).

(IV) Immunosensor principles

A biosensor that uses an antibody or fragments of an antibody as a bio-receptor is known as an immunosensor. The fundamental mechanism of analytical immunoassay lies with the ability of an antibody's recognition and subsequent binding to an antigen. Examples of target antigens are include; proteins, viruses, bacteria, organic/inorganic molecules all of which induces an immunological response.

Immunosensors can operate as either; labelled (indirect), which makes use of signal-generating labels such as enzymes, electro-active species and fluorescent molecules to or non-labelled (direct), in which physical changes during Ab-Antigen formation are directed detected. (Luppa et al., 2001). Labels aids in producing an electrochemical signal since Ab and antigens are not able to act as redox partners. The use of enzymes, like in the case of ELISA (enzyme-linked immunosorbent assay) and redox probes such as $[Fe(CN)_6]^{3-/4-}$, are a common labelled immunosensing approaches. The non-labelled approach monitors changes in physical parameters (charge, current, capacitance, impedance, mass and thickness) at the immunosensor surface as the result of Ab immobilisation onto the electrode surface and subsequent binding and recognising of the antigen (Karunakaran et al., 2015a).

The electrodes used for immunosensing are commonly composed of inert metals such as Au, Pt, Ag or carbon derivatives or semi-conductive materials. Ab immobilisation strategies onto electrode surfaces are important in insuring high sensitivity and selectively for the antigen. This can be achieved by either physical or chemical adsorption. Physical adsorption involves direct attachment of Ab onto the surface via van der Waals force, hydrophobic interaction, electrostatic interaction, and hydrogen bonding. Chemical adsorption is achieved through modification of the surface with groups such as amines, thiols, epoxides, carboxylic acids and aldehydes then immobilising the Ab onto these

groups, the amino residues of the Ab are expected bind to the respective chemical groups (Gopinath et al., 2014). The self-assembly monolayer (SAM) technique, is also a chemical biding strategy, it entails chemically bonding the SAM to the electrode surface, then using cross-linkers to covalently attach the Ab to the SAM (Bahadır and Sezgintürk, 2015).

(V) Electrochemical immunosensors

Electrochemical immunosensors combines electroanalytical measurements with Ab-antigen immune-recognition, to produce a highly sensitive and selective biosensing platform (Ju et al., 2017b). Basic electrochemical systems include three electrode system i.e. working, counter an auxiliary electrodes. The working electrode is the immobilisation and sensing platform for Ab and antigens respectively. Electrochemical techniques can be categorised according to the type of measurement been used. Amperometry, involves the measuring of current that results from the oxidation or reduction of the analyte at constant potential. Voltammetry is based on the same principle, differing in that, it involves measuring the current over a potential range. In potentiometry the analyte signal is measured as charge accumulation or potential between the working electrode and the reference electrode. Conductometry entails measuring electrical conductivity or alterations in conductive properties of the sample solution whilst impedance spectroscopy monitors electrical resistance and capacitance (Ronkainen et al., 2010). Electrochemical immunosensors are advantageous in many aspects. They are highly sensitive, easy to operate, financially viable and have the potential for miniaturization. Potential to develop hand held devices are extremely positive for point-of-care diagnostics (Wen et al., 2017).

2.4. ELECTROCHEMICAL APPLICATIONS OF TAU PROTEIN

2.4.1. Electrochemical studies of tau protein

Martic and co-workers investigated tau phosphorylation using three different protein kinases; kinase (GSK-3b), sarcoma (Src)-related kinase, and protein kinase A (PKA). Here they employ a working electrode gold electrode to which tau protein is immobilised using Lip-NHS (N-hydroxysuccinimide lipoic acid ester) binder. Ferrocenyl (Fc) adenosine triphosphate (Fc-ATP) was used as a co-substrate, which will allow for the facilitation of the kinase to transfer phosphate groups to tau. The kinase reactions involved additions of the 3 respective kinases combined with kinase assay buffer and Fc-ATP onto the electrode. The study made use of three electrochemical techniques i.e. cyclic voltammetry (CV), square-wave voltammetry (SWV) and electrochemical impedance spectroscopy (EIS). Their study demonstrated that Fc-ATP is a viable co-substrate for Fc-phosphorylation of Tau. The redox signals for GSK-3b and PKA was greater than Src, supporting the prior knowledge of the ability of GSK-3b and PKA to phosphorylate tau at serine and threonine residues, in comparison to Src kinases ability to target only tyrosine residues. (Martic et al., 2012).

Using the same principle and electrochemical setup as in the study above, The Fc-ATP in this study served a two-fold purpose, the firstly to probe singular and sequential Fc-phosphorylation of tau by multiple kinases and secondly to monitor any changes to the tau protein film properties. The kinases employed were; the threonine/serine kinase, Gsk-3β and four tyrosine kinases, Abelson tyrosine kinase (Abl), tau-tubulin kinase (TTBK), proto-oncogene tyrosine protein kinase Fyn (Fyn), and Src. It was observed that there was a decrease in current for sequential Fc-phosphorylation by GSK-3β for all other kinases. When Src-phosphorylated tau that was further phosphorylated by GSK-3β, there was a drastic decrease in current. By reversing the order of sequential Fc-phosphorylation i.e. further phosphorylate GSK-3β-phosphorylated tau by the other kinases, an increase in current was observed. This eludes to a possibility that the order and type of kinase plays a role in hyper-phosphorylation of tau. (Rains et al., 2013).

Metal cations such as copper, iron, magnesium, manganese, calcium and zinc are involved in many cellular process in the human body. They are involved in multiple functions such as; energy production, nerve transmission, muscle contraction and oxygen transport. Their involvement in brain activity is important for regulating many processes. Metals also form part of metallo-proteins and metallo-enzymes (Crichton and Ward, 2013). Metals are also

associated with neurotoxicity, they are capable of generating ROS which leads oxidative stress, aiding protein aggregation and are found in high concentrations in various neurodegenerative pathologies (Linert and Kozlowski, 2011, Kim et al., 2018). Protein/metal interactions are therefore important in understanding mechanisms of neuropathology.

Martic and co-workers studied tau protein interaction with copper, they investigated the binding of Cu^{2+} ions to both normal tau (nTau) and phosphorylated tau (pTau). Based on the current density for Cu(II) or Cu(I) remaining relatively constant, it was noted that the Cu^{2+} ions were well bound to the protein. The effects of Cu^{2+} concentration and pH was also explored. The authors noted that smaller electrochemical signals were alluded to high Cu^{2+} concentration and tau/Cu binding at lower pH was more favourable. It was also noted that pTau reaction with Cu^{2+} yielded higher current densities at varying pH than for nTau. It had been suggested that phosphorylation induces tau conformational change leading to more favourable binding to Cu. (Martic et al., 2013).

A gold electrode with nTau and pTau film deposits were used to investigate tau reactions with Fe(II) and Fe(III) by Ahmadi and co-workers. The respective tau modified electrodes were incubated with Fe^{2+} and Fe^{3+} solutions and was monitored with a $[Fe(CN)_6]^{3-/4-}$ redox probe using CV and EIS methods. The CV data indicated higher current densities for incubation with Fe^{2+}. Nyquist plots from EIS data indicated a more significant reduction in charge-transfer resistance of gold modified electrodes incubated with Fe^{2+}. The results for Fe reaction with pTau indicated the same response as for nTau with tau phosphorylated by threonine/serine Gsk-3β kinase, however the affinity of p-tau to Fe(II) significantly decreases when tau was phosphorylated by the tyrosine kinase Src. This indicates that phosphate groups present at tyrosine residues prevent Fe(II) binding. The information gained from this study suggests that tau protein's ability to absorb Fe is not enhanced but rather, regulated by phosphorylation. (Ahmadi et al., 2017).

One possible mechanism other than phosphorylation that plays a role in the aggregation tau protein is their reaction with inducing agents such as polyanions which are capable of neutralizing positive charges of tau repeat domains. Trzeciakiewicz and co-workers investigated tau binding to a herapin. Heparin, a polyanion is known to induce tau aggregation by; promoting its assembly into PHF, phosphorylation and inhibiting tau binding to microtubules (Hasegawa et al., 1997). The study employed two immobilisation strategies; the first saw tau protein been immobilised onto the Au electrode surface via the N-terminal using

Lip–NHS (N-tau-Au) and the second via the R-repeat domains at Cys291/Cys322 residues (Cys-tau-Au) using direct immobilisation where sulphur groups from Cysteine residues bind directly to the Au surface. Using EIS, it was observed that no reaction with herapin occurred on reacting with N-tau-Au whilst an increase in impedance was observed for herapin reacting with Cys-tau-Au. The lack of heparin binding on N-tau-Au suggests that the N-terminal may be necessary for heparin binding. Although previous reports indicate heparin binding to R domains of tau (Mukrasch et al., 2005), this study has displayed through electrochemistry, for the first time, the contribution of the N-terminal region of tau in polyanion binding, thus opening a pathway for therapeutic potential in preventing aggregation of tau by targeting its N-terminal region. (Trzeciakiewicz et al., 2015).

In transgenic mice models, anti-tau antibodies have shown possible treatment pathways for tauopathies. In these models anti-tau antibodies have shown to reduce; hyper-phosphorylation, aggregation, insoluble forms of tau and brain atrophy, whilst improving cognition (Yanamandra et al., 2015). The binding of anti-tau antibodies during phosphorylation of tau films on Au electrode surface by ATP and GSK-3β enzymes, have been demonstrated electrochemically. Five antibodies where used in this study, these include; Tau46, P262, D8, A10, IVIG, and IgG1 which has no binding affinity for tau protein and was used as a control. The charge transfer resistance (Rc) was measured for each antibody in relation to the measured value obtained for phosphorylation without antibodies. The results indicated that Tau46, A10, IVIG, and IgG1 induced significant increase in Rc values compared to P262 and D8 that showed only negligible increased Rc values. These results has confirmed the anti-tau antibodies ability to inhibit phosphorylation (Esteves-Villanueva and Martic-Milne, 2016).

2.4.2. Electrochemical detection of tau protein

Dai and co-workers developed an immunosensor for tau protein detection. The study used a protein ladder containing 6 recombinant Tau proteins representing each isoform. The biosensor was developed using screen-printed electrode (SPE), composed of Au working and counter electrodes and Ag/AgCl reference electrode. Anti-tau antibody was immobilised onto the bare Au working electrode surface using chemical linkers; 3-mercaptopropionic acid (MPA), N-(3-dimethylaminopropyl)-N'-ethylcarbodiimide hydrochloride (EDC), and N–hydroxysuccinimide (NHS). DPV was used to measure tau protein in both PBS (0.1M) and undiluted human serum over a concentration range of 1000 pg/mL to 100 000 pg/mL., using a

$[Fe(CN)_6]^{3-/4-}$ redox probe. There was an observed increase in anodic peak current with increasing tau concentration in both PBS and serum, this corresponding to the electron transfer reaction of $[Fe(CN)_6]^{4-}$ to $[Fe(CN)_6]^{3-}$. An R^2 value of 0.85 and 0.88 was obtained for the established linear calibration for tau in PBS and human serum respectively (Dai et al., 2017).

In another study, gold electrodes were covered with a layer of cross-linker DTSSP which was used to attach amino acid groups of protein G (an immunoglobulin-binding bacterial protein) via interaction with its sulpho-NHS ester groups. Unreacted sulpho-NHS ester groups was blocked with ethanolamine. Anti-tau antibodies were then immobilised onto the electrode binding to protein G. using EIS, it was found that the R_{ct} values increased upon addition of increasing concentrations of tau ranging from 0.01 pM to 10 nM. The LOD for this study was 0.03 pM. (Wang et al., 2017b).

Carlin and Martic tested 3 different anti bodies of tau to develop their immunosensor. The selected antibodies; D-8, A-10 and Tau-46 were chosen based on the epitope of tau441. The gold electrode surface was prepared by immobilising anti-tau antibodies using Lipoic Acid EDC/NHS. $[Fe(CN)_6]^{3-/4-}$ redox probe was used to monitor tau441 protein binding to antibody modified Au surface. Electrodes modified with D8-Au and A10-Au antibodies showed higher charge transfer resistance than Tau46-Au modified surface. The Detection range of tau441 was observed to be in the μM to nM range. The selectivity and sensitivity of the immunosensor was tested using bovine serum albumin (BSA), impedance was measured in the absence of tau replacing it with BSA. The observed change in impedance was negligible compared to tau, thus indicating that the immunosensor was selective for tau441 over BSA. (Carlin and Martic-Milne, 2018).

Derkus and co-workers developed an immunosensor for the simultaneous detection of tau protein and Myelin Basic Protein (MBP) in CSF and serum obtained from MS patients. The sensor developed in this study added another dimension to biosensors, as it makes use of signal amplifying nanomaterials. A carbon SPE was modified with graphene oxide (GO) nanomaterial following the addition of amine functionalized 1st generation trimethylolpropane tris[poly(propyleneglycol)] (pPG) dendrimers. Antibodies of tau and MBP was then immobilised onto the Carbon-SPE/GO/pPG surface. DPV and EIS was used to optimise and test the sensor. The LOD for tau was determined to be 0.15 nM. (Derkus et al., 2017)

2.5. NANOMATERIALS

Nanoparticles (NPs) can be defined as objects ranging in diameter size from 1 to 100 nm. NPs have garnered much scientific and technological interest in recent years under the umbrella of nanotechnology. Although much current emphasis is on synthetic developments, NPs do exist naturally. Naturally occurring NPs can occur as inorganically or biologically. Examples of naturally occurring inorganic NPs include: $CaCO_3$/ Al_2O_3/ SiO_2/ SiO_4^{4-}/ Fe_3O_4 in surface water: $CaSO_4$ in sea water and SiO_2/carbon soot from volcanic activity/fires/combustion (Griffin et al., 2017). NPs can also occur naturally as biological entities or products of biological process which include; magnetosomes, exosomes, lipoproteins and viruses (Stanley, 2014). Metallic nanoparticles have already been used since ancient times, in particular as colorant in glass and ceramic this is evidential from examination of historical artefacts from the ancient civilisations of Egypt to Rome across centuries and even millennia (Schaming and Remita, 2015). NPs consists of metals, metal oxides, carbon and organic matter. NPs also differ in shape, size and dimensions. They can be form spherical, cylindrical, rod shaped, spiral etc. They also exhibit surface variations. Physical and chemical properties of NPs differ from their corresponding bulk material or scaled up versions. Their higher surface are to volume ratio, together with their enhanced reactivity and stability and mechanical strength, are key factors which enable a wide variety of applications. Some of these application fields include; medicine, food, biotechnology, environmental studies, energy and electronics, construction, catalysis and cosmetics (Anu Mary Ealia and Saravanakumar, 2017).

The synthesis on NPs are commonly categorised in two ways i.e. Top-down approach and Bottom-up approach, shown in Figure 2.3. Bulk material is broken down or decomposed into smaller units which in turn is converted to NPs in the first approach, whilst in the latter, atoms in gas/liquid phase are condensed allowing for growth of NPs (Khan et al., 2017).

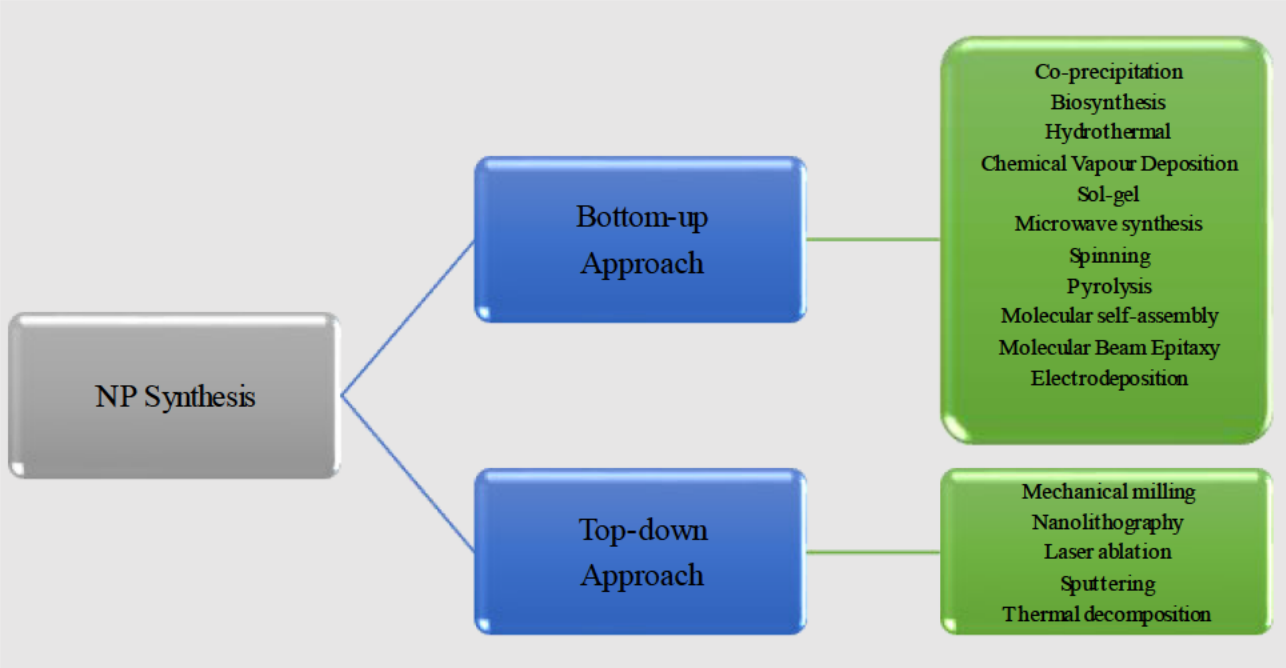

Figure 2. 3. Outline of nanoparticle synthesis techniques

A wide array of methods are employed to determine chemical and physical properties of NPs. Understanding these important characteristics of NPs are key to their applications, these include; Morphology, distribution, roughness, topography, surface area and surface chemistry, stability, dispersion, swelling, agglomeration, aggregation, purity, reactivity, hydrophobicity, magnetic properties , kinetics, thermal properties, chemical state, elemental composition and optical properties (Kumar and Dixit, 2017). Some of the most frequently characterisation techniques are listed below (Mourdikoudis et al., 2018).

- **X-ray-based techniques** - X-ray diffraction (XRD), X-ray absorption spectroscopy (XAS), Small-angle X-ray scattering (SAXS) and X-ray photoelectron spectroscopy (*XPS*) and energy dispersive X-ray analysis (*EDX*).
- **Microscopy** – Transmission electron *microscopy* (TEM), high resolution transmission electron *microscopy* (HRTEM), electron diffraction, electron tomography, scanning electron *microscope* (SEM), T-SEM-EDX, atomic force *microscopy* (AFM) and magnetic force *microscopy* (MFM)
- **Spectroscopy –** Fourier-transform infrared spectroscopy (FTIR), nuclear Magnetic resonance (NMR), UV-Vis, photoluminescence (PL), *low-energy ion scattering* spectroscopy (LEIS), dynamic light scattering (DLS), nanoparticle tracking

analysis (*NTA*), Raman spectroscopy, inductively coupled plasma mass spectrometry (ICP-MS), secondary-ion mass *spectrometry* (*SIMS*),

- Other methods include; Brunauer–Emmett–Teller (*BET*), *thermogravimetric analysis* (TGA) and zeta potential calculations.

(I) NPs as a signal enhancement strategy for electrochemical immunosensing

The role of antibodies increases affinity for antigens and enhances specificity and selectivity. Due to the large size of antibodies and specifically protein antigens, the surface area provided by electrodes are often not large enough to guarantee the sensitivity required in terms of detection limits for early diagnostic and point of care analysis. The use of nanomaterials aims to resolve this issue as they possess a wide range of properties such as a high surface-to-volume ratio, electrical conductivity, good biocompatibility and functionalisation, unique optical properties and the ability to act as potential signal labels (Ju et al., 2017a). Due to their large surface area, NPs are capable of increasing analytical sensitivity by increasing current yield by enhancing redox activity, preventing electrode fouling, lowering electrode overpotential and improving electrocatalysis efficiency (Lim and Ahmed, 2016). These properties combined with that of electrochemical sensors and antibodies provides the bases for the development of ultrasensitive immunosensors.

2.5.1. Graphene oxide (GO)

Graphene is carbon allotrope, it consists of a single layer of sp2 bonded carbon atoms arranged in a hexagonal or honeycomb lattice, as shown in Figure 2.4. Graphite is composed of multiple layers of graphene. GO is commonly synthesised from graphite by the Hummers' or modified Hummers' methods. In brief, the method involves mixing graphite powder with sodium nitrate followed by the addition of concentrated sulphuric acid gradual addition of potassium permanganate, this done at constant stirring. The modified methods often includes a pre-oxidation step or replacing some reactants with more stable, cost effective and environmentally friendly options. Other methods of GO synthesis include; Brodie and Staudenmaier methods, these methods however release chlorine dioxide gas, which has toxic effects. (Pooja and Bajapi, 2016).

GO is a two dimensional, disordered, oxygen functionalised graphene sheet to which the degree of oxidation is dependent on the method of synthesis. Functional groups include; hydroxyl, epoxy, carboxyl and carbonyl groups (Biswal et al., 2018, Sun, 2019). The distribution of these groups on GO sheets also vary according to the synthesis. Distribution and atomic arrangement plays a vital role in GO composition and properties, thus effecting its functional capabilities. Characterisation is therefore key in providing this information.

GO is considered hydrophilic due to its functional groups having high affinity to water molecules. GO is therefore able to dissolve in solvents. It has been found that with a low degree of oxidation, GO exhibits good semiconductor properties whilst a full degree of oxidation, results in GO displaying good insulating properties (Gomez et al., 2016).

GO has many applications, some examples include; biomedical, energy storage devices, catalysts, water purification, coating technology, medical and biosensors (Gupta et al., 2015).

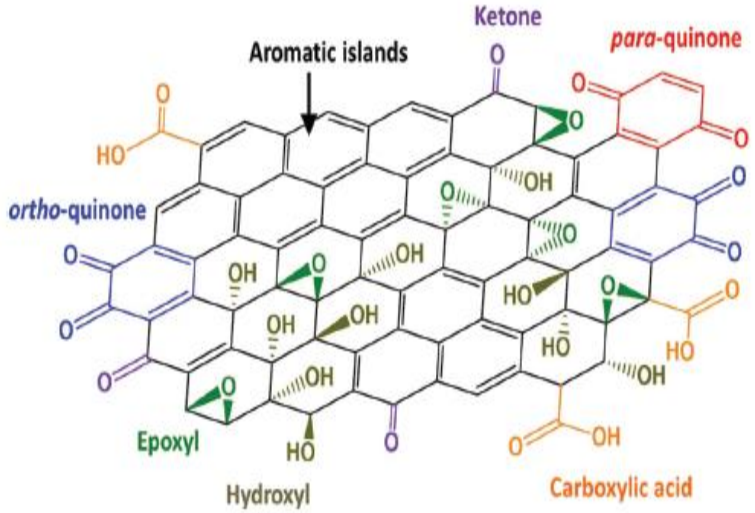

Figure 2. 4. Structure of GO (Eng et al., 2015)

(I) GO and biosensors

GO is known to have a high energy/electron transfer capability, strong electro-catalytic ability, low charge-transfer resistance, fluorescence quenching ability, high affinity toward various amphiphilic biomolecules, easy protonation of analytes by functional groups on GO, strong binding with biomolecules through pi-pi stacking and/or hydrogen bonding interactions and high surface area (Lee et al., 2016). These reported characteristics make it ideal for biosensor application and contributes to possible miniaturisation of sensors that will have

low detection limits. GO and graphene based NPs act as transducers in biosensors, converting receptor-analyte interactions into measurable signals. For immunosensing functional groups within GO permits multiple strategies for the attachment of Ab. EDC linkers, for example, allows for bio-conjugation between carboxyl groups of GO and amine groups of the Ab (Peña-Bahamonde et al., 2018).

2.5.2. Silver NPs (AgNPs)

AgNPs exhibit a wide array of properties which in turn enable a vast number of applications. These properties are highly dependent on the precursor Ag salt concentration, type and concentration of reducing agents and capping agents and method of synthesis. Morphology and size have shown to effect functioning and reactivity of AgNPs. Shapes of AgNPs include; spherical, rod, octagonal, hexagonal, triangle, flower-like. Morphology and size also effect other properties, for example smaller AgNPs are known to be more toxic due to their larger surface area, and the same can be said of the shape due to their varying surface area. Optical, thermal, magnetic, electrical properties and toxicity are all impacted by the morphology and size of AgNPs. (Syafiuddin et al., 2017)

(I) AgNPs properties and applications

The mechanism of AgNPs antimicrobial activities are both direct and indirect. It is reported that AgNPs are capable to attaching to cell surfaces causing distortions to its structure which has subsequent consequences such as interrupting cellular function, inhibiting multiplication and eventual cell death. AgNPs are reactive towards nucleophilic amino acid residues, sulfhydryl, amino, imidazole, phosphate, and carboxyl groups which permits its use as an antimicrobial agent against microbes such as fungi, viruses and bacteria. In an indirect approach, AgNPs also generates ROS and free radicals which in turn are antimicrobial (Sweet and Singleton, 2011). AgNPs has therefore found application in the medical and general health care sectors, been incorporated into products such as soaps, cosmetics and detergents, their application has also been touted as potential therapeutic agents against cancer and other illness and

disease (Zhang et al., 2016). Application also extends to food storage, textile coatings and environmental application for example, water purification (Abou El-Nour et al., 2010).

AgNPs also display some unique optical properties, having absorption and scattering characteristics in both the visible and near-infrared (NIR) regions owing to excitation of localized surface plasmon resonance (LSPR), in which surface electrons of AgNPs undergo collective oscillation when excited by light of specific wavelength. These properties give rise to optical applications of AgNPs especially when conjugated to biomolecules. Interaction between AgNPs and biomolecules occur via electrostatic adsorption, direct chemisorption of thiol derivatives or covalent binding through chemical linkers. These AgNPs-Biomolecules leads to multiple applications in biosensing, imaging, catalysis, drug delivery, diagnostics and therapy (Zeng et al., 2012). The light scattering ability of AgNPs also can be utilised in environmental analysis such as detecting heavy metals in water sources.

Thermal and electrical properties of AgNPs such as reduced melting points increased surface energy and inhibitors of electrical loss, allows for its usage in microelectronic materials, conductive fillers, solar cells and electrical optical sensor devices (Thamilselvi and Radha, 2017).

(II) Biological synthesis of AgNPs

The biological approach of synthesis employs the use of herbal extracts or microorganisms. This is considered a "green" approach, contributing to a much more eco-friendly form of chemical synthesis. There are several advantages to using such methods over traditional chemical and physical methods. $AgNO_3$ is the most common precursor salt used for AgNP production. Plants, fruit and vegetable contain carbohydrates, fats, proteins, nucleic acids, pigments and several types of secondary metabolites that are capable reducing, capping and stabilising agents. Similarly, microorganisms (bacteria, yeasts, fungi, and algae), enzymes, proteins and bio-surfactants have the same capabilities (Siddiqi et al., 2018).

The use of green synthesis is advantageous in terms of cost, energy requirements and eliminating the use of harmful/toxic reducing agents such as sodium borohydride or hydrazine and their bi-products. Water is commonly used as the solvent medium for plant extracts and do not need specific solvent extraction techniques. Reactivity is dependent on time, temperature, pH, concentrations of salt/extract solutions and volume ratio of extract to salt solution. It has been well reported that production of NPs occur within a short time frame at room temperature. Overall plants, fruit and vegetables are readily available and safe to handle. They contain a wide variety of agents capable to reducing Ag ion and stabilising AgNPs. All parts of plant/veg/fruit can be used for green synthesis, these include their roots, stems, seeds, leaves, latex, barks and peels. All these components contain chemical groups such as phenolics, terpenoids, polysaccharides, flavones, alkaloids, proteins, enzymes, amino acids, alcoholic compound, quinols, chlorophyll pigments, linalool, methyl chavicol, eugenol, caffeine, theophylline, ascorbic acid, and other vitamins, all of which have been reported as reducing and capping agents. Flavonoids and phenols in particular are known to cap NPs preventing their agglomeration. (Rauwel et al., 2015, Parveen et al., 2016)

2.5.3. Gold Nanoparticles (AuNPs)

(I) AuNPs synthesis and structures

AuNPs has generally been synthesised by reducing gold (III) salts such as hydrogen tetrachloroaurate ($HAuCl_4$). Citric acid is most commonly used, acting as both a reducing and stabilizing agent to produce spherical AuNPs by varying the ratio of $HAuCl_4$ to citric acid. Aggregation becomes a possibility when functionalised with thiolate ligands. A strategy to overcome such problems has been to use a two-phase liquid-liquid system using a tetraoctylammonium bromide (TOAB) as a phase transfer reagent and sodium borohydride (NaBH4) as a reducing agent, in the presence of dodecanethiol ($C_{12}H_2SH$) (Yeh et al., 2012). Other synthesis of methods include photo-reduction using UV and Gama radiation, Ultrasound-assisted synthesis, laser ablation strategies, electro-reduction and biosynthesis. AuNPs morphologies

exist in 1D, 2D, 3D forms as: 1D; nanorods, nanowires, nanotubes and nanobelts: 2D; nanoplates such as stars, pentagons, squares, rectangles, triangles and hexagons: 3D; spheres, tadpoles, dumbbells and branched pods, stars and dendrites (Elahi et al., 2018).

(III) AuNPs properties and applications

Similarly to other noble metal nanoparticles, AuNPs possesses unique optical properties owing to surface plasmon resonance (SPR). Spherical AuNPs are known to exist in a variety of colours when in solution which is a result of their varying size. Reported UV peaks range from 500nm to 550nm. Optical applications of include its usage in photodynamic therapy to diagnose and treat oncological and skin disease, this capability arises from their SPR and fluorescence quenching ability. AuNPs are able to accumulate in tumour cells and show optical scattering, making it an important tool for probing cancerous cells. When irradiated with EMR of between 800nm to 1200 nm, AuNPs cause heating, making it useful in the photo thermal destruction of tumours. In addition AuNPs have good biocompatibility and can be integrated easily with ligands, combined with their non- cytotoxicity AuNPs find application drug delivery and cellular uptake. (Tomar and Garg, 2013)

AuNPs are also used for sensing applications for the detection of metal ion and various molecules and biomolecules. They can be used in conjunction with various transducers giving rise commonly to colorimetric and electrochemical based sensors. For immunosensing, Ab can be functionalised on AuNPs via physical interactions which may include, the attraction of negatively charged AuNPs and a positively charged antibody, hydrophobic interactions and binding of AuNPs conducting electrons to amino acid sulphur atoms of the antibody, as shown in Figure 2.5. Chemical binding of Ab to AuNPs includes chemisorption via thiol derivatives and the use of chemical bifunctional linkers. (Jazayeri et al., 2016)

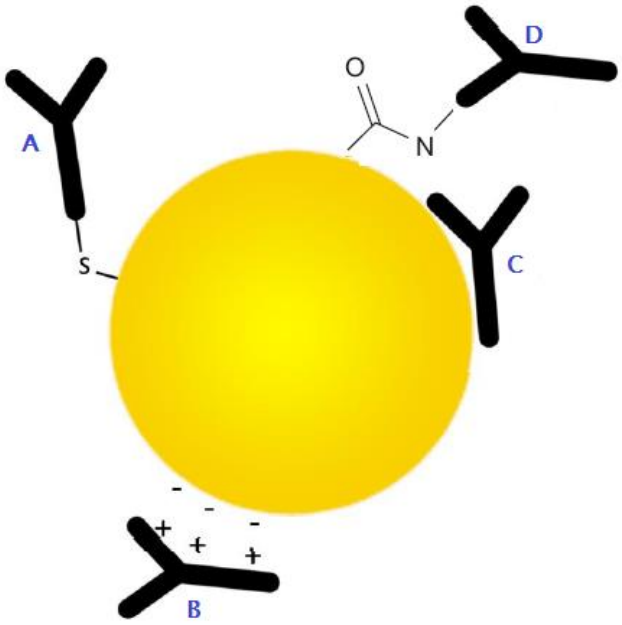

Figure 2. 5. Interaction mechanisms of AuNP with an antibody. (A) Dative binding between thiol Ab groups and AuNP (B) ionic interactions (C) hydrophobic interactions (D) EDC/NHS covalent binding, Adapted (Ljungblad, 2009).

2.6. COMPUTATIONAL CHEMISTRY

Computational chemistry relies on mathematical and non-mathematical models that aid in understanding and predicting chemical mechanisms. Computational models can be used to simulate molecular systems prior to experimental attempts, thus providing key information relating to suitability of all materials been used, thus avoiding wastage, time and labour and leading to more successful experimental work. Computational modelling can also be used to give insight into mechanisms such as molecular bonding of various experiments and natural occurring reactions and processes.

Computational chemistry allows for examination of multiple properties of a variety of substances, these properties include; molecular geometries, reactivity, rates, equilibria, and spectral. Computational methods include; molecular mechanics, molecular dynamics and quantum mechanical methods such as density functional theory (DFT), semi-empirical and ab initio (Lewars, 2011).

Theoretical studies of nanomaterials have been achieved by computational means giving rise to understanding their properties, characteristics and interactions with its surroundings and with other substances. NPs can be studied under varying conditions be it normal or extreme

conditions such as extreme temperatures, pressures, or strong electric or magnetic fields. In addition NPs can be studied in different matrixes, these factors are therefore advantages over conventional experiments in that reaction conditions and matrixes that are normally inaccessible due to factors such as cost and hazard potential are now able to be explored in a safe and cost effective manner (Barnard, 2010). NPs have application in the medical field, uses include drug delivery, and this often involves functionalisation with biomolecules. Conditions and sites of interaction between NPs and biomolecules can all be modelled, in addition cellular intake of NP/biomolecule composites can be evaluated and optimised before experimental work. Biosensors can also benefit from computational modelling by predicting the most suitable conditions, configuration and biomolecule receptor type that will enhance selectivity of a specific analyte (Angioletti-Uberti, 2017).

There have also been reports of computation chemistry been used to evaluate the pathogenies of neurodegenerative diseases. Mechanisms such as protein misfolding and aggregation can be studied by computational means (Huang, 2009, Giacomelli et al., 2017). This contributes to finding trigger and progression events of neurodegeneration which is still not well understood.

CHAPTER THREE

THEORETICAL PRINCIPLES

In this chapter the principles underlying the experimental work relating to electrochemical development and subsequent studies on the developed immunosensors are discussed together with the key principles of the characterisation and synthesis of nanoparticles used. In addition, the fundamental aspects of the appropriate computational methods, are outlined together with the software capabilities.

3.1. EXPERIMENTAL PRINCIPLES

3.1.1. Voltammetry

The most common setup for voltammetry utilises a three electrode system i.e. a working electrode (WE), reference electrode (RE) and auxiliary electrode (AE). The basic function involves the applying a potential to the WE, varying its potential relative to the fixed potential of the RE and then measuring the current (i) that flows between the WE and AE over a period of time (t). Voltammetric techniques can therefore be described as some function E, I, t. Applying a potential to an electroactive species present on the WE causes its reduction and/or oxidation.

3.1.1.1. Cyclic voltammetry (CV)

CV provides qualitative information about electrochemical reactions. In CV, a linear potential sweep is applied to the WE at a fixed rate between two values, V_1 and V_2. This sweep is reversible, occurring in both directions i.e. form V_1 to V_2 then from V_2 to V_1, as shown in Figure 3.1. During this reversible sweep, the analyte is either oxidised or reduced by the current that flows through the WE as illustrated by equations 3.1a and 3.1b, where species O is reduced to form species R, then O oxidised back to R.

$$O + ne^- \rightleftharpoons R \qquad (3.1a)$$

$$R \rightleftharpoons O + ne^- \quad (3.1b)$$

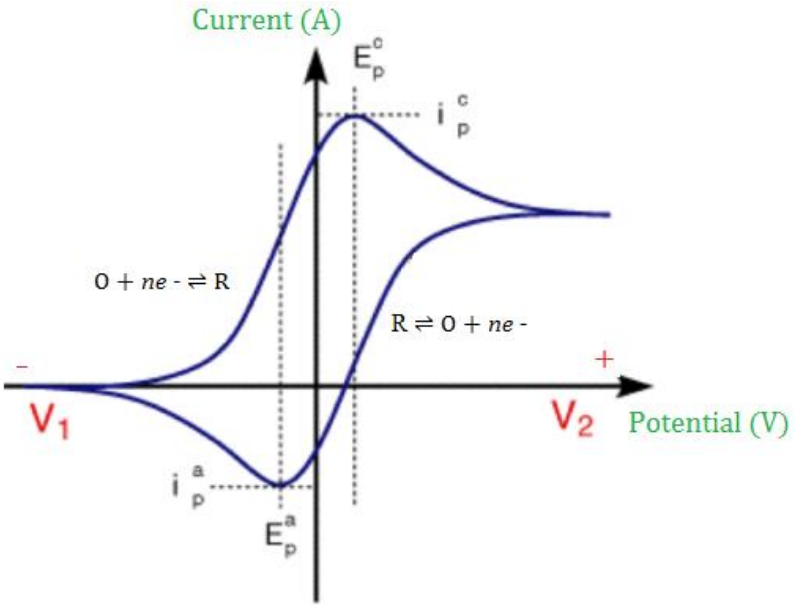

Figure 3. 1. Cyclic Voltammogram showing the redox reaction of species O and R, where i_{pc}/E_{pc} and i_{pa}/E_{pa} indicate the peak cathodic and anodic current/potential respectively for a reversible reaction.

The peak current is given by the Randles-Sevcik equation:

$$i_p = (2.69\times10^5)n^{3/2} AD^{1/2} C\nu^{1/2} \quad (3.3)$$

where n is the number of electrons in the redox reaction, A is the area of the WE, D is the diffusion coefficient for the electroactive species, ν is the scan rate, and C is the concentration of the electroactive species.

CV is therefore a useful technique that could be used in the evaluation of thermodynamic and kinetic parameters, conduct diffusion and adsorption studies, investigate chemical mechanisms and monitor the behaviour of modified electrodes.

3.1.1.2. Differential Pulse Voltammetry (DPV)

Pulse voltammetric methods are based on the difference in rate of decay of the charging current and faradaic currents after when the potential between the WE and RE as a pulses of increasing amplitude. In DPV the current measured before and after the application of each pulse, with the difference in current been plotted against the base potential and been at a maximum around the redox potential of the reacting species or analyte. DPV is considered to be a highly sensitive method having a high signal to noise ratio, as shown in Figures 3.2 and 3.3.

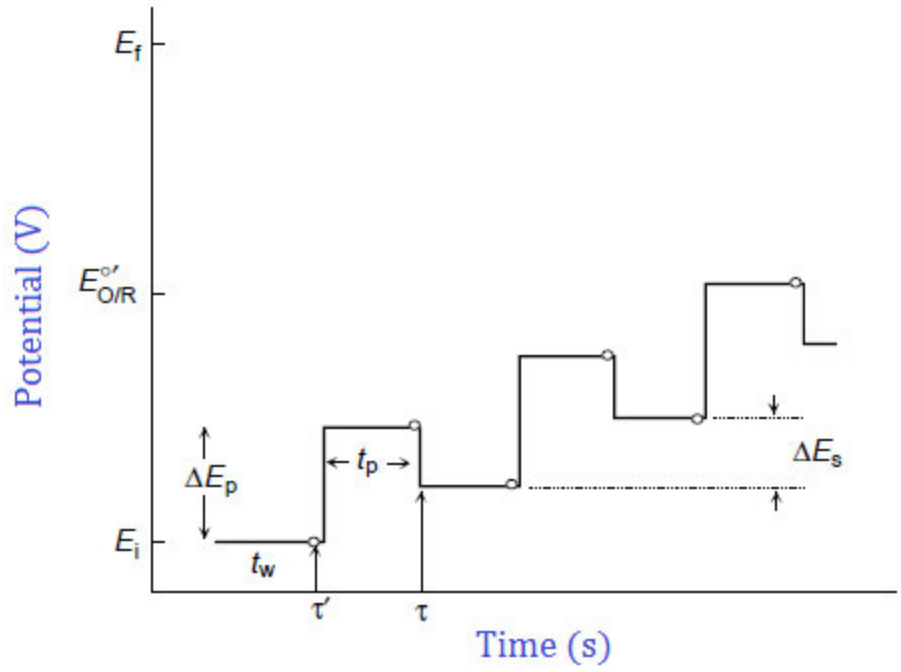

Figure 3. 2. DPV waveform, showing; pulse time, t_p; waiting time, t_w; pulse amplitude, E_p; base potential, E_s and the two points of current measurements, τ' and τ.

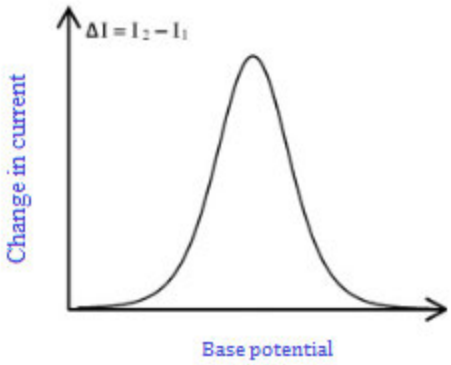

Figure 3. 3. Resulting DPV curve of change in current (i_2 - i_1, *from points* τ *and* τ'*, respectively*) versus the base potential.

3.1.1.3. Square wave voltammetry (SWV)

SWV is a form of pulse voltammetry and is similar to DPV as it employs a waveform, shown in Figure 3.2. This waveform is a result of superimposing symmetrical pulses of constant amplitude onto base staircase potential increments. The output of this waveform is a voltammogram of the net current against potential. SWV also takes into account both forward and reverse reaction signals, whereas DPV considers only the forward reaction. SWV is considered to be a highly sensitive and relatively quick method.

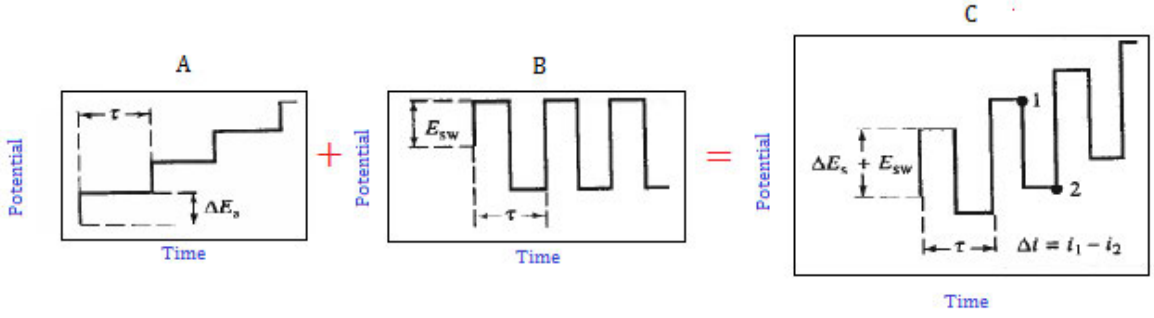

Figure 3. 4. Steps in SWV signal development. (A) Staircase signal, (B) symmetrical pulses, (C) SWV waveform.

.

3.1.2. UV-Visible Spectroscopy

The UV-Visible range of the electromagnetic spectrum is between 210 to 900 nm. Absorption of UV or visible radiation results in the excitation of electrons from the ground state to the excited state, for a given substance. Figure 3.5 shows types of electronic transitions that occur, can involve π, σ, n electrons and may also include d and f orbital electrons.

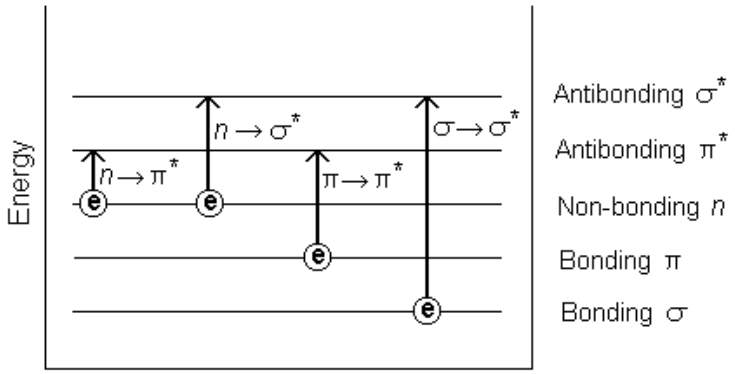

Figure 3. 5 Illustration of the electronic transitions by UV/Vis absorption

Each wavelength of light has a particular energy associated with it. A large gap between the energy levels requires more energy to promote the electron to higher energy level, this results in absorption of light of a higher frequency, and shorter wavelength. The probability that a substance will absorb light is dependent on its molecular orbital structure.

The absorption spectrum of a compound is one of its most useful physical characteristics and can be used for both qualitative and quantitative analysis. A UV-visible spectrometer is the instrument used to measure the absorbance of ultra violet or visible light by a sample, either at a single wavelength or perform a scan over a range in the spectrum. These instruments contain a light source, such as halogen, tungsten, deuterium lamps. The output from the light source is focused onto a dispersion device, normally monochromator, which splits the incoming beam of light into its component wavelengths and then allowing only the selected wavelength(s) to pass through the reference and the sample, contained inside a cuvette. Some of this light will then be absorbed by the sample and the rest will pass through to a detector, which in turn converts the incoming transmitted light into a current signal. Transmission is the ratio of the intensity of the transmitted light to the incident light, and is correlated to absorbance. The absorbance is related to the concentration of the sample by the Beer-Lambert law, which states

that the concentration of a substance in solution is directly proportional to the absorbance of the solution by defining the relationship between absorbance (A) and transmittance (T) (equation 3.4.), where is, ε is molar absorptivity ($dm^3\ mol^{-1}\ cm^{-1}$), c is molar concentration ($mol.dm^{-3}$), and b is path length of the sample cell (cm). A graphic representation is shown in Figure 3.6.

$$A = \log \frac{I_o}{I} = \log \frac{100}{T} = \varepsilon\ c\ b \qquad (3.4)$$

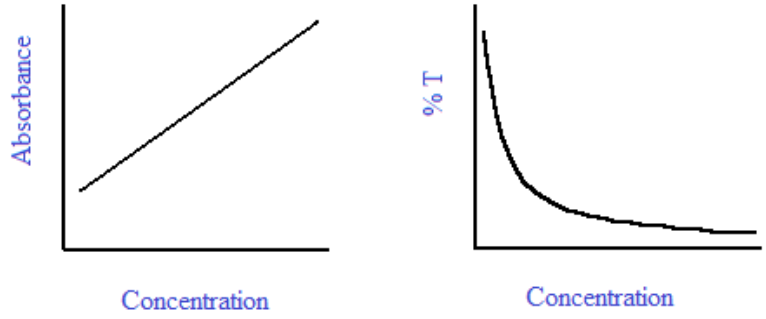

Figure 3. 6. Graphical representation of the output of UV-Visible spectrometry

3.1.3. Transmission electron microscopy

In TEM, a beam of electrons is passed through the sample specimen. The transmission of the electron beam is dependent on the properties of sample specimen. TEM consists of an electron source or cathode which is usually a V-shaped filament made of tungsten or lanthanum hexaboride that accelerates monochromatic electrons into the surrounding vacuum (Figure 3.7). The optical aspect involves the uses of three lenses, i.e. condenser lenses, the objective lenses, and the projector lenses. These lenses play a role in forming and focusing electron beams, then magnifying them onto the imaging platform device (phosphor screen, made of fine particulate zinc sulphide). The image strikes the phosphor screen, generating light and allowing for image observation. Darker area of the image indicate, that fewer electrons are transmitted in that area compared to the lighter areas. TEM images are useful in providing topographical, morphological, compositional and crystalline information of a substance.

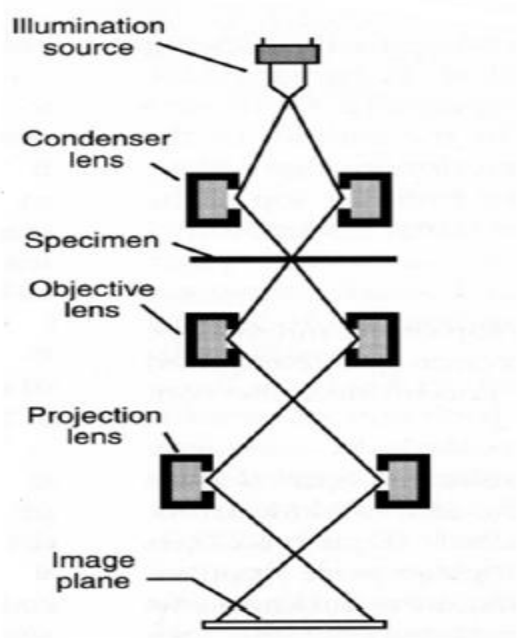

Figure 3. 7. General components and setup of TEM instrumentation

3.1.4. Field-flow fractionation (FFF)

FFF is a separation technique, based on an applied gradient or field of force, as shown in Figure 3.8. These force fields can be, centrifugal, thermal-gradient, electrical, magnetic, gravitational or flow fields. In FFF the sample is dissolved or suspended in a carrier liquid, this carrier liquid is pumped through a channel, which contains an inlet flow and a perpendicular field flow. The carrier liquid enters the column via the inlet flow, creating a parabolic laminar flow profile, propelling the sample towards the channel outlet, a subsequent diffusion influx is also created which drives the analyte back towards the centre of the channel. The sample forms different equilibrium layers as a result of this phenomenon. The laminar flow is fastest in the centre of the channel and slowest next to the channel walls. The sample separation elution can be observed in terms of particle size, where the smaller particles are transported faster through the channel than the bigger ones and are therefore eluted first.

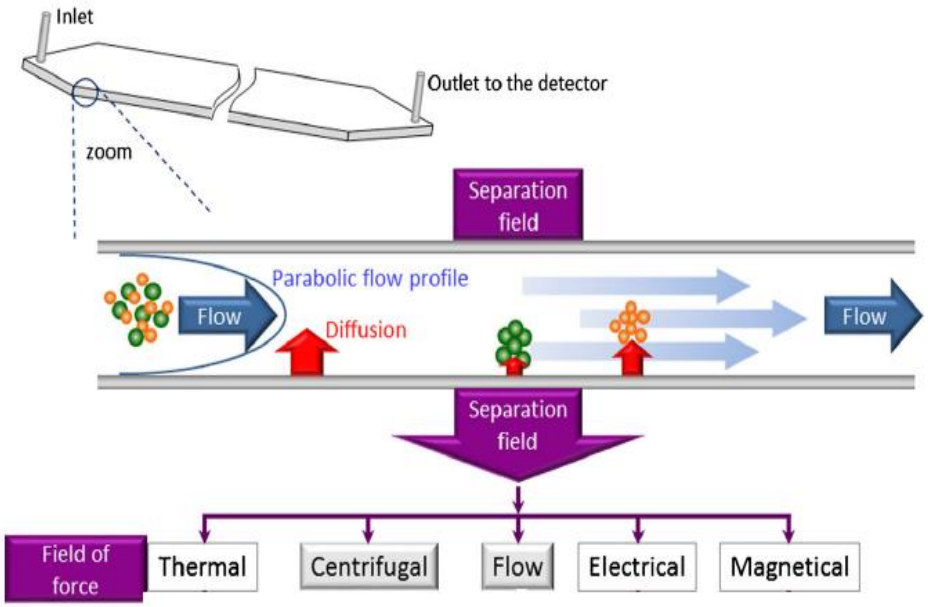

Figure 3. 8. Scheme of FFF operation (Contado, 2017)

3.1.5. Asymmetric flow – field flow fractionation (AF4)

In AF4 the sample fractionates according to its molecular weight and hydrodynamic size (Meier and Heinzmann, 2017). AF4 utilises a semi-permissive membrane that has a specific cut off size, allowing retention of sample component of interest above the membrane cut of size. The sample accumulates at the bottom of the channel due to the cross-flow, which acts perpendicular to the forward channel flow. The sample components are separated due to differences in their diffusion coefficients. The cross flow can be adjusted, thus allowing for optimisation and enabling a wide variety of sample types and sizes to be analysed. In addition to cross flow, other factors that affect the signal include; the Channel height, which effects the parabolic laminar flow rate profile which in turn has an effect on separation resolution, it also affects the quantity of sample that can be analysed. The choice of membrane is also important as it should not interact or bind with the sample. Finally the amount of sample injected should also be optimised. (Zhang and Lyden, 2019)

3.2. COMPUTATIONAL CHEMISTRY

With computational chemistry, investigations into a substance's molecular geometry, shape, bond lengths, bond angles, energies, transition states and reactivity, can easily be done using computer software. Some of the tools employed include molecular mechanics, molecular dynamics and quantum mechanical methods such as Ab Initio calculations, semi-empirical calculations and density functional theory calculations (Young, 2001).

3.2.1. Density functional theory (DFT)

The following principles are key in the development and application of DFT. (Koch et al., 2001, Lewars, 2011, Band and Avishai, 2013)

- Schrödinger equation

  The Schrödinger equation is a powerful mathematical tool and is considered the basis of many applications of quantum mechanics by describing the wave function or state function of a system. For chemical approaches, solving the time independent equation (3.5) aids in the description of molecular, atomic, and subatomic systems.

$$\hat{H}\Psi_i(\vec{x}_1,\vec{x}_2,\ldots,\vec{x}_N,\vec{R}_1,\vec{R}_2,\ldots,\vec{R}_M) = E_i\Psi_i(\vec{x}_1,\vec{x}_2,\ldots,\vec{x}_N,\vec{R}_1,\vec{R}_2,\ldots,\vec{R}_M) \quad (3.5)$$

  Where $\hat{H}$, is the differential Hamilton operator, representing the total energy (kinetic and potential) of the system. M and N represent the nuclei and electrons respectively. Ψ, the wave function, containing all possible information about the quantum system. E_i, is an energy value of the system and x and R, are spin co-ordinates of the electrons and spatial co-ordinates of the nuclei respectively. Expanding the Hamilton operator gives equation (3.6).

$$\hat{H} = -\frac{1}{2}\sum_{i=1}^{N}\nabla_i^2 - \frac{1}{2}\sum_{A=1}^{M}\frac{1}{M_A}\nabla_A^2 - \sum_{i=1}^{N}\sum_{A=1}^{M}\frac{Z_A}{r_{iA}} + \sum_{i=1}^{N}\sum_{j>i}^{N}\frac{1}{r_{ij}} + \sum_{A=1}^{M}\sum_{B>A}^{M}\frac{Z_A Z_B}{R_{AB}} \quad (3.6)$$

- Born-Oppenheimer approximation

  This approximation separates the motion of nuclei and electrons by virtue of their difference is mass, where electrons are much smaller and therefore move much faster, hence the basis of the approximation is that the nuclei in a molecule are stationary with respect to the electrons. The Born-Oppenheimer approximation, therefore reduces the Hamilton operator equation (3.6) and effectively simplifying the Schrödinger equation.

$$\hat{H}_{elec} = -\frac{1}{2}\sum_{i=1}^{N}\nabla_i^2 - \sum_{i=1}^{N}\sum_{A=1}^{M}\frac{Z_A}{r_{iA}} + \sum_{i=1}^{N}\sum_{j>i}^{N}\frac{1}{r_{ij}} = \hat{T} + \hat{V}_{Ne} + \hat{V}_{ee}. \tag{3.7}$$

- The Hartree-Fock Approximation

  Hartree-Fock theory was developed to solve the Schrödinger equation, it is considered an output determinant capable of lowering the average value of the Hamilton operator. It is an approximation an electron wave function by using an anti-symmetrised product, known as a Slater determinant (Φ_{SD}).

$$\Psi_0 \approx \Phi_{SD} = \frac{1}{\sqrt{N!}}\begin{vmatrix} \chi_1(\vec{x}_1) & \chi_2(\vec{x}_1) & \cdots & \chi_N(\vec{x}_1) \\ \chi_1(\vec{x}_2) & \chi_2(\vec{x}_2) & & \chi_N(\vec{x}_2) \\ \vdots & \vdots & & \vdots \\ \chi_1(\vec{x}_N) & \chi_2(\vec{x}_N) & \cdots & \chi_N(\vec{x}_N) \end{vmatrix} \tag{3.8}$$

- The Hohenberg–Kohn Theorems

  The first of these two theorems states that the electron density determines ground state properties using only 3 spatial coordinates, thus determining the Hamilton operator and enabling computation of the wave functions of all states and all material properties. The second Hohenberg–Kohn Theorem establishes a variational principle. The theorem states that the energy and density of the ground state corresponds to a functional delivering the lowest energy, provided that the input density is the true ground state

density. These theorems enables the calculation of molecular properties from the electron density.

- The Kohn-Sham equation

  This approach makes use of a fictitious non-interacting reference electron system in which density is the same as that of the interacting electrons of a real system. This reference system is built from a set of one electron functions and enables the determination of a systems kinetic energy. The Kohn-Sham approach makes use of orbitals to calculate the non-interacting kinetic energy using the following equation.

$$\left[\frac{-1}{2}\sum_{i}^{N}\nabla_i^2 + \hat{V}_{ext}(r) + \int\frac{\rho(r')}{|r-r'|}dr' + \nu_{xc}(r)\right]\phi_i(r) = \varepsilon_i\phi_i(r) \tag{3.9}$$

DMoL^3 is a computer modelling program that utilises DFT to simulate chemical reactions and predict properties of atoms, molecules, clusters, surfaces and other materials in all three phases of matter. Some of DMol^3 capabilities include; *geometry optimization; transition-state search and optimization*, enabling geometry stabilisation by bringing the energy of the structure to a stationary point; and *molecular dynamics*, which permits the simulation of atom motion as a function of time taking account temperature effects. DMol^3 also performs numerous calculations such as; *total and single-point energy*, which is generally negative and corresponding to a bound state; *elastic constants*, providing mechanical properties of a substance by an elastic constants tensor calculated from energies corresponding to an applying finite displacement distortion; *reaction kinetics*, estimated from the transition state theory; and *electron transport*, which enables the calculation of electron transmission or currents.*(*BIOVIA Materials Studio, 2019).

CHAPTER FOUR

MATERIALS AND METHODS

This chapter outlines the equipment, software and chemicals employed in this study and details the stepwise approaches and protocols used; to develop, optimise and test the two immunosensors for tau protein detection. Furthermore, all methodologies relating to the accompanying computational analysis are also detailed here.

4.1. EXPERIMENTAL

4.1.1. Reagents and chemicals

All reagents used were of analytical grade and prepared in deionised water, unless otherwise stated. Sodium dihydrogen phosphate (NaH_2PO_4), disodium hydrogen phosphate ($Na_2HPO_4.7H_2O$), sodium hydroxide (NaOH), potassium chloride (KCl), potassium dihydrogen phosphate (KH_2PO_4), sodium hydrogen phosphate (Na_2HPO_4), sodium chloride (NaCl), potassium ferrocyanide ($K_4[Fe(CN)_6]$) and potassium ferricyanide ($K_3[Fe(CN)_6]$), Tris(hydroxymethyl)aminomethane ($NH_2C(CH_2OH)_3$), were purchased from were supplied by Capital Lab Supplies (Durban, SA). Silver nitrate ($AgNO_3$), sodium borohydride ($NaBH_4$), trisodium citrate ($Na_3C_6H_5O_7$), chloroauric acid ($HAuCl_4$), sodium hydroxide (NaOH), ammonium chloride (NH_4Cl), graphene oxide ($C_xO_yH_z$), anti-tau antibody, produced in rabbit (polyclonal), tau-441 (recombinant) and N-Hydroxysuccinimide ($C_4H_5NO_3$) were purchased from Sigma Aldrich (Durban, SA).

4.1.2. Preparation of working solutions

(i) Preparation of phosphate buffer solution

300 mL of deionised water was placed into a 500 mL volumetric flask, to this 1.6970g of Sodium dihygrogen phosphate (NaH_2PO_4) and 10.1045g disodium hydrogen phosphate ($Na_2HPO_4.7H_2O$) was added. After the dissolution of the salts, the flask was made to make using deionised water to produce a 0.1 M phosphate buffer solution. The pH of the buffer was

then adjusted to its desired pH, using either 0.01 M, NaOH or HCl solutions. The buffer solutions were then stored at 4°C in a refrigerator and used for a maximum period of two weeks.

(ii) Preparation of PBS buffer solution

300 mL of deionised water was placed into a 500 mL volumetric flask, to this 4g of sodium chloride (NaCl), 0.1g potassium chloride (KCl), 0.72g disodium hydrogen phosphate (Na_2HPO_4) and 0.12g potassium dihydrogen phosphate (KH_2PO_4), was added. After the dissolution of the salts, the flask was made to make using deionised water to produce a 0.01 M PBS buffer solution. The pH of the buffer was then adjusted to its desired pH, using either 0.01 M, NaOH or HCl solutions. The buffer solutions were then stored at 4°C in a refrigerator and used for a maximum period of two weeks.

(iii) Preparation of Tris-HCl buffer

1.2114g of Tris(hydroxymethyl)aminomethane ($NH_2C(CH_2OH)_3$) salt was weighed and dissolved in 200 mL of deionised water, the pH of the solution was adjusted using concentrated HCl (32%) to a pH of 7.4.

(iv) Preparation of $[Fe(CN)_6]^{3-/4-}$ redox probe

The $[Fe(CN)_6]^{3-/4-}$ redox probe was prepared by adding 0.8231g of potassium ferricyanide ($K_3[Fe(CN)_6]$) and 1.0560g potassium ferrocyanide ($K_4[Fe(CN)_6]$) into a 500 mL volumetric flask, the salts were then dissolved and made to mark with 0.01M PBS buffer, pH 7.

(v) Preparation of anti-tau antibody solutions

Using a micro-pipette an appropriate amount of the 1mg/mL (1000 ppm) liquid solution of polyclonal anti-tau antibody was diluted accordingly with ultra-pure deionised water to produce anti-tau antibody solutions ranging from 1-10 ppm.

(vi) Preparation of tau protein standard solutions

The 50 µg lyophilized powder of tau protein was made to a 100 ppm solution by the addition of 50 µL of ultra-pure deionised water. 25 µL of the 100 ppm tau protein stock standard was then added to a 5 mL volumetric flask then made to mark with ultra-pure deionised water, to produce a 5 ppm standard solution of tau. This 5 ppm tau solution was then used to make the all subsequent standards solutions of varying concentration.

(vii) Preparation of NHS binding agent

0.0575g of N-Hydroxysuccinimide ($C_4H_5NO_3$) salt was added to a 10 mL volumetric flask, then was dissolved and the flask made to mark using deionised water, to produce a 0.05 M NHS binding agent solution.

4.1.3. Synthesis of gold and silver nanoparticles

(i) A 50 mL solution of 2.5mM trisodium citrate ($Na_3C_6H_5O_7$) combined with 50 mL of 0.5mM chloroauric acid ($HAuCl_4$) solution. This resulting mixture was then cooled and then was reduced by the addition of 1 mL of 0.1M sodium borohydride ($NaBH_4$) under rapid stirring in an ice bath, to produce citrate capped gold nanoparticles. (Calzolai et al., 2011)

(ii) The green synthesis of silver nanoparticles was achieved by the chemical reduction of silver nitrate ($AgNO_3$) by an extract of patty-pan squash (*Cucurbita pepo var. ovifera*) (Figure 4.1). Methodologies were adapted from (Gonnelli et al., 2015) and (Roy et al., 2015).

Figure 4. 1. Image of patty-pan squash (*Cucurbita pepo var. ovifera*)

(I) Preparation of patty-pan squash (*Cucurbita pepo var. ovifera*) extract

200g of a mixture of yellow and green patty-pans were washed with deionised water, then cut into small pieces. The cut pieces were then blending with 200 mL of deionised water using an electric hand blender. The mixture was then heated to about 70 – 80^{0}C for 10 minutes. After cooling, the mixture was then separated into four centrifuge vials and centrifuged at 5000 rpm. The supernatant was then collected, combined and then filtered through a Whatman filter paper no.1. The filtrate was then collected and stored at 4^{o}C in a refrigerator for further use.

(II) Production of silver nanoparticles

10 mL of solution of $AgNO_3$ was added to varying volumes of the prepared patty-pan extract respectively, followed by mixing them for 5 minutes using a magnetic stirrer. The resulting mixture was then incubated overnight at room temperature. To obtain high yielding nanoparticles, the effect of both; $AgNO_3$ concentration and extract volume was tested as shown in Table 4.1.

Table 4. 1. Concentration of $AgNO_3$ and volumes of patty-pan extract used to investigate optimum conditions for Ag nanoparticle formation.

Concentration of $AgNO_3$ (mM)	**Volume of patty-pan extract (mL)**
5	1
	2
	0.5
10	1
	2
	0.5

4.1.4. Electrochemical methods

A 797 VA Computrace instrument from Metrohm (Herisau, Switzerland) was employed for voltammetric measurements, using a 3-electrode system in an electrochemical cell. The cell was composed of; a rotating disk electrode working electrode with a 3 mm diameter gold surface; a platinum wire as the counter electrode and Ag/AgCl (saturated AgCl, 3 M KCl) as a reference electrode. The instrument was used in three different modes, i.e. cyclic voltammetry (CV), differential pulse voltammetry (DPV) and square-wave voltammetry (SWV). All the solutions analysed, were first purged with purified nitrogen gas for a specified amount of time and occurred at room temperature.

The phosphate and PBS buffers, together with all working solutions were prepared using deionized water obtained from a water purification system, AquaMax ™ Basic360 (Trilab, South Africa). All necessary pH adjustments of buffer solutions were carried out using 781 pH/ion meter coupled with an 801 stirrer (Metrohm, Herisau, Switzerland).

4.1.5. Characterisation methods

Optical studies of the synthesised gold and silver nanoparticles involved obtaining the UV-Visible spectra using a VARIAN Cary 50 spectrophotometer, in the EMR range of 200 to 800nm. Size and morphological studies involved Transmission Electron Microscopy (TEM) using JEM-2100, 200 kV Electron Microscope (JEOL Ltd.), equipped with a LaB_6 electron gun capable of TEM resolution as high as 0.19 nm. Further size related studies were conducted using Field-flow fractionation (FFF), the POSTNOVA, Asymmetric Flow FFF (AF4) and CF2000 Centrifugal systems**,** coupled with UV, DLS and MALS detectors.

I. UV-Visible spectroscopy

The optical characteristics of both the synthesised gold and silver nanoparticles were examined using the VARIAN Cary 50 spectrophotometer. The analysis was performed by placing the sample in a quartz cell of 10 mm path length and scanning in the range of 200 – 800 nm using a single beam mode.

II. Transmission electron microscopy (TEM)

JEM-2100, 200 kV Electron Microscope (JEOL Ltd.) was used to analyse the size, distribution and morphology of the nanoparticles and nanocomposites. The nanoparticles (liquid) were diluted to a volume of 50% using ethanol, followed by sonication for 30 minutes. A supporting carbon film was then immersed in the sample solution, the film was allowed to dry at room temperature which was then placed into the microscope for analysis.

III. Field flow fractionation (FFF)

AF4 system (AF2000 Postnova Analytics, Germany), containing a 29 cm channel and 10 kDa regenerated cellulose membrane, was employed for studying the nanoparticle size and distribution. The AF4 system was coupled to both, Postnova PN3621 Multi-Angle Light Scattering Detector (MALS) (21 angles) and PN3211 UV detector systems. Samples were first sonicated for 15 minutes before injecting 10 µL into the system via the injection valve. The separation of the sample was achieved by a cross flow, generated inside in channel. NovaChem Surfactant 100, of a specified concentration, was used as an eluent for this study. Table 4.2. States all the necessary parameters used for the analysis of AuNPs and AgNPs. Prior to sample analysis the instrument was calibrated using latex standards to test the efficiency of the detectors.

4.1.6. Fabrication of immunosensors

(i) Cleaning of Au rotating disk electrode (Au RDE)

The electrodes were first cleaned chemically, in which the electrodes were cleaned with piranha solution (H_2SO_4/H_2O_2, 4:1, v/v) for 5 minutes, followed by rinsing with deionised water. The electrodes were then polished with alumina slurry and were then sonicated in deionised water to remove leftover alumina. Finally electrochemical cleaning of the electrodes were performed by running cyclic voltammetry, first in 0.5M KOH in a potential range of –2 to 0 V and secondly in 0.5M H_2SO_4 in a potential range of 0 to 1.5 V.

4.1.6.1. Sensor 1 – AuE/AuNPs/Anti-tau antibody

5 µL of AuNPs was cast onto the Au working electrode, this was then dried for 15 min at 30^0C in an oven. After cooling for 30 min at room temperature, 5 µL of N-Hydroxysuccinimide ($C_4H_5NO_3$) binder was added to the modified surface. 5 µL of the anti-tau antibody was then added and was left to dry in a refrigerator overnight. For tau protein analysis, 5 µL of tau protein standard was added onto the fabricated sensor, then allowed to dry at room temperature for 3 hours.

4.1.6.2. Sensor 2 – AuE/GO/AgNPs/Anti-tau antibody

2 µL of 100 ppm GO was places onto the surface of the Au working electrode, so to cover the whole surface. The electrode was then dried in an oven at 30^0C for 15 min. after cooling for a period of 10 min at room temperature, 5 µL of AgNPs was added to the AuE/GO surface and the electrode was further dried at 30^0C for 15 min. After cooling for 30 min at room temperature, 5 µL of N-Hydroxysuccinimide ($C_4H_5NO_3$) binder was added to the modified surface. 5 µL of anti-tau antibody was then added and was left to dry in a refrigerator overnight. 5 µL of tau protein standard was added onto the fabricated sensor, then allowed to dry at room temperature for 3 hours.

For tau protein analysis, both sensors were incubated with 50 nM $Cu(ClO_4)_2$ solution in Tris buffer for 30 min at room temperature. The sensors were finally rinsed with Tris buffer followed by rinsing with de-ionised water (Martic et al., 2013). Methodologies for the immobilisation of anti tau antibodies were adapted from (Esteves-Villanueva and Martic-Milne, 2016, Esteves-Villanueva et al., 2014).

4.1.7. Procedure for the electrochemical measurements with the fabricated sensors

4.1.7.1. Cyclic voltammetry

I. A $[Fe(CN)_6]^{3-/4-}$ redox probe was employed to monitor the effect of each electrode modification step on the working electrode surface for sensor 1. Cyclic voltammograms were obtained at a scan rate of 0.1 $V.s^{-1}$ in a 5mM $[Fe(CN)_6]^{3-/4-}$ redox probe solution between -1 V and +1 V potential range. For sensor 2, cyclic voltammograms for the

monitoring of each modification step, were obtained at a scan rate of 0.1 $V.s^{-1}$ in 10 mM phosphate buffer (Table 4.2).

Table 4. 2. Step wise electrode modification for sensor 1 and 2.

Sensor 1	**Sensor 2**
Bare AuE	AuE/GO
AuE/AuNPs	AuE/GO/AgNPs/NHS
AuE/AuNPs/NHS/Anti-tau antibody	AuE/GO/AgNPs/NHS/Anti-tau antibody

II. For optimisation studies:

a. The AuE electrode was modified according to methodologies described in 4.1.5.2 and 4.1.5.3 respectively. The concentration of anti-tau antibody was first optimised by varying its concentration and observing the highest current peak produced for tau protein detection. Previous literature suggests that the concentration of anti-tau antibody should be higher than the concentration of tau protein to avoid the possibility of becoming a rate limited component of the system (Dai et al., 2017). Concentrations of anti-tau antibody investigated, ranged from 1-5 ppm.

b. For pH studies, the optimised concentration anti-tau antibody was used. Tau protein concentration was kept constant at 20 nM, the scan rate used was 0.1 $V.s^{-1}$ and the deposition time of 60 sec. pH range of 6.0, 6.5, 7.0, 7.5, and 8.0 was invested for both sensors.

c. Optimisation of scan rate was investigated in a range of 0.025 $V.s^{-1}$ to 0.125 $V.s^{-1}$ for both sensors with increments of 0.025. The other parameters, i.e. deposition time (60 sec) and pH (optimised) was kept constant.

d. Optimisation of deposition was subsequently investigated in the range of 50 to 90 seconds for sensor 1 and a range of 40 to 120 seconds for sensor 2. The scan

rate and pH used was that of the optimised values obtained from their respective optimisation studies.

III. To test the signal amplification strategies employed in this study, Table 4.3, indicates the stepwise approach used to improve the detection of tau protein. Both electrodes where modified according to methods described in 4.1.5.2 and 4.1.5.3. Cyclic voltammograms were then obtained at optimised pH, scan rate and deposition time in 10 mM phosphate buffer. The concentration of tau protein was set as 20 nM with the anti-tau antibody concentration set according to the optimum results obtained from the study described in 4.1.6.1. (II, b).

Table 4. 3 Analysis of tau protein at each step of electrode modification

Sensor	**Modified sensor**
1	Bare AuE/Tau protein
	AuE/AuNPs/Tau protein
	AuE/AuNPs/NHS/Anti tau/Tau protein
2	AuE/GO/Tau protein
	AuE/GO/AgNPs/ Tau protein
	AuE/GO/AgNPs/NHS/Anti-tau antibody/Tau protein

4.1.8. Quantitative studies

After the qualitative studies described above, quantitative techniques i.e. Differential pulse voltammetry (DPV) and Square wave voltammetry (SWV) were employed to establish calibration curves for each of the developed immunosensors. The same procedures described in 4.1.5.2 and 4.1.5.3 for the fabrication of the two immunosensors was used, with the optimised electrochemical parameters and antibody concentration. The concentration of tau protein was varied. Voltammograms were obtained in 10 nM phosphate buffer using a copper (II) redox probe (50 nM $Cu(ClO_4)_2$ solution). Differential pulse voltammetry and Square wave voltammetry with concentrations of tau (5, 10, 15, 20, 30 nM) was used to establish a calibration curve for sensor 1. For sensor 2, the concentrations of tau included 2, 4, 6, 8, 10 and 12 nM.

4.2. COMPUTATIONAL

4.2.1 Computational adsorption studies

The structure of N-Hydroxysuccinimide (NHS) was constructed using the drawing utilities of the Material Studio 2016 (MS, http://accelrys.com/products/collaborative-science/biovia-materials-studio/). The structure of NHS was optimized using the DFT – based techniques implemented in the DMol3 module (Delley, 2000) of the MS on the basis of B3LYP functional theory. Furthermore, the characteristic structures of gold electrode surface, citrate doped AuNPs and AgNPs/GO were constructed using the utilities present in "Build module" of the MS. These generated structure were placed on each other in order to construct the layer-by-layer electrode surface. The NHS and Anti-Tau was adsorbed onto the layered structures separately using the "Adsorption locator" module of the MS and the corresponding outputs were generated in the form of total and adsorption energies.

4.2.2 Molecular docking

The optimized structure of NHS and 1-Ethyl-3-(3-dimethylaminopropyl)carbodiimide EDC were docked against anti-Tau protein using the AutoDock 4 (Morris et al., 2009) package. The AutoDock 4 perform the prediction of the bound conformation on the basis of the free energy based empirical force field coupled with Lamarckian Genetic Algorithm (Morris et al., 2009). The grid box of dimensions 126 x 126 x 126 Å along the XYZ directions with grid spacing of 0.375 Å was established by using the AutoGrid module. In order to increase the efficiency, the parameters associated with Lamarckian genetic algorithm were set to the maximum efficiency value such as number of individuals in population was set to 250 while the maximum number of energy evaluations was set to "longer". As a result around 100 docked conformations were obtained which were grouped according to the RMSD tolerance of 2.0 Å. The generated conformations were rescored on the basis of the scoring function present in DrugScoreX server (Neudert and Klebe, 2011) and the conformation with the highest score was selected for the validation using Molecular Dynamics (MD) simulations.

4.2.3 MD simulations

These docked complex of NHS and anti-Tau protein was subjected to MD simulations using GROMACS (Pronk et al., 2013) (version 2018-2). The topology of anti-Tau protein was produced on the basis of GROMOS96 53a6 force field (Oostenbrink et al., 2004). Due to the unavailability of suitable force field parameters for drug-like molecules in the GROMACS package, the PRODRG server (Schuttelkopf and van Aalten, 2004) was used for the generation of the NHS topology and coordinate files. The partial charges were corrected by using DFT method of Gaussian which utilized the B3LYP 6-31G (d,p) basis set and CHELPG program (Frisch et al., 2009). After the successful topology generation, the system was immersed in SPC/E water model (Zielkiewicz, 2005) and subsequently neutralized by adding the counter ions. The neutralized system was energetically minimized by utilizing the steepest descent and conjugate gradient algorithms with a convergence criterion of 0.005 kcal mol^{-1}. In order to increase the reliability of the MD simulations the restrains were applied to the structure of the piperine before the equilibration phase.

The equilibration phase was carried out separately in NVT (constant volume) as well as NPT (constant pressure) ensemble conditions, each for 1 ns time scale. The temperature of the system was maintained at 300 K by using Berendsen weak coupling method in both ensemble conditions along with pressure which was maintained at 1 bar by utilizing Parrinello-Rahman barostat in constant pressure ensemble. The final MD simulations were produced on the basis of LINCS algorithm at 100 ns time scale. The knowledge extracted from the trajectory files were utilized for the analyses of each complex behaviour in the explicit water environment. The distances, H-bonds, Rg (Radius of Gyration) and RMSD (Root Mean Square Deviations) of NHS and anti-Tau protein complex were analysed.

CHAPTER FIVE

RESULTS AND DISCUSSION

In this section the results for the development of the two immunosensors are presented. The mechanisms, reactions and statistical evaluation of each step in developing and testing of the immunosensors are outlined and explained. The successes and shortcomings of the methodologies employed are also discussed in relation to the signal enhancement strategies, i.e. nanomaterials and antibody bio-receptors. Results are presented and discussed in relation to the synthesis of nanomaterials and its characterisation, the fabrication of immunosensors and finally the qualitative and quantitative analysis. Also outlined in this chapter is the accompanying computational studies which aims to supplement and correlate the experimental data.

5.1. EXPERIMENTAL STUDIES – SENSOR 1

5.1.1. Gold nanoparticles – Synthesis, reactions and mechanisms

AuNPs were synthesised using chemical reduction methodologies in a typical bottom-up approach of nanoparticle synthesis. Sodium borohydride and sodium citrate were employed as reducing and capping agents, respectively. This methodology is known to produce high yielding, stable AuNPs and the experiment itself is easy to conduct (Freitas de Freitas et al., 2018). Equation 5.1 shows the reduction of Au(III) by strong reducing agent, sodium borohydride, with the formation of Au nuclei resulting from the reduction and collisions between Au ions, atoms and clusters. Coalescence of the nuclei eventually lead to the formation of the nanoparticles.

$$HAuCl_4 + NaBH_4 \rightarrow Au^0 + B(OH)_3 + NaCl + H_3O^+ \qquad (5.1)$$

The formed AuNPs were stabilised by citrate ions via electrostatic interactions between anionic carboxylate groups of citrate and AuNPs, thus giving rise to an overall negative surface charge. Three possible forms of binding geometries between the carboxylate group and the AuNPs surface have been reported by Aljohani and co-workers, i.e. monodentate monocarboxylate binding (A), monocarboxylate bridging (B), and dicarboxylate bridging (C), as illustrated in Figure 5.1.

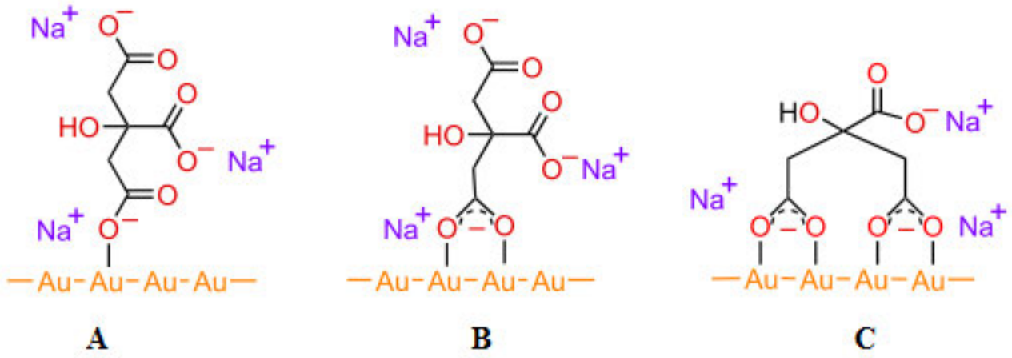

Figure 5. 1. Possible binding modes of carboxylate group and AuNPs (Aljohani et al., 2017)

5.1.2. Characterisation of AuNPs

5.1.2.1. UV-Visible spectroscopy

The obtained liquid AuNPs were visually red in colour, this owing to its surface plasmon resonance (SPR) properties. The wavelength for maximum absorbance was around 528 nm as illustrated in Figure 5.2. The results confirmed the presence of AuNPs as previous work indicate their absorption band around 500 – 600 nm.

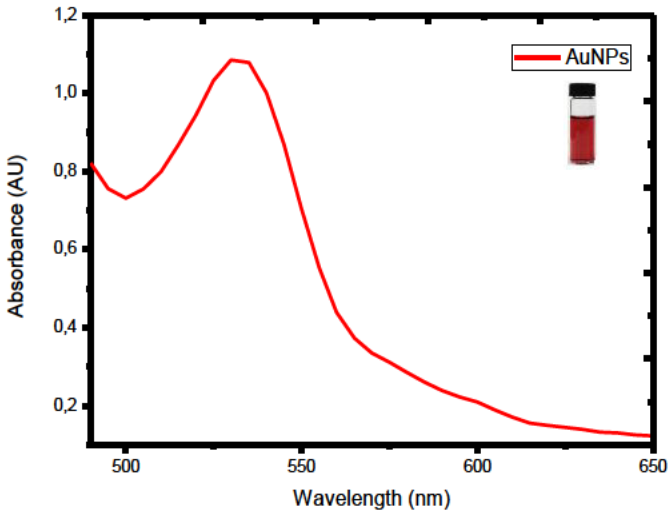

Figure 5. 2. UV-Visible absorption spectra for citrate capped AuNPs

5.1.2.2. TEM imaging

The structural properties of the AuNPs were characterized using high-resolution transmission electron microscopy (HRTEM). Figure 5.3 shows the TEM image obtained for the synthesised AuNPs. The image revealed that the nanoparticles have a spherical morphology. The nanoparticles can be seen to have good dispersion and display an absence of agglomeration, which is an indication of successful capping of the AuNPs by the citrate ions. Using ImageJ software, the size of the nanoparticles were determined to be approximately 8 nm in diameter (Figure 5.4).

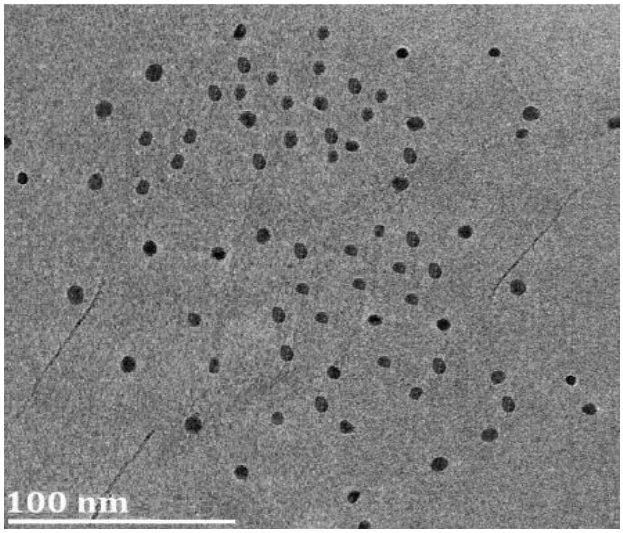

Figure 5. 3. HRTEM image of AuNPs

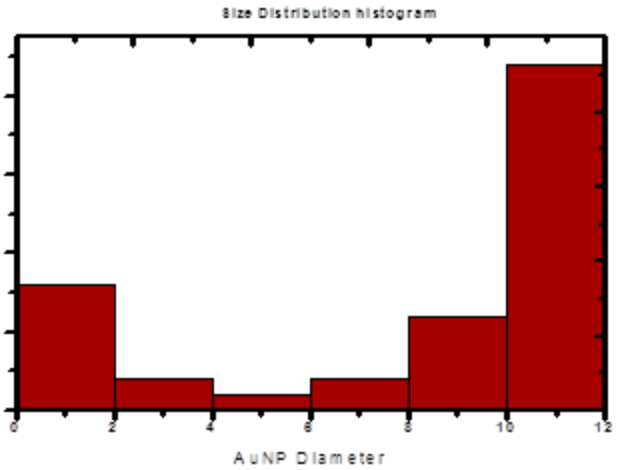

Figure 5. 4. AuNPs size distribution graph

5.1.2.3. Field flow fractionation – AF4

The field-flow fractionation technique is capable of separating AuNPs according to its sizes and hence provides key information relating to the size and distribution of the nanoparticles (Calzolai et al., 2011). Prior to the sample analysis, latex standards were used to calibrate the instrument and test the efficiency of the detectors. The baseline separation of latex mixture with particle sizes; 60 nm, 125 nm and 350 nm are displayed in Figure 5.5 below.

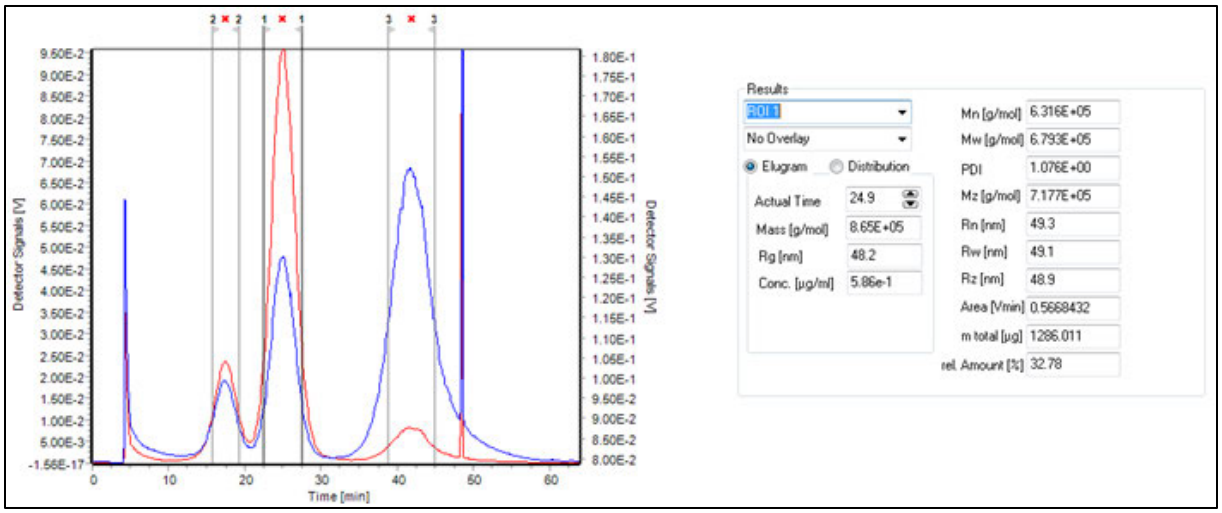

Figure 5. 5. Results for AF4 analysis of latex standards

The results for the AuNPs analysis, illustrated in Figure 5.6 below show distribution patterns of both molar mass (A) and radius (B). In asymmetric FFF, smaller particles are transported faster along the channel, therefore they elute before larger particles (Johann et al., 2009), as seen in the fractogram (B). The results indicated a radius of gyration (R_g) of 74.1 nm which translates to a hydrodynamic radius (R_h) of 95.6 nm calculated from Equation 5.2. The size measured using FFF reflects the gold nanoparticle together with its citrate coating, which is the reason why is the result is significantly larger than results obtained for TEM imaging that reflect only the inner, electron dense, Au core.

$$R_g = (3/5)^{1/2} R_h = 0.775 R_h \qquad (5.2)$$

.

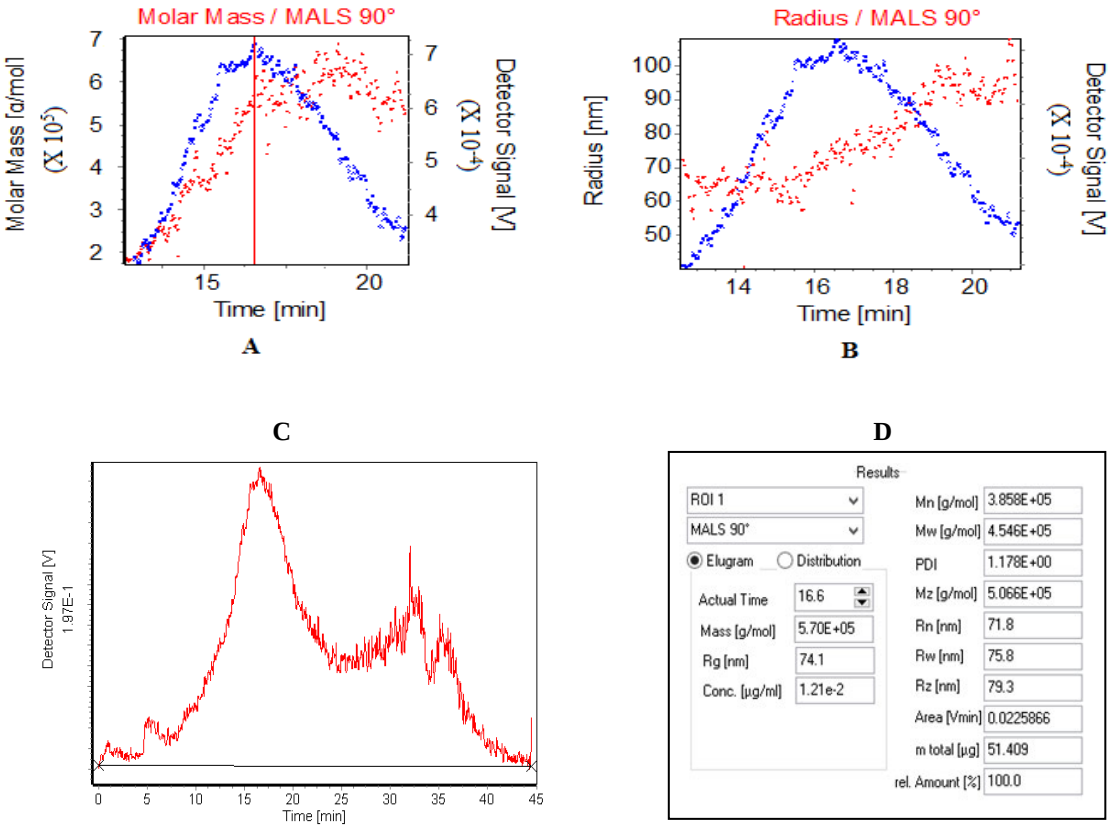

Figure 5. 6. AuNPs analysis data from FFF

5.1.3. Fabrication of Sensor 1 – AuE/AuNPs/EDC-NHS/Anti-tau antibody

Immobilisation of anti tau antibodies was achieved via the binding of its amine group to NHS ester groups. The lysine residues of antibodies contain amine groups present on the exterior which act a common anchoring points for attachments (Yu et al., 2014). Carboxylic acid groups present on the citrate ion that surrounds the AuNPs, reacts with 1-Ethyl-3-(3-dimethylaminopropyl)carbodiimide (EDC) to form an intermediate carboxylic ester, this in turn reacts with N-Hydroxysuccinimide (NHS) to form an NHS ester. The EDC/NHS served to activate the carboxyl group of the citrate, thus allowing for covalent attachment of the antibody. This reaction scheme is displayed in Figure 5.7.

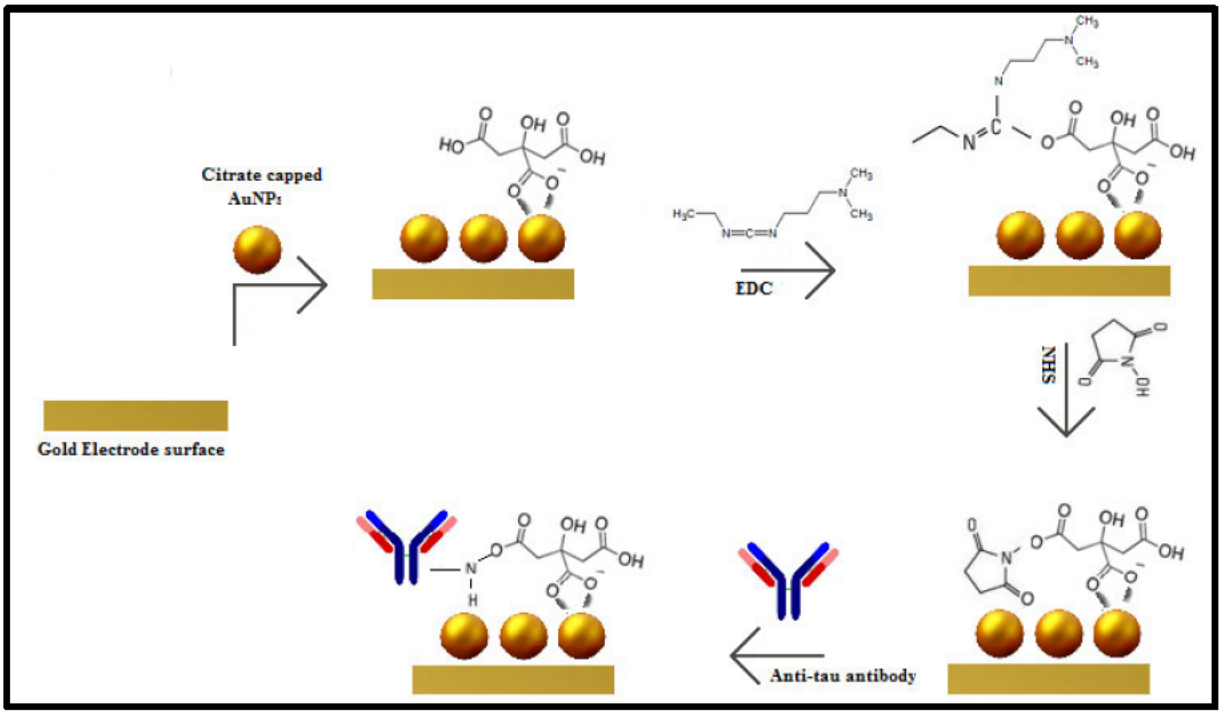

Figure 5. 7. Scheme representing the immobilisation of anti tau antibodies onto gold electrode surface, modified with gold nanoparticles

The stepwise modification was monitored by cyclic voltammetry, using a ferrocyanide/ferricyanide redox couple $[Fe(CN)_6]^{3-4-}$, as illustrated in Figure 5.8. The forward scan is represented by Equation 5.3, where the anodic current is due to Fe^{2+} been oxidised to Fe^{3+}. Equation 5.4, represents the reverse reaction in which the cathodic current is a result of the reduction of Fe^{3+} to Fe^{2+}. An anodic peak current of 2 μA is observed for the bare Au electrode. The current amplitude is then observed to be enhanced when the electrode surface has been modified with AuNPs, the current signal increases to 3.5 μA. This increase in current can be attributed to the conductive properties of AuNPs together with increased surface area for electron transfer to occur. An inverse effect is observed when the surface contains the immobilised antibody. This decrease in current is owing to the insulating nature of the antibody as it hinders electron transfer (Gomes-Filho et al., 2013). These observations thus confirms electrode surface modification.

$$[Fe(CN)_6]^{4-} \rightarrow [Fe(CN)_6]^{3-} + e \quad (5.3)$$

$$[Fe(CN)_6]^{3-} + e \rightarrow [Fe(CN)_6]^{4-} \quad (5.4)$$

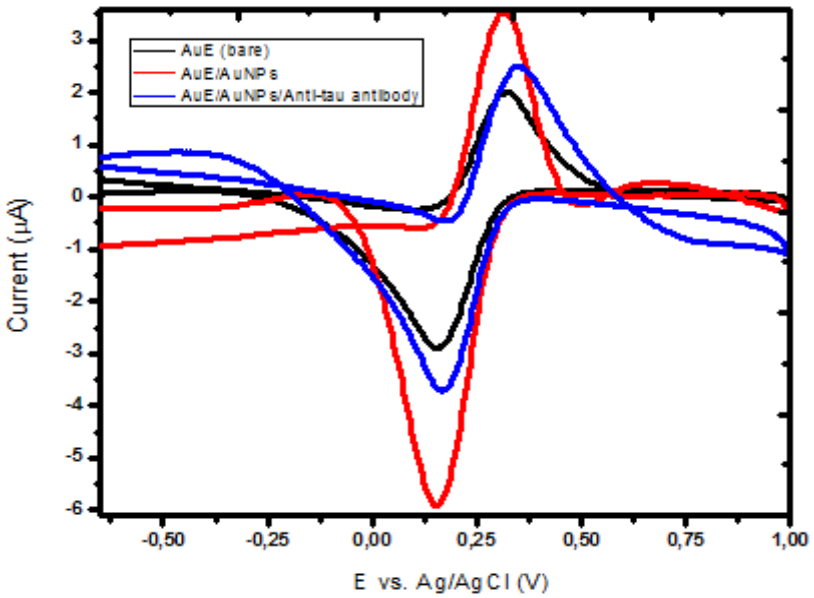

Figure 5. 8. Cyclic voltammogram of stepwise modification of gold electrode with AuNPs and anti-tau antibody immobilisation

5.1.4. Electrochemical studies – Sensor 1

The electrochemical signal produced in Figure 5.9 is due to the Cu(II)/Cu(I) redox probe that co-ordinates to tau protein, forming a tau/copper complex. The observed redox potentials are observed at 0.16 V for the forward reaction and 0.43 V for the reverse reaction, this owing to the oxidation of Cu(II) to Cu(I) and the reduction of Cu(I) to Cu(II), respectively. No signal was obtained for the blank measurements for both; bare AuE and modified electrode (AuE/AuNPs/Anti-tau antibodies).

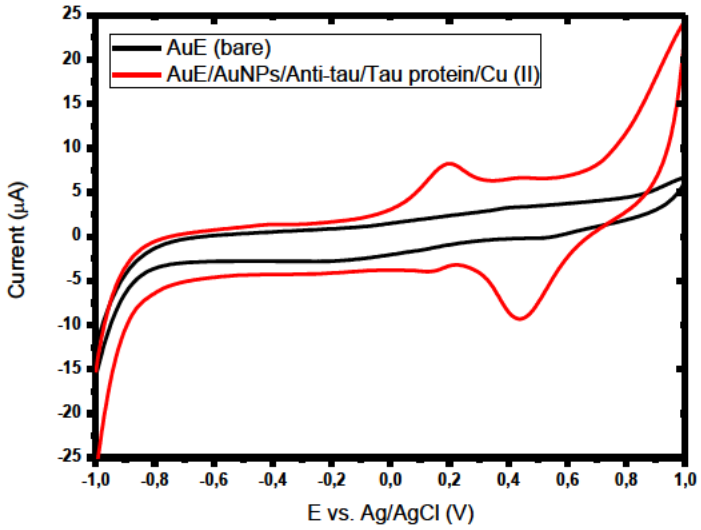

Figure 5. 9. Cyclic voltammogram showing the blank measurement of bare electrode in phosphate buffer (black) and signal produced on the addition of tau protein analyte and copper redox probe on a modified electrode surface (red)

5.1.4.1. Optimisation of parameters

I. Effects of pH

To the determine the optimum pH value for the detection of tau protein, cyclic voltammetry analysis was done in the pH range between 6 to 8 in phosphate buffer solution. The concentration level of tau protein was constant at 20 nM. pH values above 7 gave the least favourable current response with broad shaped oxidation peaks in comparison to values below 7 that produced higher peak currents with oxidation peaks that were more defined. The optimum current response was achieved at pH 7.0 as shown in Figure 5.10 and is the pH value at which all further experiments were conducted. This pH value is in keeping with literature which indicate strong antigen-antibody binding between pH 6.5 and 8. Extreme pH values tend to cause conformational change of the antibody (sigmaaldrich.com, 2019)

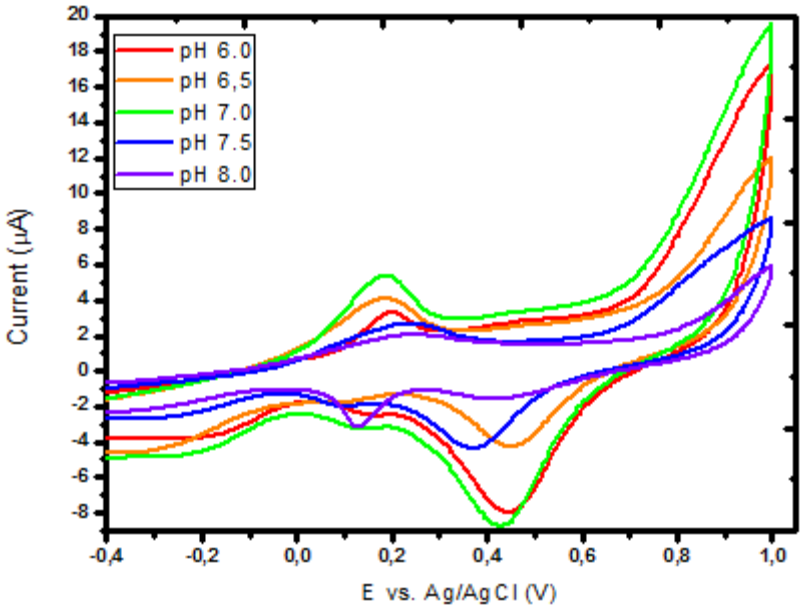

Figure 5. 10. Cyclic voltammogram of pH optimisation for sensor 1

II. Effect of scan rate

Figure 5.11 shows the cyclic voltammograms of 20 nM tau protein with varying scan rates, ranging from 0.025 Vs^{-1} to 0.125 Vs^{-1}. The anodic peak current is seen to increase proportionally with increase in scan rate. This is rationalised through the Cottrell equation (Equation 5.5) which relates current dependency on the rate at which the analyte diffuses to the electrode and the Randles-Sevcik equation (Equation 5.6) which describes how the peak current increases linearly with the increasing scan rate (Elgrishi et al., 2017). The linearity of the scan rate versus the oxidation peak current is confirmed by the regression equation, $y = 0.6313x + 1.329$ with a coefficient of $R^2 = 0.9865$. A rate of 0.125 Vs^{-1} was selected as the optimum.

$$I = \frac{nFA\sqrt{D}\,c}{\sqrt{\pi t}} \qquad (5.5)$$

$$\mathbf{i_p = 269n^{3/2}AD^{1/2}v^{1/2}C^b} \qquad (5.6)$$

.

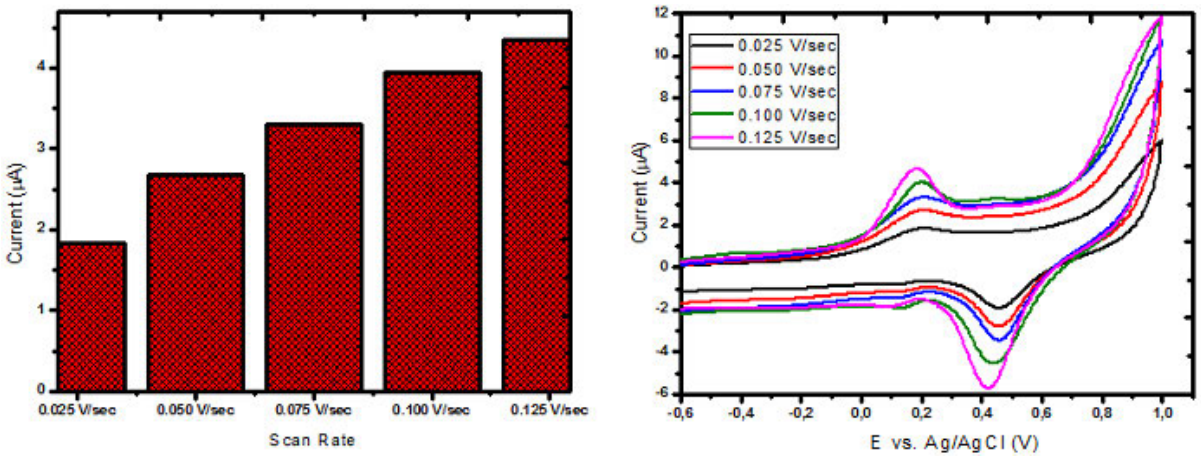

Figure 5. 11. Cyclic voltammogram of scan rates optimisation (right) and corresponding bar graph (left), for sensor 1

III. Effect of deposition time

The effects of deposition time on current response was investigated. Figure 5.12 shows that the aniodic current increases with increasing deposition time up, then begins to decrease when the deposition time exceeds 80 seconds. From the graphs it can be noted that more analyte is absorbed onto the surface of the electrode when as time increases but then begins to saturate the electrode sufrace preventing electron movement beyond the time of 80 seconds.

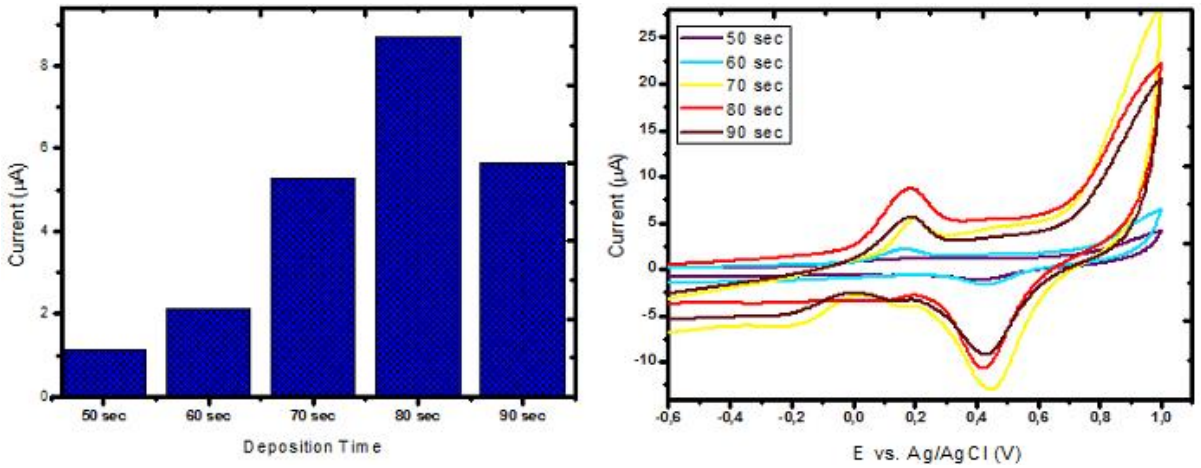

Figure 5. 12. Cyclic voltammogram of deposition time optimisation (right) and corresponding bar graph (left), for sensor 1

5.1.4.2. Effects of electrode modification on current response of tau protein analyte

Table 5.1 shows the effect of electrode modification on the current response. The addition of AuNPs is shown to significantly improve the signal for tau protein by 79.32 % compared to the use of a bare gold electrode. This is owing to the general properties of nanomaterials that serve to increase the electrode surface area, by increasing the number of sites for reactions to occur on the surface which then leads to higher current signals. In addition the larger surface are permits the immobilisation of larger biomolecules such as the tau protein and anti-tau antibodies used in this study (Wang et al., 2017a). The signal is further amplified with the addition of anti-tau antibodies onto the electrode surface, this together with lower standard deviation and % RSD values supports the idea of antibodies been used to enhance the selectivity for the tau protein analyte.

Table 5. 1. Results of signal response for analyte at each electrode surface modification step

Step	**Modified sensor layers**
1	Bare AuE/Tau protein
2	AuE/AuNPs/Tau protein
3	AuE/AuNPs/NHS/Anti tau/Tau protein

Electrode modification step	**Current / µA**			**Average current/ µA**	**Standard deviation**	**% RSD**	**% Current improvement**
1	3.19	2.93	3.59	3.24	0.27	8.34	-
2	6.21	5.84	5.38	5.81	0.34	5.84	79.32
3	7.37	6.73	6,96	7.02	0.26	3.77	20.83

5.1.4.3. Quantitative Analysis

The current signal was investigated as a function of tau protein concentration. DPV and SWV were employed as electrochemical techniques to establish calibration curves for tau protein detection using the developed immunosensor. The results for both DPV and SWV as seen in Figures, 5.13 and 5.17, show that the peak current increases with increase in tau proein concentration. In this study concentrations of tau protein (5, 10, 15, 20, 25, 30 nM) were added onto the electrode whilst keeping the concentration of copper solution constant. Measurements were carried out at pH 7 in phosphate buffer.

I. DPV

The calibration resulted in a linear curve with an R^2 value of 0,9890, indicating good linearity as seen in Figure 5.14. No observable trend could be noted in terms of standard error and standard deviation relating to calibration points, the standard residual plot reveals that all data points are well within ± 2 standard error and therefore indicates a good regression model. An LOD of 3.31 nM and LOQ 11.04 nM was calculated.

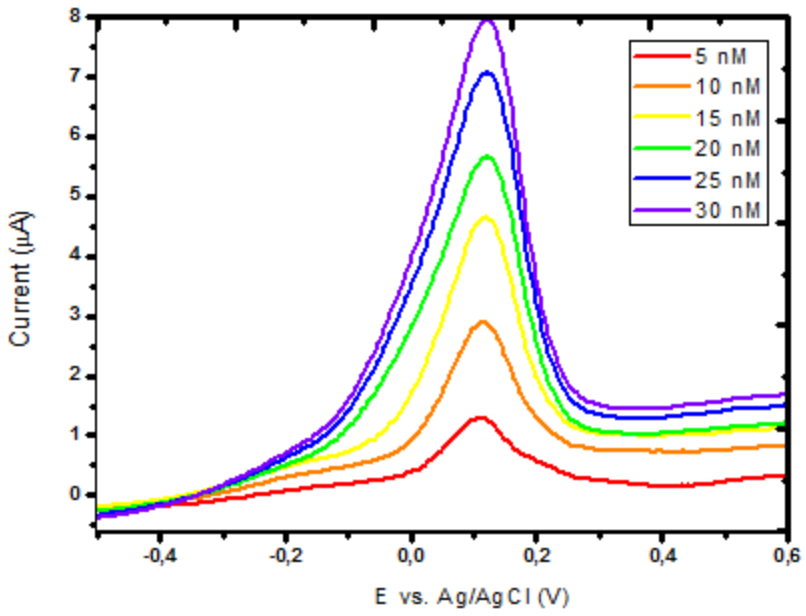

Figure 5. 13. Differential pulse voltammogram showing the immunosensor response for varying concentrations of tau protein

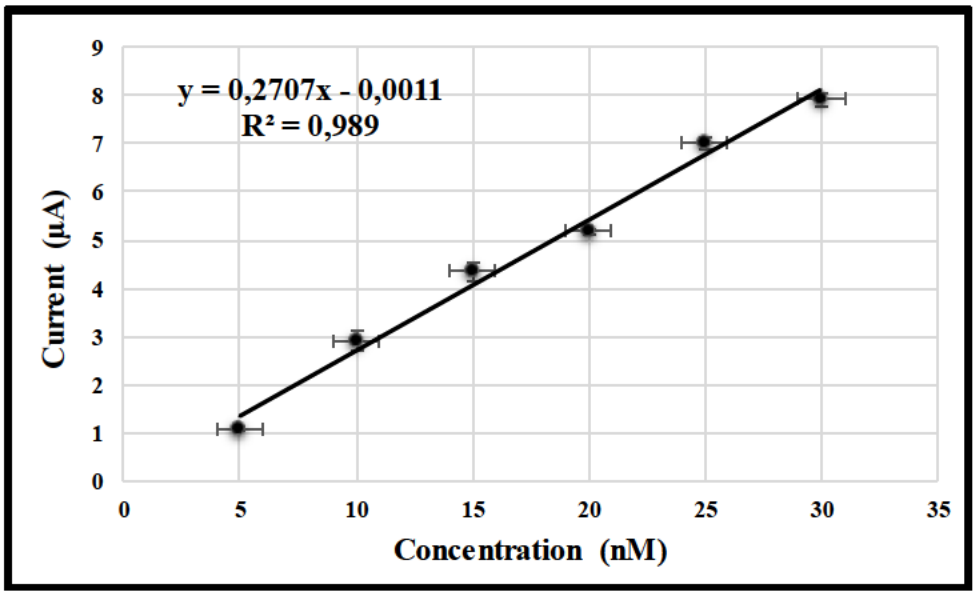

Figure 5. 14. Calibration curve with standard deviation error bars, showing the immunosensor response for tau protein, ranging between 5 and 35 nM concentration

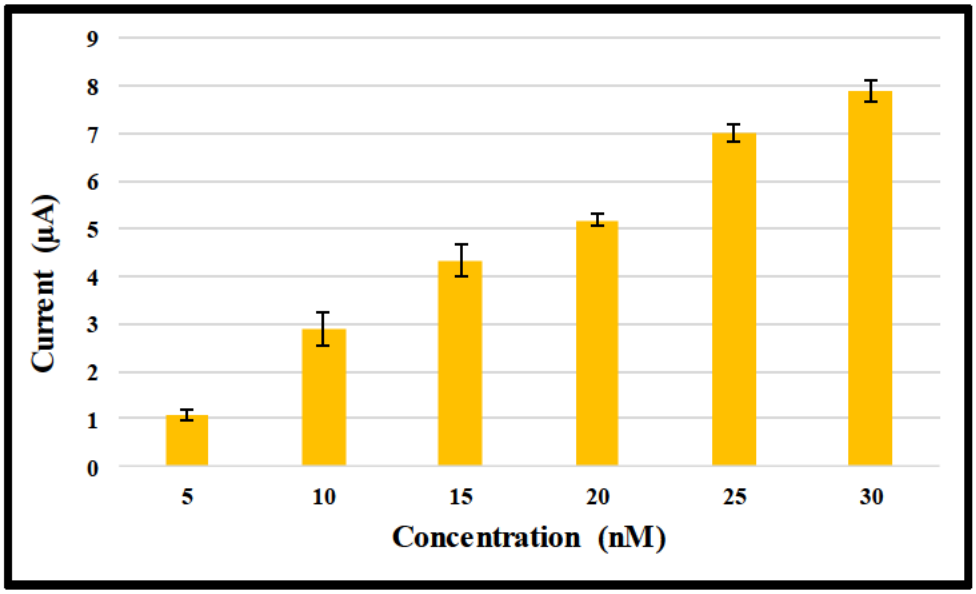

Figure 5. 15. Calibration bar graph with error bars for standard error, showing the immunosensor response for tau protein, ranging between 5 and 35 nM concentration

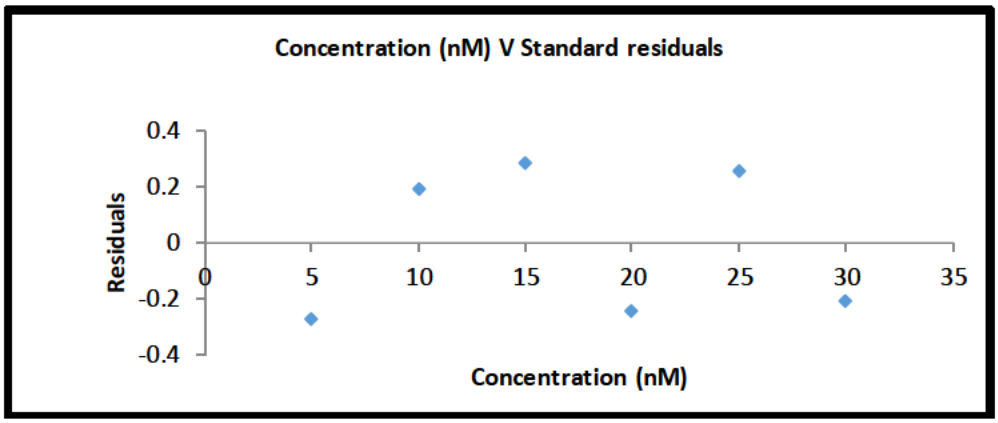

Figure 5. 16. Residual plot showing tau protein concentration against standard residuals, calculated from regression statistics

II. SWV

The calibration resulted in a linear curve with an R^2 value of 0,9722 as seen in Figure 5.18. Figures 5.19 and 5.20, shows the standard error and standard deviation of each data point, from this it can be noted that the values were relatevily low compared to that of the DPV results. Although there is an observable increase in peak current with increasing concentration of tau protein, it is noted that the current increments decrease with higher concentrations of tau protein. The standard residual plot reveals that all data points are well within ± 2 standard error and therefore indicates a good regression model. An LOD of 5.31 nM and LOQ 17.70 nM was calculated.

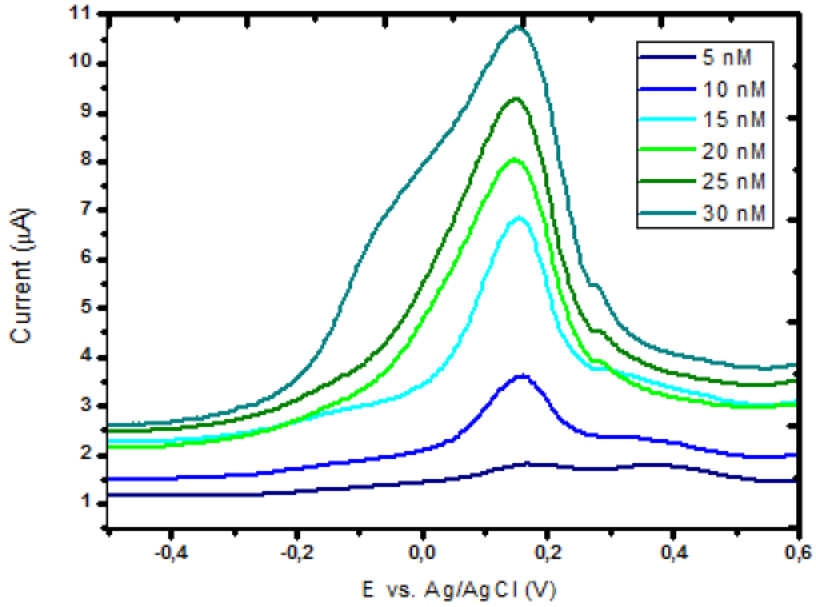

Figure 5. 17. Square wave voltammogram showing the immunosensor response for varying concentrations of tau protein

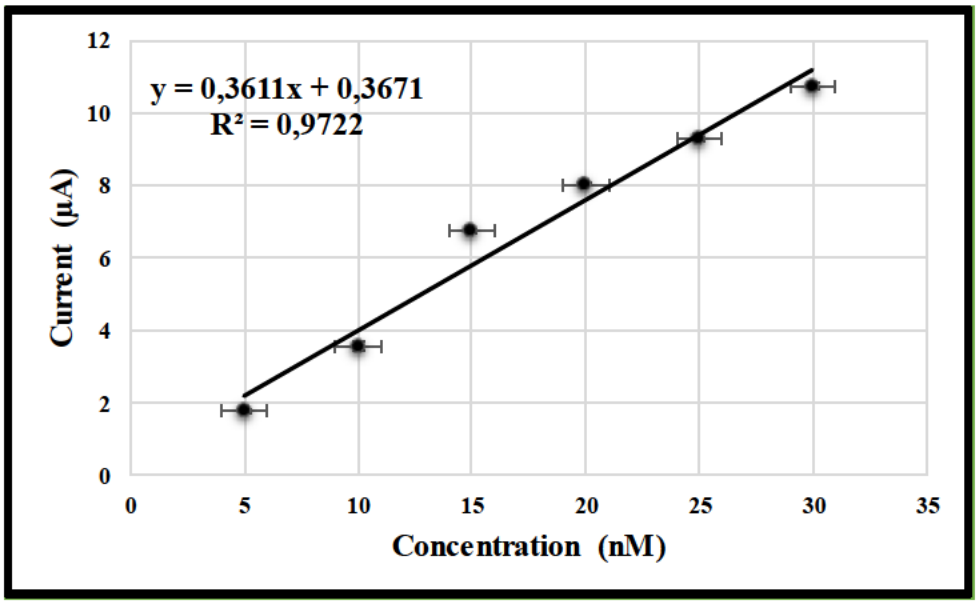

Figure 5. 18. Calibration curve with standard deviation error bars, showing the immunosensor response for tau protein, ranging between 5 and 30 nM concentration

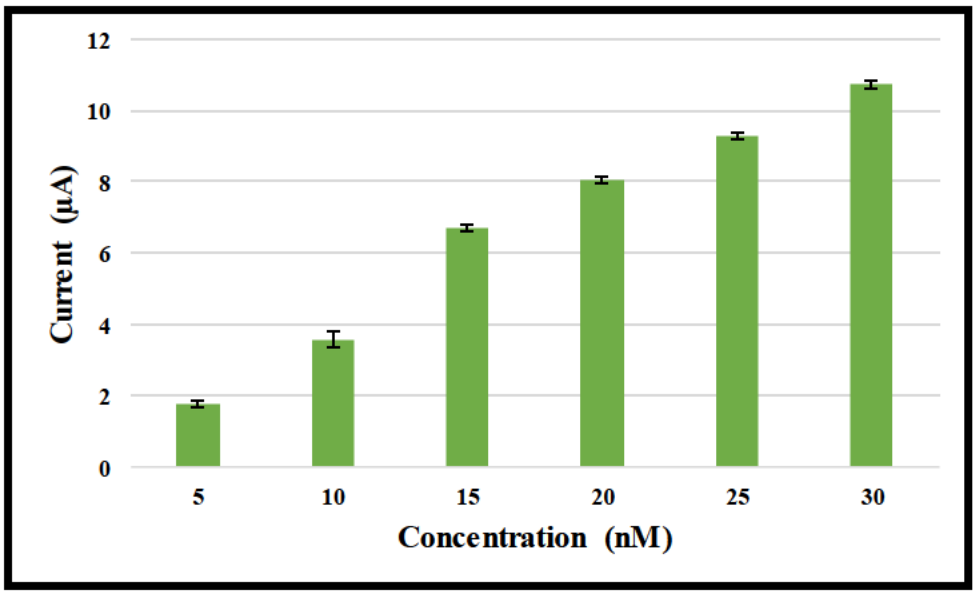

Figure 5. 19 Calibration bar graph with error bars for standard error, showing the immunosensor response for tau protein, ranging between 5 and 30 nM concentration

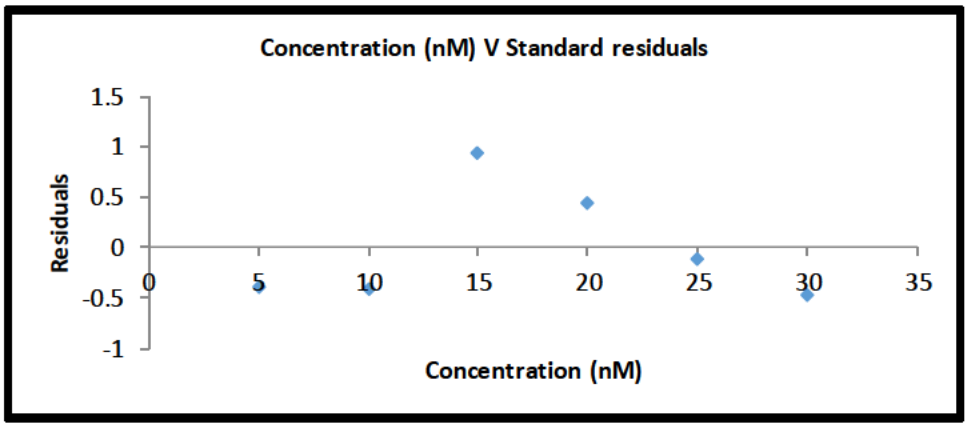

Figure 5. 20. Residual plot showing tau protein concentration against standard residuals, calculated from regression statistics

III. Tau protein recover studies

Table 5.2 and Table 5.3 shows the results for analysis of tau protein using the developed immunosensor and calculating the results from the established DPV and SWV calibration curves. The tau protein was prepared in PBS buffer, to simulate the pH and ionic composition of biological fluid. Three tau protein concentrations (5, 10, 20 nM) were used to test the lower, mid and upper levels of the calibration plot. The results for DPV yielded higher % recovery for all three concentrations of tau protein compared to SWV. % recovery was also higher for higher concentrations of tau protein. The differences in these recoveries between the two electrochemical methodologies is a result of the differences in detection limits. Both methods, however, indicate low standard deviations and standard error between replicate measurements. % RSD is also seen to decrease at higher concentration levels of tau protein. From these results, both methodologies seem to favour the detection of higher concentration levels of tau protein. This could be the result of the greater interaction between the tau protein and the anti-tau antibodies.

Table 5. 2. DPV Results for sample analysis

Sample	Concentration Added (nM)	Concentration Recovered (nM)	Mean	% Recovery	Standard error	Standard deviation	% RSD
1	5	3.71 4.10 3.62	3.81	76.24	0.15	0.26	6.76
2	10	8.31 8.86 9.24	8.78	87.79	0.19	0.33	3.71
3	20	19.14 19.28 19.59	19.34	96.6	0.13	0.23	1.19

Table 5. 3. SWV Results for sample analysis

Sample	Concentration Added (nM)	Concentration Recovered (nM)	Mean	% Recovery	Standard error	Standard deviation	% RSD
1	5	1.45 1.90 1.81	1.78	35.54	0.18	0.31	17.40
2	10	6.06 5.55 5.77	5.82	58.19	0.17	0.30	5.12
3	20	18.79 19.16 18.99	18.94	94.71	0.08	0.14	0.73

5.2. EXPERIMENTAL STUDIES – SENSOR 2

5.2.1. Silver nanoparticles - Synthesis, reactions and mechanisms

A green synthesis methodology was employed in the production of AgNPs using an extract of patty-pan squash (*Cucurbita pepo var. ovifera*). The main chemical constituents of patty-pan squash are: water (94.64%), total fibre (1.1%), total sugars (2.2%), protein (1.21g/100g), amino acid containing molecules (0.905g/100g), ion content (0.35g/100g), Vitamin C (0.02g/100g), fatty acids (saturated – 0,044g/100g) and fatty acids (unsaturated – 0.105g/100g) (USDA, 2019). The chemical components have the capabilities to reduce Ag salt to AgNPs and also have the ability to stabilise the formed nanoparticles. Various reports indicate that plant metabolites such as sugars, terpenoids, polyphenols alkaloids, phenolic acids and proteins have bio-reduction capabilities. Carbonyl groups of amino acids and proteins are known to play a role in the capping of nanoparticles due to their ability to, bind metal ions to form nanoparticles and act to prevent agglomeration, thereby stabilising the medium. Many of the extract components such as amino acids that contain varying groups such as; C=O, -NH2, -COOH, R−SH, and aromatic heterocyclic compounds like imidazole and indole, also have dual capability of been both reducing and stabilising agents (Chandra and Singh, 2016).

The largest chemical constituents of the patty pan extract, apart from water is its carbohydrate content, mainly in the form of monosaccharide reducing sugars, fructose and glucose which account for almost 2% of the total content. The open, linear form of these sugars allows for the interaction between its aldehyde group and a metal ion. Glucose, considered to be a stronger reducing agent than fructose, is known for its ability to reduce silver ions present in $AgNO_3$ into silver atoms and in turn be oxidized to gluconic acid as $AgNO_3$ itself is an oxidant. This oxidation of an aldehyde into a carboxyl group is reportedly due to nucleophilic addition of a free hydroxide group and leads to the synthesis of nanoparticles (Makarov et al., 2014). **Scheme 5.1** shows the possible mechanism involved in the formation of AgNPs by the glucose component of the extract.

Another possible mechanism of AgNPs synthesis by the use of glutamic acid, is illustrated in **Scheme 5.2**. Glutamic acid is a major amino acid present in patty pan vegetable and it has been reported that it has strong affinity for Ag+ ions (Chandra and Singh, 2018). The proposed mechanism shows the binding of glutamic acid to silver ions via its amino group.

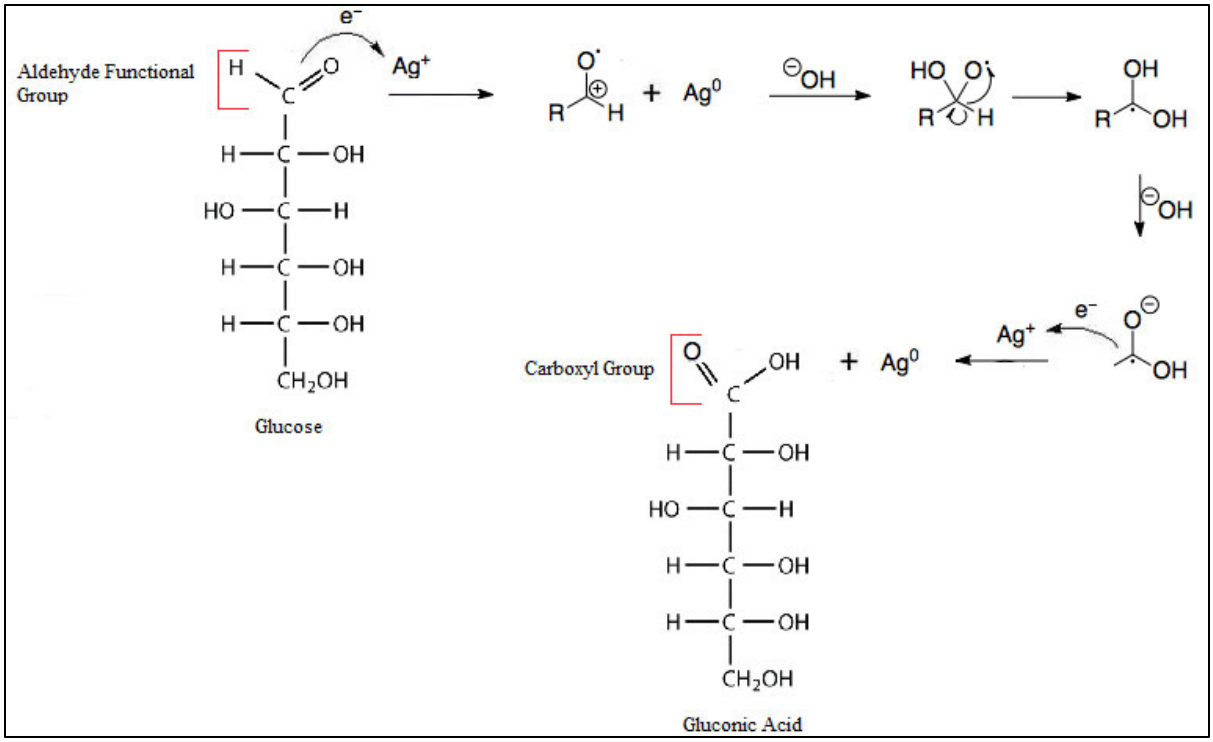

Scheme 5.1. Reduction of $AgNO_3$ to AgNPs using glucose

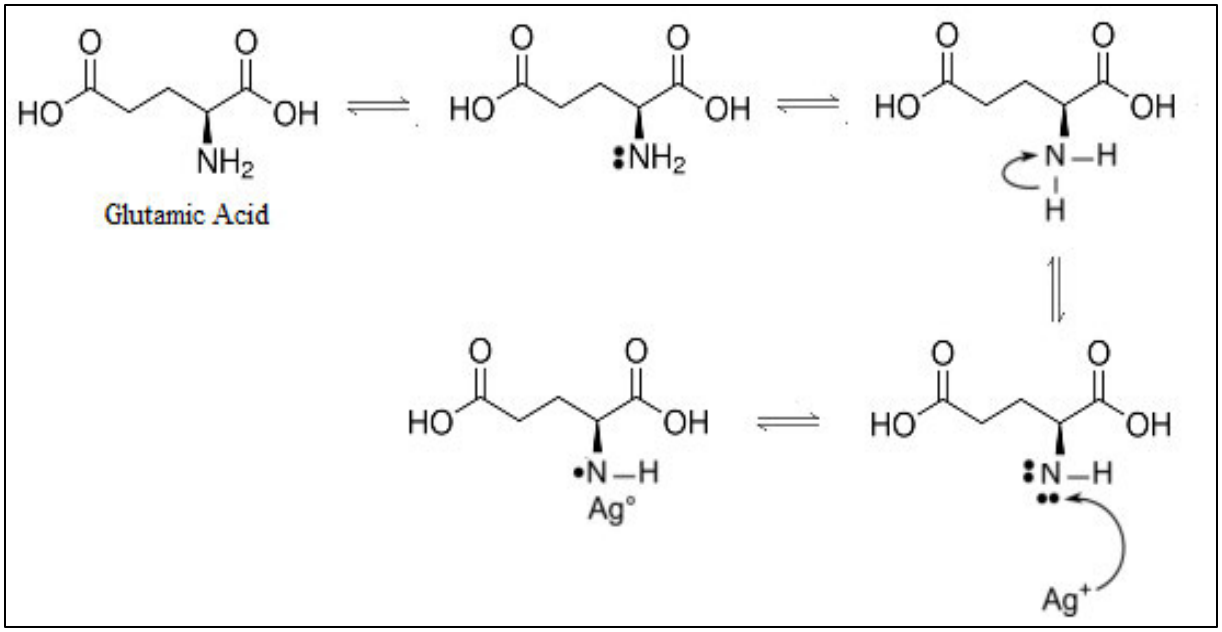

Scheme 5.2. Formation and stabilization of AgNPs with glutamic acid

5.2.2. Characterisation of AgNPs

5.2.2.1. UV-Visible spectroscopy

UV-Visible spectra reveals an increase in absorbance with increasing volumes of extract added to both 5 mM and 10 mM $AgNO_3$ solutions. The absorption peaks for 10 mM AgNO3 solutions were broad shaped in comparison to more narrow and defined peaks observed for 5 mM concentration of $AgNO_3$. The reduction of 5 mM AgNO3 also produced a higher absorbance reading across all corresponding extract volumes. The differences in band width is likely due the size distribution of the nanoparticles with a narrow peak indicating a more cohesive size distribution, whilst higher absorbance values can be attributed to higher concentrations of AgNPs. The observed λ_{max} is around 450 nm and thus confirms the formation of AgNPs as reported in literature (Lee and Jun, 2019).

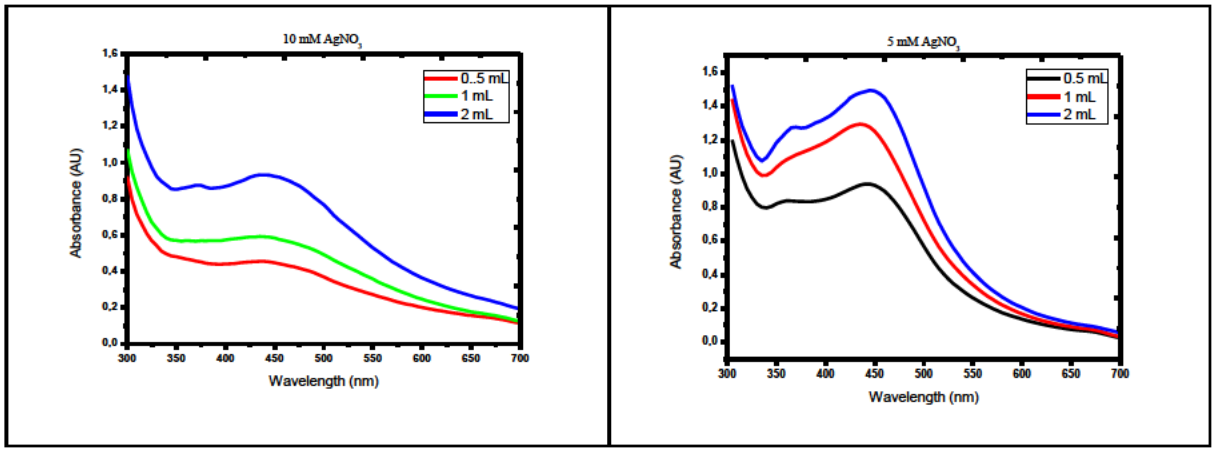

Figure 5. 21. UV-Visible spectra of AgNPs synthesised from varying concentration/volume ratios of extract

5.2.2.2. TEM

The nanoparticles synthesised are observed to be spherically shaped as seen in **Figure 5.22**. The calculated diameter was revealed to be approximately 9.5 nm. The size distribution indicated that a higher percentage of nanoparticles have diameters below the calculated mean. The nanoparticles are however, seen to have meagre dispersion which could be due to inadequate stabilisation by molecules groups present in the extract. It is also noted that some particles are much darker than others, which can be attributed to successful capping of the AgNPs. The inability to control volumes and concentrations of molecules present in the extract,

which act as reducing and stabilising agents lends to a downside of green methods. Graphene oxide was employed as a supporting material for the AgNPs, with the two nanomaterials been composited in equal ratios. It can also be seen in **Figure 5.22** that the AgNPs does interact with GO, with the AgNPs been concentrated on the edges of the pockets formed on the GO layer.

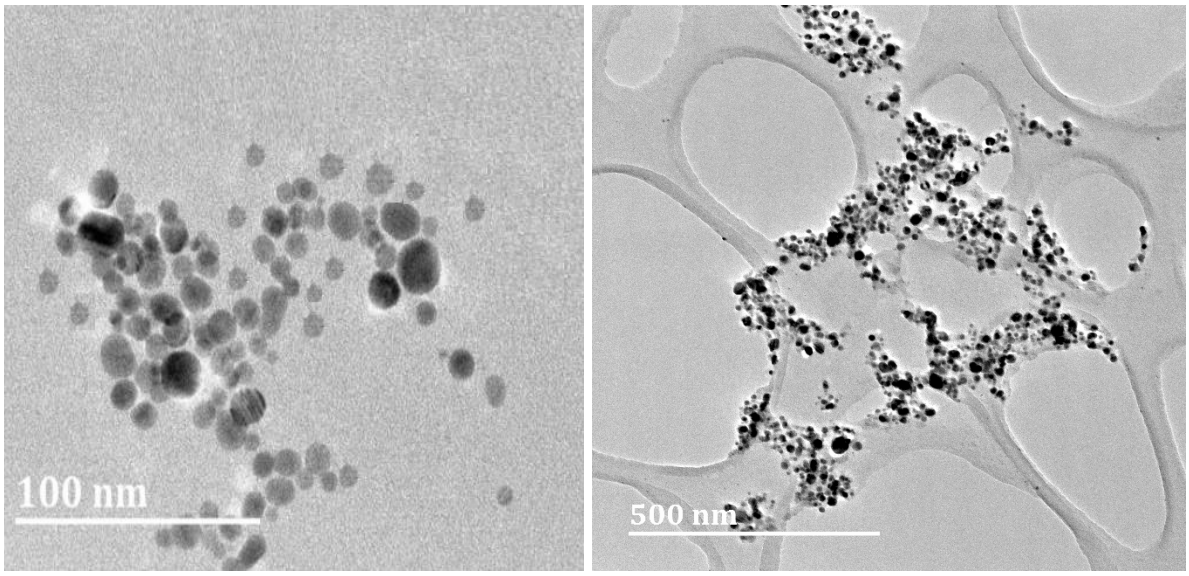

Figure 5. 22. TEM images of AgNPs (left) and AgNPs on graphene oxide (right)

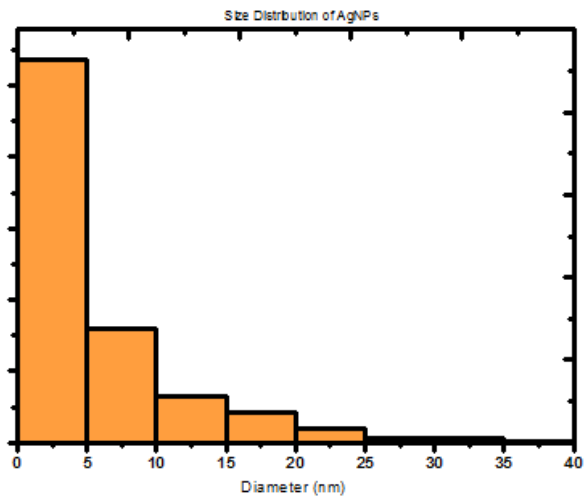

Figure 5. 23. AgNPs size distribution graph

5.2.2.3. Field flow fractionation – AF4

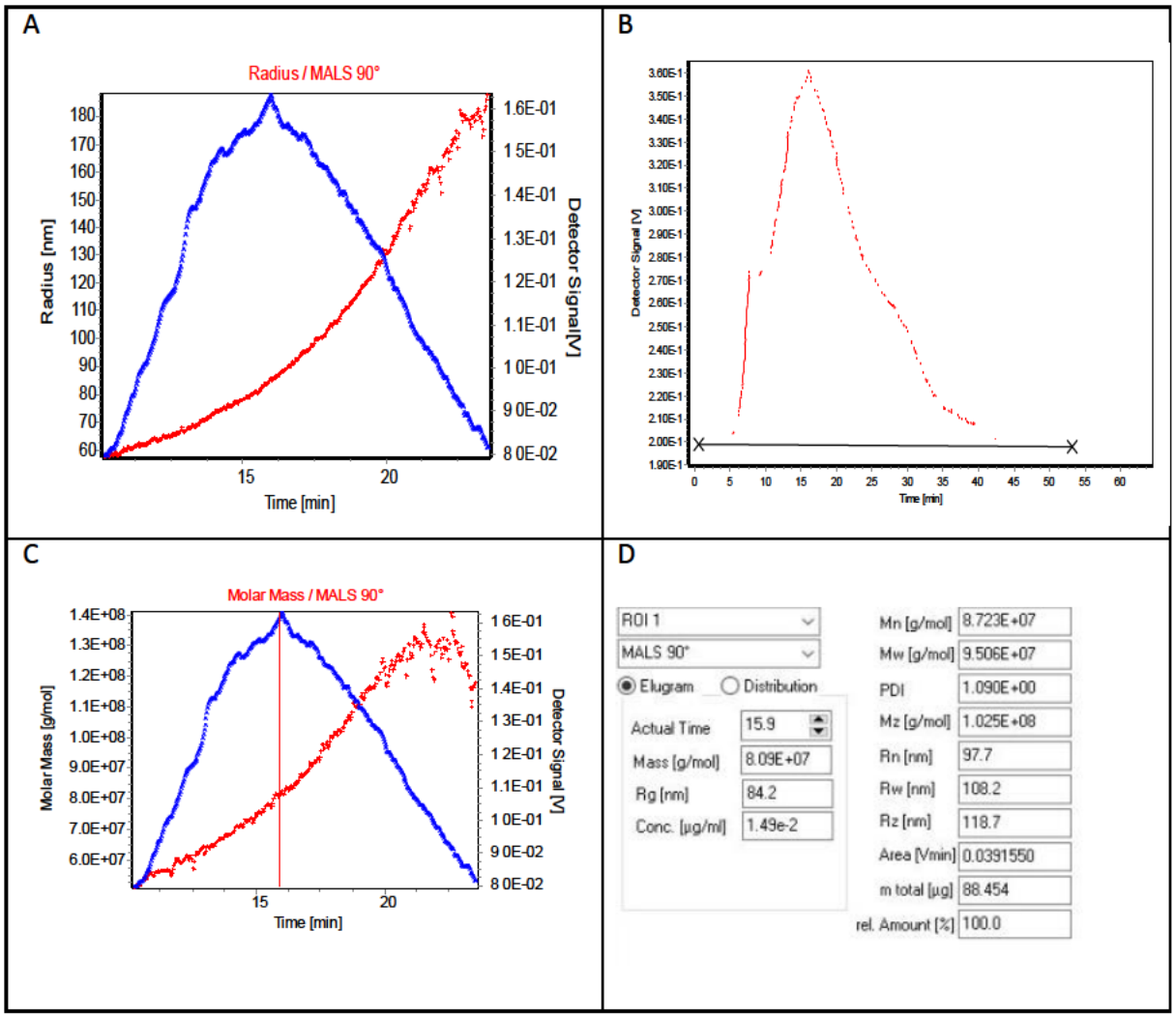

Figure 5. 24. AgNPs analysis data from FFF

The FFF-AF4 analysis of AgNPs, illustrated in Figure 5.24 above, shows the distribution patterns of both molar mass (C) and radius (A). The results indicated a radius of gyration (R_g) of 84.2 nm which translates to a hydrodynamic radius (R_h) of 108.65 nm calculated from Equation 5.2. As with the case of AuNPs, the results are reflective of the AgNPs with the capping agents and not only the electron dense Ag core as seen using TEM imaging. The FFF-AF4 results does confirm the successful synthesis of AgNP using the patty-pan extract and it further indicates that the particles are capped/coated as reflected in the size of the particle measurement.

5.2.3. Fabrication of Sensor 2 - AuE/GO-AgNPs/NHS/Anti-tau antibody

The use of a green methodology does not afford precise information regarding molecules surrounding or capping the silver nanoparticle. In Figure 5.25, the immobilisation of antibodies onto the silver nanoparticles were conducted using EDC/NHS surface chemistry, similar to sensor 1, where amine groups of the antibody binds to aldehyde groups of NHS esters. This approach is applicable where carboxyl groups are present in molecules that bind to the silver nanoparticle.

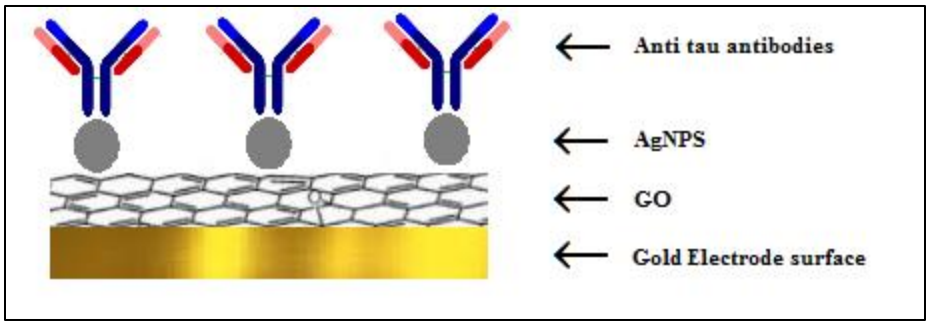

Figure 5. 25. Layer by layer modification of gold electrode surface by nanomaterials and anti-tau antibody

5.2.4. Electrochemical studies – Sensor 2

Figure 5.26 illustrates the cyclic voltammogram showing the blank bare AuE (red), after the electrode modification with GO and AgNPs (green) and finally the full modified electrode, inclusive of the anti-tau antibodies, tau protein and Cu(II)/Cu(I) redox probe (purple). These were carried out at pH 7 in phosphate buffer. The electrochemical signals at -0.04 V and -0.3 V are attributed to Cu(II)/Cu(I) redox probe that co-ordinates to tau protein and the signals at 0.1 V and -0.03V that are due to the redox reactions of the silver nanoparticles attributed to; $Ag \rightarrow Ag_2O$ and $Ag_2O \rightarrow Ag$, with potentials in keeping with reported literature (Choi and Luo, 2011). It must also be noted that no electrochemical peak was observed on the addition of GO onto the AuE surface.

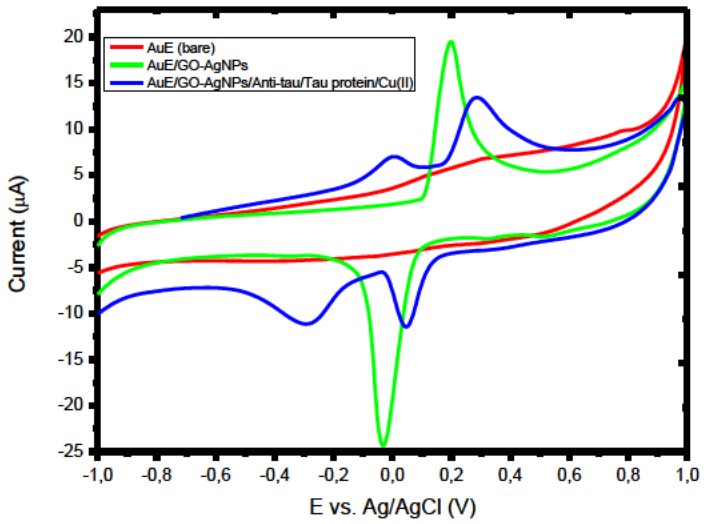

Figure 5. 26. Cyclic voltammogram showing the effects of electrode modification on the addition of nanomaterials and tau protein analyte

5.2.4.1. Optimisation of parameters

I. Effects of pH

The pH dependence of the immunosensor was investigated between pH 6.0 and 8.5 with 0.5 increments, in phosphate buffer in the presence of 20 nM tau protein. Higher pH values are seen to produce lower current signals with the optimum current response achieved at pH 7.0 as shown in Figure 5.27.

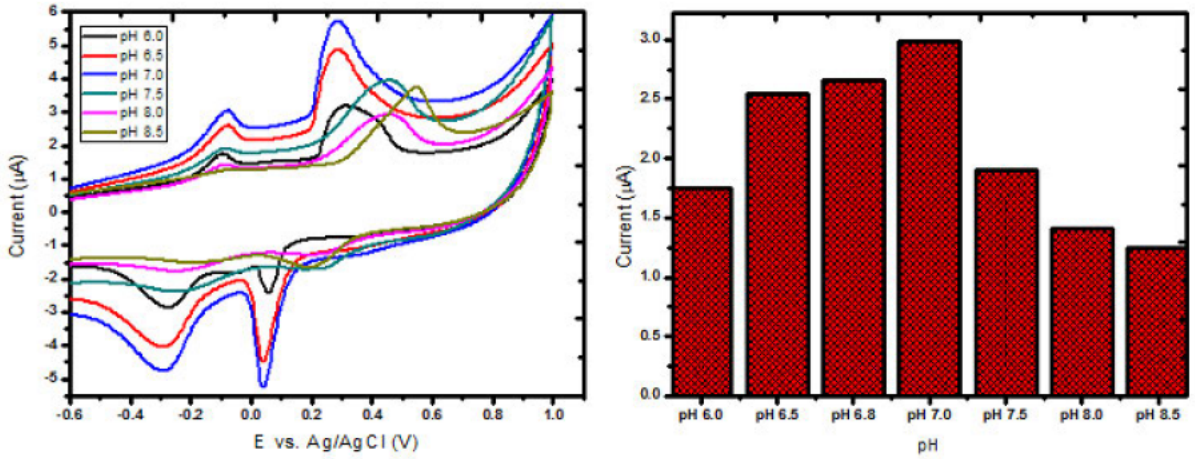

Figure 5. 27. Cyclic voltammogram of pH optimisation for sensor 1

II. Effects of scan rates

The effect of scan rates on peak currents signals of tau protein was studied at pH 7 in phosphate buffer. Figure 5.28 reveals a linear increase in oxidation peak current for both tau/copper complex and AgNPs from 0.025 $V.s^{-1}$ to 0.1 $V.s^{-1}$. The peak current then decreases above 0.1 $V.s^{-1}$. The highest peak current correspondes to a scan rate of 0.1 $V.s^{-1}$, which was use as the optimum rate for all further studies. The linear increase in tau/copper complex current with increase in scan rates in the range of 0.025 $V.s^{-1}$ to 0.1 $V.s^{-1}$, indicates that there is adsoption of the complex onto the modified electrode surface and that tau has sucessfully co-ordinated to copper II solution.

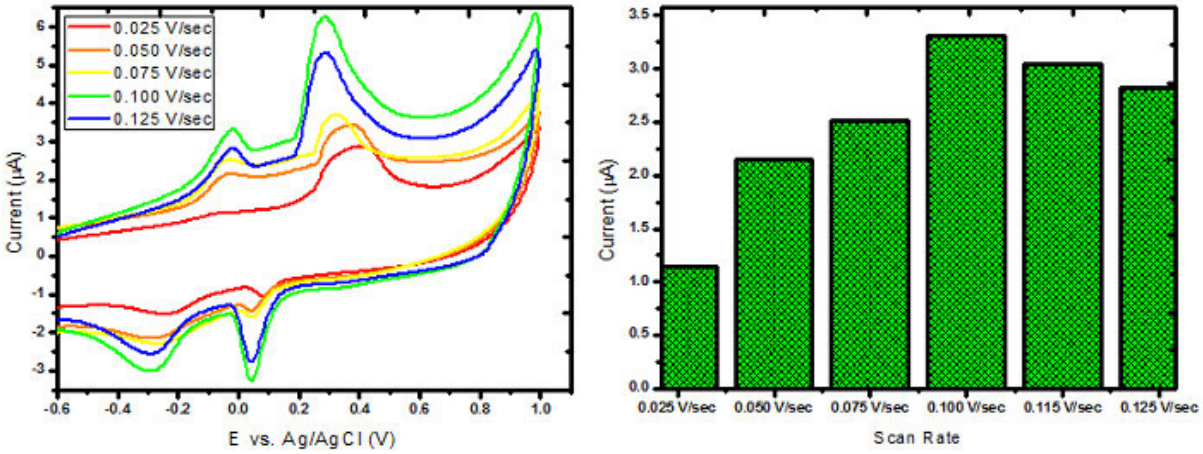

Figure 5. 28. Cyclic voltammogram of scan rates optimisation (right) and corresponding bar graph (left), for sensor

III. Effects of deposition time

The effects of deposition time on current response was investigated as seen in Figure 5.29. the results show that the aniodic current for tau/copper complex (first oxidation peak) increases with increasing deposition time up, then begins to decrease when the deposition time exceeds 100 seconds. From the graphs it can be noted that more analyte is absorbed onto the surface of the electrode when as time increases but then begins to saturate the electrode sufrace preventing electron movement beyond the time of 100 seconds.

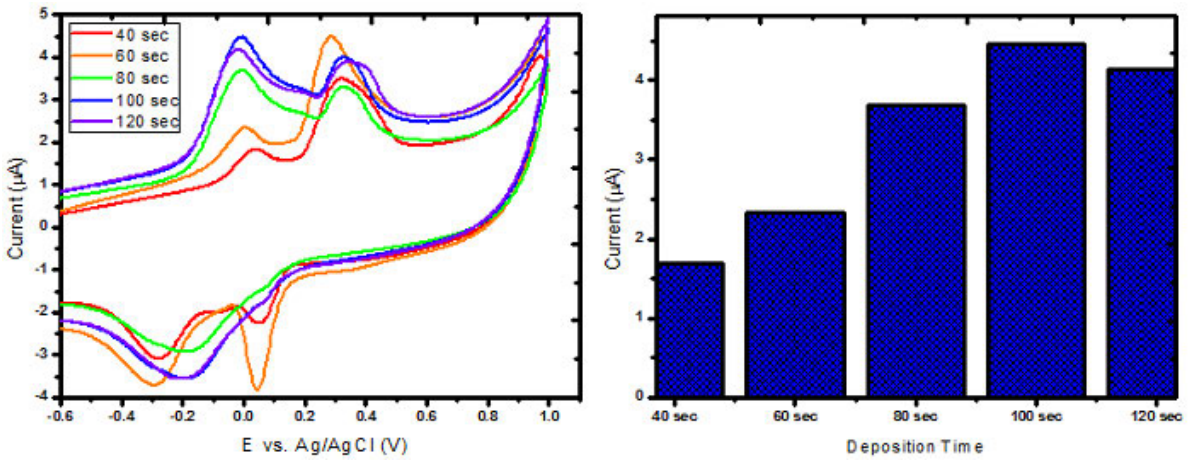

Figure 5. 29. Cyclic voltammogram of deposition time optimisation (right) and corresponding bar graph (left), for sensor 1

5.2.4.2. Effects of electrode modification on current response of tau protein analyte

Table 5.4 shows the effect of electrode modification on the current response. The addition of GO/AgNPs nanocomposite onto the gold electrode surface is shown to significantly improve the signal for tau protein by 125.62 % compared to the signal obtained using the unmodified, bare gold electrode. The variety of oxygen based functional groups present of GO allow its electrostatic interaction with AgNPs. The electrocatalytic activity is thus enhanced by the addition of AgNPs, owing to its high electrical conductivity and excellent catalytic properties (Pichaimuthu et al., 2018). The GO serves to enhance the surface area of the electrode, thus providing a larger volume of AgNPs to be accommodated, the number of sites for reactions are thus increased which then leads to higher current signals. The larger surface area also allows for the accommodation of the large anti-tau antibody. On the addition of the antibody onto the surface modified with the GO/AgNPs nanocomposite, the peak current corresponding to tau/copper complex is further enhanced by 23.39 % up from the previous modification step. The developed immunosensor with the use of nanomaterials and antibodies provided a 3-fold increase in analyte peal current signal compared to a bare gold electrode.

Table 5. 4. Results of signal response for analyte at each electrode surface modification step

Step	Modified sensor layers
1	Bare AuE/Tau protein
2	AuE/GO/AgNPs/Tau protein
3	AuE/ GO/AgNPs /NHS/Anti tau/Tau protein

Electrode modification step	Current / µA			Average current/ µA	Standard deviation	% RSD	% Current improvement
1	3.19	2.93	3.59	3.24	0.27	8.34	-
2	7.64	7.50	6.80	7.31	0.37	5.02	125.62
3	8.66	9.12	9.27	9.02	0.26	2.88	23.39

5.2.4.3. Quantitative Analysis

The current signal was investigated as a function of tau protein concentration (2, 4, 6, 8, 10, 12 nM). Using DPV and SWV calibration curves for tau protein detection was established. Figures 5.30 and 5.34 are voltammograms of DPV and SWV respectively and shows an increase in the peak current with increase in tau proein concentration. The optimum pH, scan rate and deposition time, established in section 5.1.5.1. The concentration of copper II solution was kept constant thus confirming the peak current increase due to to adddition of tau protein.

DPV

The results for DPV analysis showed a linear relationship between tau protein concentration and peak current. This is indicated in the establish calibration curve that yielded an R^2 value of 0,9814 as seen in Figure 5.31. The same figure illustrates the standard deviation of each concentration data point, from this is can be seen that the error is associated with each point similar in magnitude and does not give heed to an observable trend. The error bars seen in Figure 5.32 reflects the standard error about each data point and is higher for lower concentrations of tau protein. The standard residual plot reveals that all data points are well

within ± 2 standard error and therefore indicates a good regression model. An LOD of 1.88 nM and LOQ 6.27 nM was calculated.

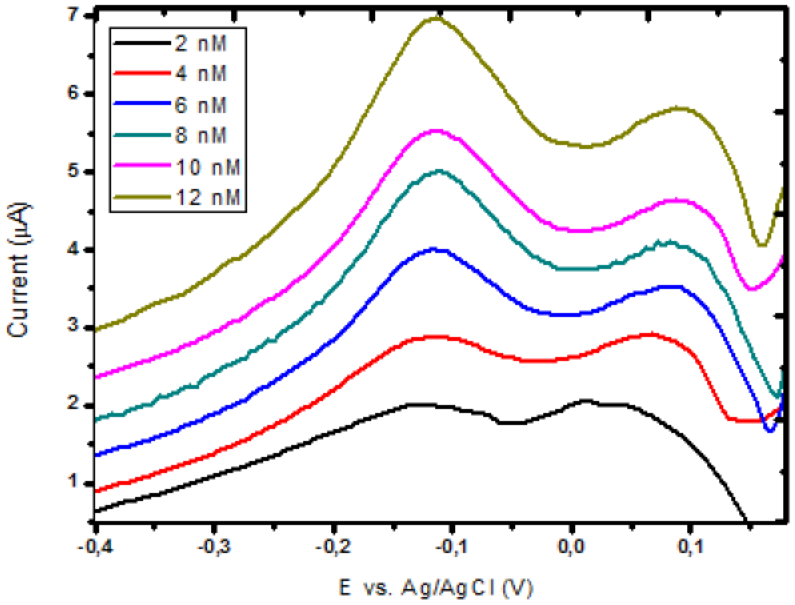

Figure 5. 30. Differential pulse voltammogram showing the immunosensor response for varying concentrations of tau protein

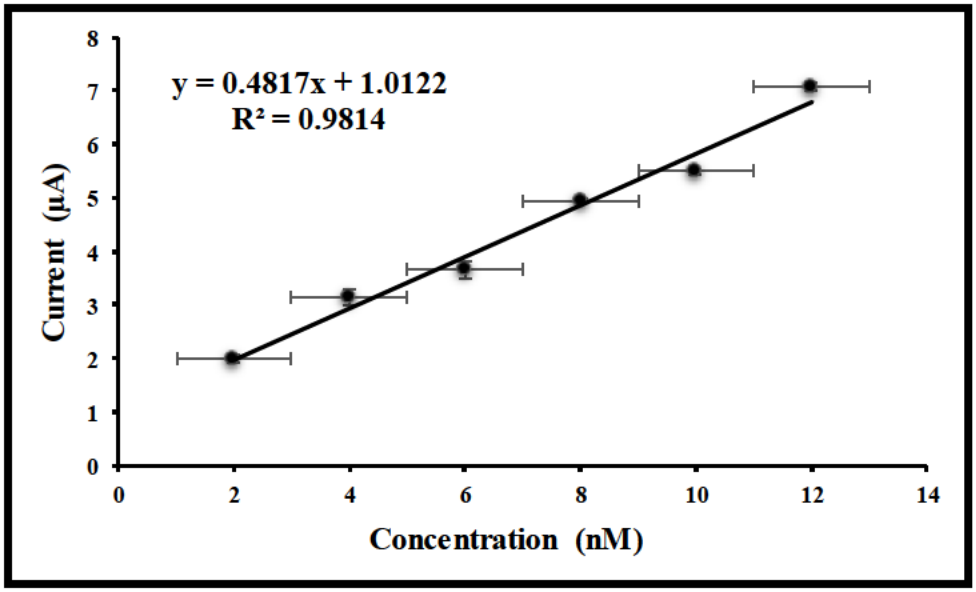

Figure 5. 31. Calibration curve with standard deviation error bars, showing the immunosensor response for tau protein, ranging between 5 and 35 nM concentration

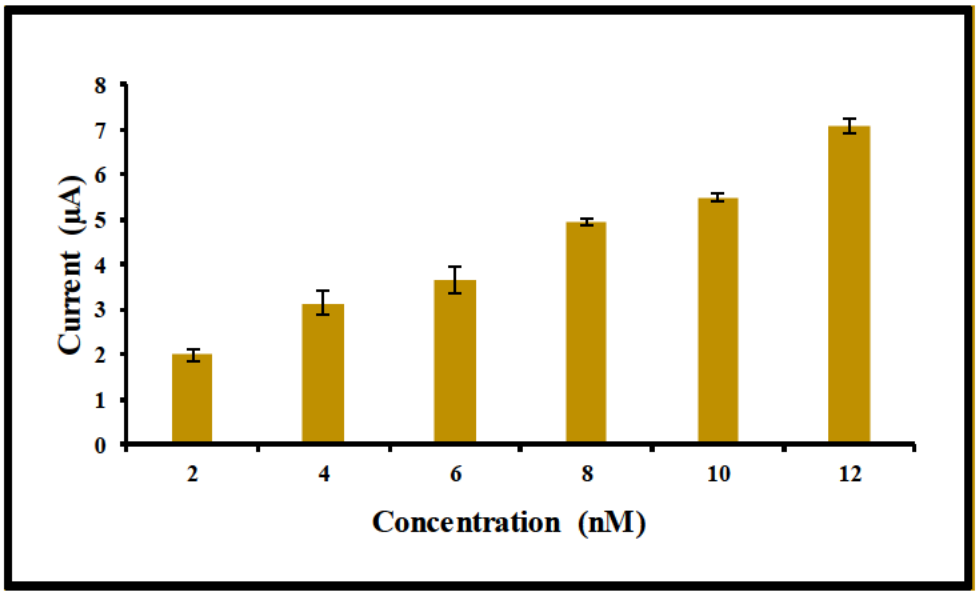

Figure 5. 32. Calibration bar graph with error bars for standard error, showing the immunosensor response for tau protein, ranging between 5 and 35 nM concentration

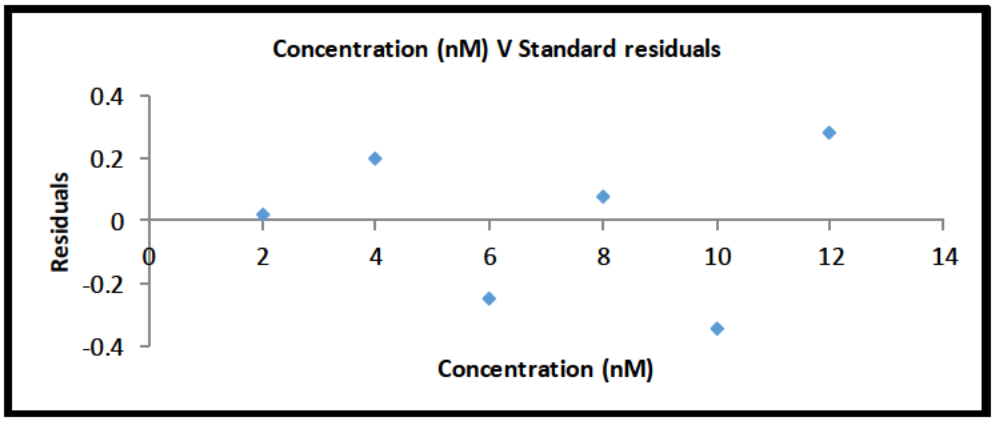

Figure 5. 33. Residual plot showing tau protein concentration against standard residuals, calculated from regression statistics

I. SWV

The calibration resulted in a linear curve with an R^2 value of 0,9780 as seen in Figure 5.35. The large errors bars are reflective of the standard deviation of each data point. Figure 5.36 shows the standard error is higher for lower concentrations of tau protein. The standard residual plot reveals that all data points are within ± 2 standard error and therefore indicates an acceptable regression model. It can be noted that results for DVP analysis yielded lesser error, howeer these are not relected in the calculation of detection limits which was found to be an LOD of 1.73 nM and and of LOQ 5.76 nM.

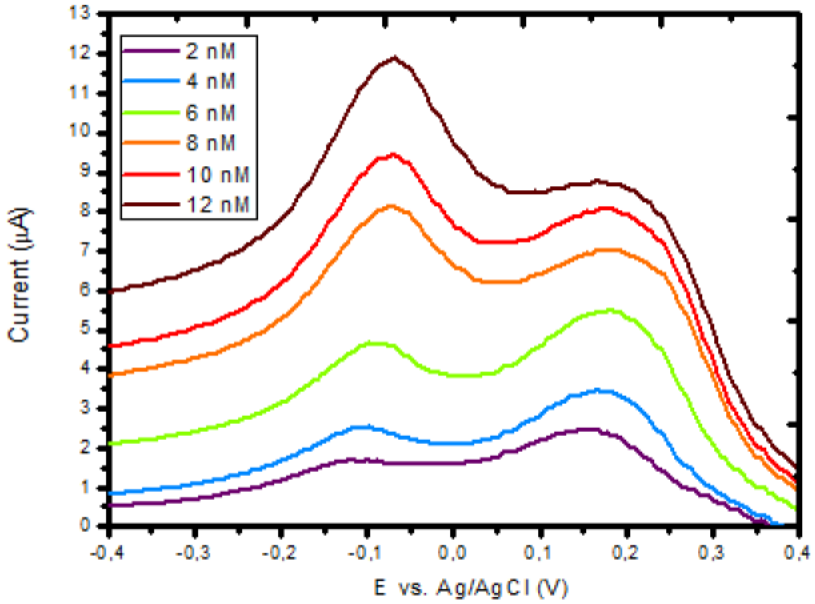

Figure 5. 34. Square wave voltammogram showing the immunosensor response for varying concentrations of tau protein

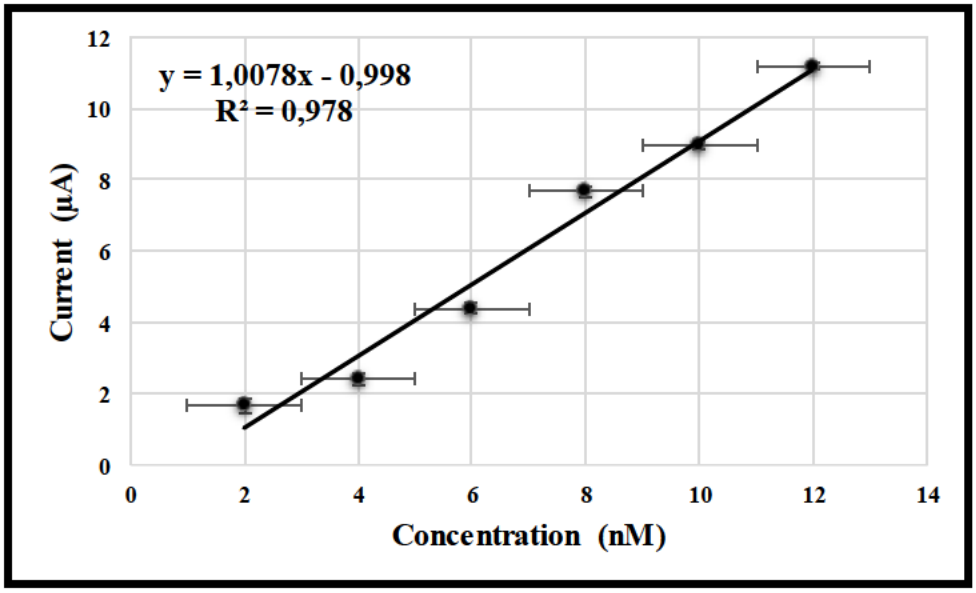

Figure 5. 35. Calibration curve with standard deviation error bars, showing the immunosensor response for tau protein, ranging between 5 and 30 nM concentration

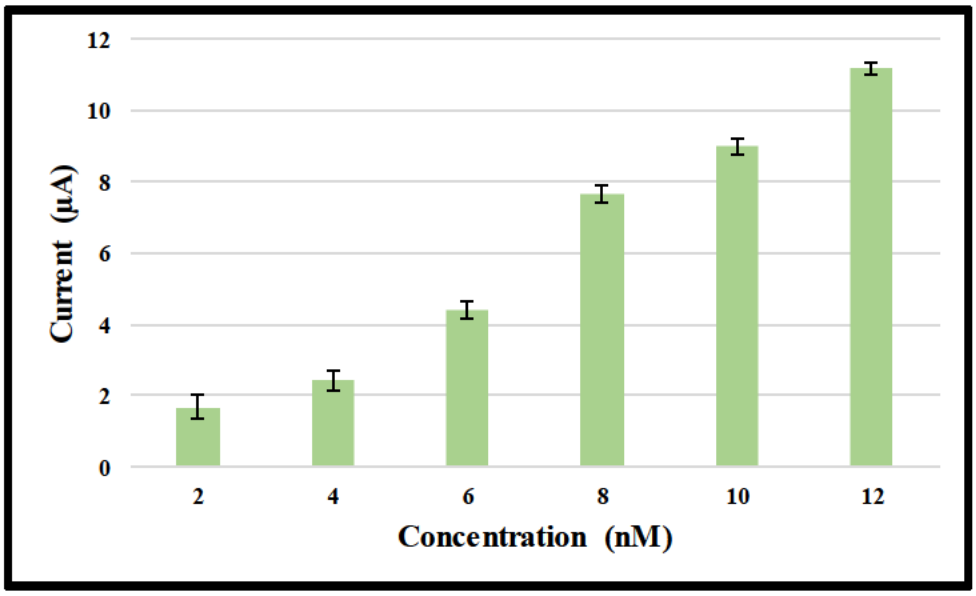

Figure 5. 36. Calibration bar graph with error bars for standard error, showing the immunosensor response for tau protein, ranging between 5 and 30 nM concentration

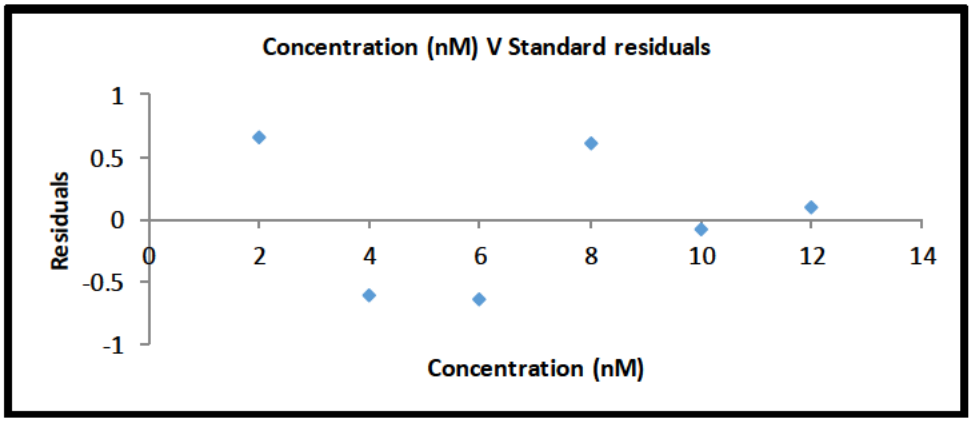

Figure 5. 37. Residual plot showing tau protein concentration against standard residuals, calculated from regression statistics

Table 5. 5. DPV Results for sample analysis

Sample	Concentration Added (nM)	Concentration Recovered (nM)	Mean	% Recovery	Standard error	Standard deviation	% RSD
1	5	4.45 4.13 3.74	4.10	82.10	0.21	0.36	8.68
2	10	5.74 6.17 6.40	6.10	61.01	0.19	0.33	5.48

Table 5. 6. SWV Results for sample analysis

Sample	Concentration Added (nM)	Concentration Recovered (nM)	Mean	% Recovery	Standard error	Standard deviation	% RSD
1	5	4.75 5.24 4.33	4.77	95.46	0.26	0.45	9.49
2	10	13.73 12.47 12.90	13.03	130.34	0.37	0.64	4.91

II. Tau protein recover studies

Two concentrations of tau protein (5 and 10 nM) was selected to test the developed immunosensor using DPV and SWV analysis and calculating the % recovery from the established calibration equations. The tau protein was prepared in PBS buffer, to simulate the pH and ionic composition of biological fluid in the absence of biological samples. Table 5.5 and Table 5.6 shows the results for analysis, where it can be seen that the SWV analysis yield a higher recovery percentage than DPV for the 5 nM sample. The 10 nM sample showed that the SWV analysis having a recovery higher than 100%. Both standard error and standard deviation values are higher for SWV compared to DPV. Both techniques seem to favour the detection of lower concentrations of tau protein.

5.3. COMPUTATIONAL STUDIES

5.3.1 Adsorption Studies

The adsorption locator was employed to generate the most stable configuration of the target molecules onto the selected electrode surfaces for sensor 1 and sensor 2 respectively. Here, the Monte Carlo-based function searches the favourable configurational space of the nanoparticulate adsorbate molecules towards the layer I, containing the electrode along a slowly decreasing temperature. Prior to MC simulation, the nanoparticulate adsorbate is constructed and optimized using the Forcite-Geometry code. The geometry optimization process was performed through an iterative procedure, in which the atomic coordinates are modified until the total energy is suitably minimized. This process represents a local minimum of the potential energy surface. The basis of the geometry optimization of the nanoparticulate adsorbate molecules were based on decreasing the magnitude of the calculated forces, until the selected values of the convergence tolerances were revealed.

Using the adsorption locator simulation module, the surface configurations for sensor 1 and sensor 2 were sampled from a canonical ensemble. In this ensemble, the loading (or number) of the nanoparticulate adsorbate molecules as well as the temperature, were kept fixed. The configuration probability, m, in the ensemble is provided by Equation 5.7 (Shi and Atrens, 2011).

$$Pm=Ce-\beta Em \tag{5.7}$$

Where C corresponds to a constant of arbitrary normalization, β is the reciprocal temperature, and Em is the total energy of configuration (m). Further, the reciprocal temperature is specified as Equation 5.8 (BIOVIA, 2016b) below.

$$\beta=1kBT \tag{5.8}$$

Where Kb is the Boltzman constant and T corresponds to the absolute temperature. The total energy of configuration, m, is determined as the following sum:

$$Em=EmAA+EmAS+UmA \quad (5.9)$$

Where $EmAA$, $EmAS$, and UmA are the intermolecular energy between adsorbate molecules, interaction energy between adsorbate and the substrate, and the total intramolecular energy of the absorbate molecules, respectively. The intramolecular energy within the substrate is not considered since its structure is kept fixed during simulations and therefore, the distribution of intramolecular energy is constant.

The first step of the simulation involves the adsorption of the specified loading of the electrode surface molecule. This step was carried out by a random series of insertion steps and equilibration phase until the selected loading is accomplished. For this step, only the insertion steps which do not produce structures with intermolecular close contacts and enable to pass all adsorbates location constraints are allowed. The initial configuration takes numerous steps for adjusting to the current temperature. An adsorption location is thus, divided into equilibrium and production stages. The last trajectories comprising of the lowest energy configuration are based on the production stage, particularly (Khaled and El-Sherik, 2013, BIOVIA, 2016b).
At the stages of equilibration and production, each step was started by choosing a step type by means of the selected parameters prior to the simulation run. This step type corresponds to either rotation or translation procedure. Upon the selection of the step type, a random component is selected and the step type is implemented to random adsorbate of the corresponding component. Metropolis Monte Carlo algorithm is subsequently used to determine the acceptability of the change to be accepted or rejected (Khaled and El-Sherik, 2013, BIOVIA, 2016b).

The adsorption energy distributions of all the loading molecules are depicted in Figure 5.38, while the corresponding outputs and descriptor are shown in Table 5.7.

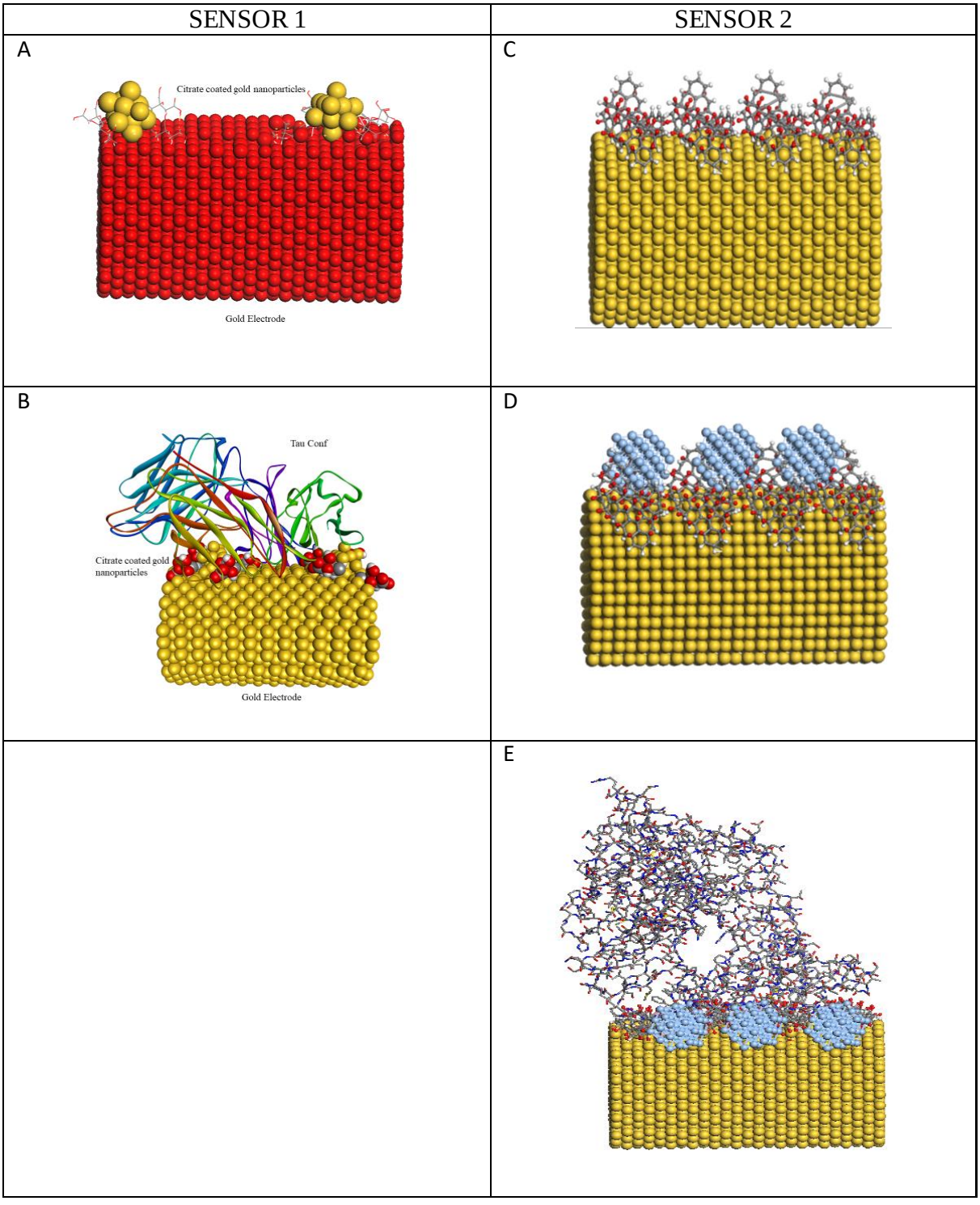

Figure 5. 38. (A) Adsorption of citrate capped gold nanoparticles onto gold electrode surface
(B) Adsorption of tau configuration (Anti-tau antibody/Tau protein) onto modified gold electrode surface for sensor 1
(C) Adsorption of graphene oxide onto gold electrode surface
(D) Adsorption of silver nanoparticles onto modified gold electrode surface
(E) Adsorption of tau configuration (Anti-tau antibody/Tau protein) onto modified gold electrode surface for sensor 2

Table 5. 7. Adsorption energies for sensor 1 and sensor 2

Layer-by-layer system	**Energy - ΔG (**kcal/mol)
SENSOR 1	
AuE/AuNPs	-23.74
AuE/AuNPs/EDC-NHS	-10.42
AuE/AuNPs/EDC-NHS/Anti tau/Tau	-142.97
SENSOR 2	
AuE/GO	-7.60
AuE/GO/AgNPs	-8.81
AuE/GO/AgNPs/NHS	-10.45
AuE/GO/AgNPs/NHS/Tau	-45.61
AuE/GO/AgNPs/NHS/ Anti tau/Tau	-127.82

Table 5.7 also demonstrates the dEads/dNi, which explains the energy in kcal/mol, of substrate-adsorbate configurations where one of the adsorbate molecules has been eliminated (BIOVIA, 2016b). The trends of adsorption energy distribution, consistent with the average total energy. For the overall adsorbate concentrations, the highest adsorption energy is generated by the lowest number of adsorbate loading i.e. 1 molecule (-23.74 kcal/mol) (Table 5.7). This trend emphasizes that the number of absorbate molecules (or concentrations) provide a direct influence upon its adsorption capability onto the electrode surface.

5.3.2. Molecular docking studies

Molecular docking was performed to reveal binding modes between chemical binders NHS, EDC and MPA to the anti-tau antibody/tau protein configuration. The results indicate that a low ΔG value of – 4.72 kcal/mol (Table 5.8) for NHS, confirms the proposed binding mode displayed in Figure 5.38, in which amine groups of the anti-tau antibody binds to NHS ester groups.

Table 5. 8. Docking results for chemical binders; NHS and EDC

Compounds	ΔG (Docking- Binding Affinity) (kcal/mol)
NHS	-4.72
EDC	-3.10

Residues such as Val177, Ser186, Thr178, Ser40, Gln39, Pro123 and Asp122 were identified as active binding sites on the tau protein as seen in Figure 5.39.

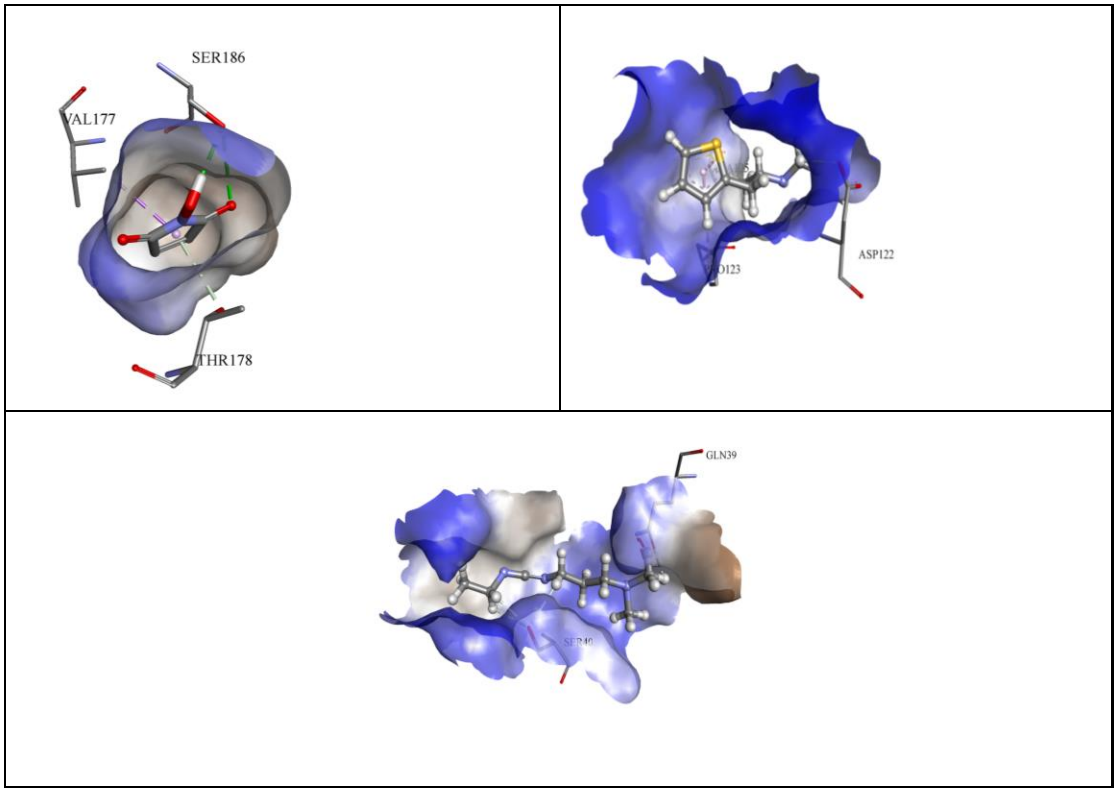

Figure 5.39. Possible binding sites for tau protein and anti-tau antibody, showing participating residuals

The Root Mean-Square Deviation (RMSD) was used to monitor the stability of the system, Figure 5.40 shows that the system becomes and remains stable after 20 000 ps, thus confirming that equilibration was achieved. The radius of gyration (Rg) aids in predicting the structural activity and statistic behaviour of tau protein, it further aids in predicting the compactness and binding patterns of the anti-tau antibody and tau protein as any change in the protein conformation results in changes in the radius of gyration (Sneha and George Priya Doss, 2016).

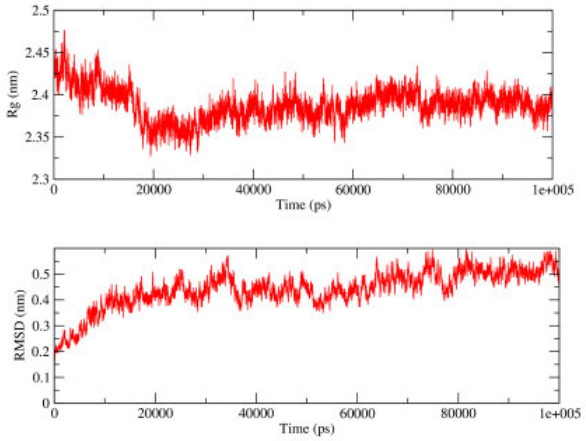

Figure 5. 40. Root Mean Square Deviation (RMSD) and Radius of Gyration (Rg) plot for the docked tau protein configuration

The results in Figure 5.40 show a steady decrease in Rg value between 0 and 20 000ps, followed by an increase is between 20 000ps to 30 000ps and then an eventual steadying beyond 30 000ps. This could indicate the effective binding to tau protein to the anti-tau antibody and effective binding of the tau configuration to the modified electrode. Table 5.7 shows the binding energies at each of the modified electrode layers for sensor 1 and sensor 2, respectively.

The results for sensor 1 indicate an increase in binding affinity at each modification step of the gold electrode, as observed in the lowering of energy, this corresponds to the electrochemical monitoring of the layer by layer modification, in which there was a decrease in current potential on the addition of chemical binders and the anti-tau antibody as seen in Figure 5.8.

It can be seen for sensor 2, a ΔG value of – 45.61 kcal/mol is observed for the addition of tau protein onto the modified electrode surface. A significantly lower ΔG value of – 127.82 kcal/mol is observed for the addition of the anti-tau/ tau configuration onto the modified electrode surface. These difference in energy values indicate a stronger interaction between tau protein and the electrode surface with the addition of the anti-tau antibody. This confirms the signal enhancing ability of the anti-tau antibody which can also be seen in Table 5.4, indicating an improvement of 23.39% in current potential, on the addition of the anti-tau antibody onto the electrode modified with GO and AgNPs.

CHAPTER SIX

CONCLUSIONS AND RECOMMENDATIONS

6.1. SUMMARY AND CONCLUSIONS

The aim of this research was to develop an electrochemical sensor for the detection of tau protein using novel approaches. Two different immunosensors were developed, the first containing gold nanoparticles and the second containing a nanocomposite of graphene oxide and silver nanoparticles. Both immunosensors utilised an anti-tau antibody which served to increase selectivity for the tau protein analyte. Both the use of nanomaterials and the antibody served to enhance the electrochemical signal of the tau protein analyte, thus leading significantly lower detection limits.

Methodologies employed for the synthesis of nanomaterials were successfully executed as revealed in the characterisation studies using U-Visible spectroscopy, TEM imaging and Field flow fractionation. Silver nanoparticles were synthesised using novel green approach, which eliminated the use of organic reagent and energy.

The results for the first sensor (AuE/AuNPs/Anti-tau antibody) revealed that the current signal improved more than double for the modified sensor compared to that of the bare electrode. The quantitative analysis done showed an LOD of 3.31 nM for DPV analysis, whilst the SWV analysis produced an LOD of 5.31 nM. Both DPV and SWV analysis produced good regression models, the analysis for recovery studies revealed that both techniques recovered ± 95 % for the upper concentration limit of the calibration curve, whilst recovery slightly decreased for DPV in the lower concentration range, a much lower recovery was observed for SWV.

The second immunosensor (AuE/GO-AgNPs/ Anti-tau antibody) showed an almost three-fold improvement in peak current for the modified electrode over the bare electrode. DPV calibrations revealed an LOD of 1.88 nM. SWV calibrations showed an LOD of 1.73 nM. Recovery studies showed a higher % for lower concentration limits of the established calibration curves. The computational studies corresponded well with experimental results and aided in confirming chemical mechanisms involved in the interaction of tau protein with the anti-tau antibody as well as with the nanomaterials. Overall both sensors produced low limits of detection which fall within the specified limits for tau protein analysis for neurodegenerative

diagnosis. The roles of nanomaterials and antibody transducers have also shown to significantly amplify current signals, which indicate the important contribution they could make in the role of detecting biomolecules present in low concentrations in the human body, thus contributing to diagnosing and monitoring neurodegenerative disease.

6.2. RECOMMENDATIONS FOR FUTURE WORK

Further work may involve the study of other nanomaterials/ nanocomposites and their properties that could prove to further enhance electrochemical signals which could lead to even lower detection limits. Methodologies of nanomaterials synthesis could also be explored, particularly the field of engineered nanoparticle in which the size and shape of the particles could be controlled. This in turn will assist in obtaining and more stable and consistent surface chemistry reactions. Other antibodies or transducers could be explored to enhance sensitivity and selectivity of the sensor. Computational chemistry could be used as a reference for experimental work instead of an accompanying validation tool. This will be favourable as computational methods are able to predict the best possible combinations and outcomes for possible experimental work, thus saving on time and expenditure.

REFERENCES

ABOU EL-NOUR, K. M. M., EFTAIHA, A. A., AL-WARTHAN, A. & AMMAR, R. A. A. 2010. Synthesis and applications of silver nanoparticles. *Arabian Journal of Chemistry,* 3**,** 135-140.

AHMADI, S., EBRALIDZE, I. I., SHE, Z. & KRAATZ, H.-B. 2017. Electrochemical studies of tau protein-iron interactions—Potential implications for Alzheimer's Disease. *Electrochimica Acta,* 236**,** 384-393.

ALBAYRAM, O., ANGELI, P., BERNSTEIN, E., BAXLEY, S., GAO, Z. J., LU, K. P. & ZHEN ZHOU, X. 2018. *Targeting Prion-like Cis Phosphorylated Tau Pathology in Neurodegenerative Diseases*.

ALJOHANI, H., ABOU-HAMAD, E., JEDIDI, A., WIDDIFIELD, C., VIGER-GRAVEL, J., SANGARU, S. S., GAJAN, D., H. ANJUM, D., OULD-CHIKH, S., HEDHILI, M., GURINOV, A., KELLY, M., EL ETER, M., CAVALLO, L., EMSLEY, L. & BASSET, J. 2017. *The structure and binding mode of citrate in the stabilization of gold nanoparticles*.

ALONSO, A. D., COHEN, L. S., CORBO, C., MOROZOVA, V., ELIDRISSI, A., PHILLIPS, G. & KLEIMAN, F. E. 2018. Hyperphosphorylation of Tau Associates With Changes in Its Function Beyond Microtubule Stability. *Frontiers in cellular neuroscience,* 12**,** 338-338.

ANGIOLETTI-UBERTI, S. 2017. Theory, simulations and the design of functionalized nanoparticles for biomedical applications: A Soft Matter Perspective. *npj Computational Materials,* 3**,** 48.

ANU MARY EALIA, S. & SARAVANAKUMAR, M. P. 2017. A review on the classification, characterisation, synthesis of nanoparticles and their application. *IOP Conference Series: Materials Science and Engineering,* 263**,** 032019.

ARENDT, T., STIELER, J. T. & HOLZER, M. 2016. Tau and tauopathies. *Brain Research Bulletin,* 126**,** 238-292.

BAHADıR, E. B. & SEZGINTÜRK, K. M. 2015. Applications of electrochemical immunosensors for early clinical diagnostics. *Talanta,* 132**,** 162-174.

BAND, Y. B. & AVISHAI, Y. 2013. 15 - Density Functional Theory. *In:* BAND, Y. B. & AVISHAI, Y. (eds.) *Quantum Mechanics with Applications to Nanotechnology and Information Science.* Amsterdam: Academic Press.

BARNARD, A. S. 2010. Modelling of nanoparticles: approaches to morphology and evolution. *Reports on Progress in Physics,* 73**,** 086502.

BAZAN, N. G., HALABI, A., ERTEL, M. & PETASIS, N. A. 2012. Chapter 34 - Neuroinflammation. *In:* BRADY, S. T., SIEGEL, G. J., ALBERS, R. W. & PRICE, D. L. (eds.) *Basic Neurochemistry (Eighth Edition).* New York: Academic Press.

BEACH, T. G. 2017. A Review of Biomarkers for Neurodegenerative Disease: Will They Swing Us Across the Valley? *Neurology and therapy,* 6**,** 5-13.

BISWAL, S., BHASKARAM, D. S. & GOVINDARAJ, G. 2018. Graphene oxide: structure and temperature dependent magnetic characterization. *Materials Research Express,* 5**,** 086104.

BLENNOW, K., DE LEON, M. J. & ZETTERBERG, H. 2006. Alzheimer's disease. *Lancet,* 368**,** 387-403.

BUEE, L., BUSSIERE, T., BUEE-SCHERRER, V., DELACOURTE, A. & HOF, P. R. 2000. Tau protein isoforms, phosphorylation and role in neurodegenerative disorders. *Brain Res Brain Res Rev,* 33**,** 95-130.

CALZOLAI, L., GILLILAND, D., GARCÌA, C. P. & ROSSI, F. 2011. Separation and characterization of gold nanoparticle mixtures by flow-field-flow fractionation. *Journal of Chromatography A,* 1218**,** 4234-4239.

CARLIN, N. & MARTIC-MILNE, S. 2018. Anti-Tau Antibodies Based Electrochemical Sensor for Detection of Tau Protein Biomarkers. *Journal of The Electrochemical Society,* 165**,** G3018-G3025.

CHANDRA, A. & SINGH, M. 2016. Amino Acid Coated Silver Nanoparticles: A Green Catalyst for Methylene Blue Reduction. *International Journal of Chemical, Molecular, Nuclear, Materials and Metallurgical Engineering,* 10.

CHANDRA, A. & SINGH, M. 2018. Biosynthesis of amino acid functionalized silver nanoparticles for potential catalytic and oxygen sensing applications. *Inorganic Chemistry Frontiers,* 5**,** 233-257.

CHEN-PLOTKIN, ALICE S. 2014. Unbiased Approaches to Biomarker Discovery in Neurodegenerative Diseases. *Neuron,* 84**,** 594-607.

CHENG, H.-C., QI, R. Z., PAUDEL, H. & ZHU, H.-J. 2011. Regulation and Function of Protein Kinases and Phosphatases. *Enzyme Research,* 2011**,** 3.

CHOI, Y.-J. & LUO, T.-J. M. 2011. Electrochemical Properties of Silver Nanoparticle Doped Aminosilica Nanocomposite. *International Journal of Electrochemistry,* 2011**,** 1-6.

CLEVELAND, D. W., HWO, S.-Y. & KIRSCHNER, M. W. 1977a. Physical and chemical properties of purified tau factor and the role of tau in microtubule assembly. *Journal of molecular biology,* 116**,** 227-247.

CLEVELAND, D. W., HWO, S.-Y. & KIRSCHNER, M. W. 1977b. Purification of tau, a microtubule-associated protein that induces assembly of microtubules from purified tubulin. *Journal of molecular biology,* 116**,** 207-225.

CONROY, P. J., HEARTY, S., LEONARD, P. & O'KENNEDY, R. J. 2009. Antibody production, design and use for biosensor-based applications. *Semin Cell Dev Biol,* 20**,** 10-26.

CONTADO, C. 2017. Field flow fractionation techniques to explore the "nano-world". *Anal Bioanal Chem,* 409**,** 2501-2518.

CRICHTON, R. & WARD, R. 2013. Role of Metal Ions in Brain Function, Metal Transport, Storage and Homoeostasis. *Metal-based Neurodegeneration.*

DAI, Y., MOLAZEMHOSSEINI, A. & LIU, C. C. 2017. A Single-Use, In Vitro Biosensor for the Detection of T-Tau Protein, A Biomarker of Neuro-Degenerative Disorders, in PBS and Human Serum Using Differential Pulse Voltammetry (DPV). *Biosensors (Basel),* 7.

DELLEY, B. 2000. From molecules to solids with the DMol3 approach. *The Journal of Chemical Physics,* 113**,** 7756-7764.

DERKUS, B., ACAR BOZKURT, P., TULU, M., EMREGUL, K. C., YUCESAN, C. & EMREGUL, E. 2017. Simultaneous quantification of Myelin Basic Protein and Tau proteins in cerebrospinal fluid and serum of Multiple Sclerosis patients using nanoimmunosensor. *Biosens Bioelectron,* 89**,** 781-788.

DISABATO, D. J., QUAN, N. & GODBOUT, J. P. 2016. Neuroinflammation: the devil is in the details. *Journal of neurochemistry,* 139 Suppl 2**,** 136-153.

DUTHEY, B. 2013. Background paper 6.11: Alzheimer disease and other dementias. *A Public Health Approach to Innovation***,** 1-74.

ECHKO, M. M. & DOZIER, S. K. 2010. Recombinant Antibody Technology for the Production of Antibodies Without the Use of Animals.

ELAHI, N., KAMALI, M. & BAGHERSAD, M. H. 2018. Recent biomedical applications of gold nanoparticles: A review. *Talanta,* 184**,** 537-556.

ELGRISHI, N., ROUNTREE, K. J., MCCARTHY, B. D., ROUNTREE, E. S., EISENHART, T. T. & DEMPSEY, J. L. 2017. A Practical Beginner's Guide to Cyclic Voltammetry. *Journal of Chemical Education,* 95**,** 197-206.

ENG, A. Y. S., CHUA, C. K. & PUMERA, M. 2015. Refinements to the structure of graphite oxide: absolute quantification of functional groups via selective labelling. *Nanoscale,* 7**,** 20256-20266.

ESTEVES-VILLANUEVA, J. O. & MARTIC-MILNE, S. 2016. Electrochemical detection of anti-tau antibodies binding to tau protein and inhibition of GSK-3beta-catalyzed phosphorylation. *Anal Biochem,* 496**,** 55-62.

ESTEVES-VILLANUEVA, J. O., TRZECIAKIEWICZ, H. & MARTIC, S. 2014. A protein-based electrochemical biosensor for detection of tau protein, a neurodegenerative disease biomarker. *Analyst,* 139**,** 2823-31.

FACECCHIA, K., FOCHESATO, L.-A., RAY, S. D., STOHS, S. J. & PANDEY, S. 2011. Oxidative toxicity in neurodegenerative diseases: role of mitochondrial dysfunction and therapeutic strategies. *Journal of toxicology,* 2011**,** 683728-683728.

FREITAS DE FREITAS, L., VARCA, G. H. C., DOS SANTOS BATISTA, J. G. & BENÉVOLO LUGÃO, A. 2018. An Overview of the Synthesis of Gold Nanoparticles Using Radiation Technologies. *Nanomaterials (Basel, Switzerland),* 8**,** 939.

FRENKEL-PINTER, M., SHMUELI, M. D., RAZ, C., YANKU, M., ZILBERZWIGE, S., GAZIT, E. & SEGAL, D. 2017. Interplay between protein glycosylation pathways in Alzheimer's disease. *Science Advances,* 3**,** e1601576.

FRISCH, M. J., TRUCKS, G. W., SCHLEGEL, H. B., SCUSERIA, G. E., ROBB, M. A., CHEESEMAN, J. R., SCALMANI, G., BARONE, V., MENNUCCI, B., PETERSSON, G. A., NAKATSUJI, H., CARICATO, M., LI, X., HRATCHIAN, H. P., IZMAYLOV, A. F., BLOINO, J., ZHENG, G., SONNENBERG, J. L., HADA, M., EHARA, M., TOYOTA, K., FUKUDA, R., HASEGAWA, J., ISHIDA, M., NAKAJIMA, T., HONDA, Y., KITAO, O., NAKAI, H., VREVEN, T., MONTGOMERY JR., J. A., PERALTA, J. E., OGLIARO, F., BEARPARK, M. J., HEYD, J., BROTHERS, E. N., KUDIN, K. N., STAROVEROV, V. N., KOBAYASHI, R., NORMAND, J., RAGHAVACHARI, K., RENDELL, A. P., BURANT, J. C., IYENGAR, S. S., TOMASI, J., COSSI, M., REGA, N., MILLAM, N. J., KLENE, M., KNOX, J. E., CROSS, J. B., BAKKEN, V., ADAMO, C., JARAMILLO, J., GOMPERTS, R., STRATMANN, R. E., YAZYEV, O., AUSTIN, A. J., CAMMI, R., POMELLI, C., OCHTERSKI, J. W., MARTIN, R. L., MOROKUMA, K., ZAKRZEWSKI, V. G., VOTH, G. A., SALVADOR, P., DANNENBERG, J. J., DAPPRICH, S., DANIELS, A. D., FARKAS, Ö.,

FORESMAN, J. B., ORTIZ, J. V., CIOSLOWSKI, J. & FOX, D. J. 2009. Gaussian 09. Wallingford, CT, USA: Gaussian, Inc.

GAURAB, K. 2018. *Antibody: Structure, classes and functions* [Online]. Available: https://www.onlinebiologynotes.com/antibody-structure-classes-functions/ [Accessed 20 March 2019].

GIACOMELLI, C., DANIELE, S. & MARTINI, C. 2017. Potential biomarkers and novel pharmacological targets in protein aggregation-related neurodegenerative diseases. *Biochemical Pharmacology,* 131**,** 1-15.

GOEDERT, M., SPILLANTINI, M. G., JAKES, R., RUTHERFORD, D. & CROWTHER, R. A. 1989. Multiple isoforms of human microtubule-associated protein tau: sequences and localization in neurofibrillary tangles of Alzheimer's disease. *Neuron,* 3**,** 519-26.

GOMES-FILHO, S. L. R., DIAS, A. C. M. S., SILVA, M. M. S., SILVA, B. V. M. & DUTRA, R. F. 2013. A carbon nanotube-based electrochemical immunosensor for cardiac troponin T. *Microchemical Journal,* 109**,** 10-15.

GOMEZ, C. V., ROBALINO, E., HARO, D., TENE, T., ESCUDERO, P., HARO, A. & ORBE, J. 2016. Structural and Electronic Properties of Graphene Oxide for Different Degree of Oxidation1. *Materials Today: Proceedings,* 3**,** 796-802.

GONG, C. X., LIU, F., GRUNDKE-IQBAL, I. & IQBAL, K. 2005. Post-translational modifications of tau protein in Alzheimer's disease. *J Neural Transm (Vienna),* 112**,** 813-38.

GONNELLI, C., CACIOPPO, F., GIORDANO, C., CAPOZZOLI, L., SALVATICI, C., SALVATICI, M. C., COLZI, I., DEL BUBBA, M., ANCILLOTTI, C. & RISTORI, S. 2015. Cucurbita pepoL. extracts as a versatile hydrotropic source for the synthesis of gold nanoparticles with different shapes. *Green Chemistry Letters and Reviews,* 8**,** 39-47.

GOPINATH, S. C. B., TANG, T.-H., CITARTAN, M., CHEN, Y. & LAKSHMIPRIYA, T. 2014. Current aspects in immunosensors. *Biosensors and Bioelectronics,* 57**,** 292-302.

GRIESHABER, D., MACKENZIE, R., VÖRÖS, J. & REIMHULT, E. 2008. Electrochemical Biosensors - Sensor Principles and Architectures. *Sensors (Basel, Switzerland),* 8**,** 1400-1458.

GRIFFIN, S., MASOOD, M. I., NASIM, M. J., SARFRAZ, M., EBOKAIWE, A. P., SCHAFER, K. H., KECK, C. M. & JACOB, C. 2017. Natural Nanoparticles: A Particular Matter Inspired by Nature. *Antioxidants (Basel),* 7.

GRUNDKE-IQBAL, I., IQBAL, K., QUINLAN, M., TUNG, Y. C., ZAIDI, M. S. & WISNIEWSKI, H. M. 1986. Microtubule-associated protein tau. A component of Alzheimer paired helical filaments. *J Biol Chem,* 261**,** 6084-9.

GUPTA, D. K., RAJAURA, R. S. & SHARMA, K. 2015. Synthesis and Characterization of Graphene Oxide Nanoparticles and their Antibacterial Activity. *Suresh Gyan Vihar University International Journal of Environment, Science and Technology,* 1**,** 16-24.

HAMMOND, J. L., FORMISANO, N., ESTRELA, P., CARRARA, S. & TKAC, J. 2016. Electrochemical biosensors and nanobiosensors. *Essays Biochem,* 60**,** 69-80.

HASEGAWA, M., CROWTHER, R. A., JAKES, R. & GOEDERT, M. 1997. Alzheimer-like changes in microtubule-associated protein Tau induced by sulfated glycosaminoglycans. Inhibition of microtubule binding, stimulation of phosphorylation, and filament assembly depend on the degree of sulfation. *J Biol Chem,* 272**,** 33118-24.

HIPPIUS, H. & NEUNDÖRFER, G. 2003. The discovery of Alzheimer's disease. *Dialogues in clinical neuroscience,* 5**,** 101-108.

HUANG, A. 2009. *Computational Studies of Tau Protein: Implications for the Pathogenesis and Treatment of Neurodegenerative Diseases.* Doctorate Doctor of Philosophy in Electrical and Biomedical Engineering Massachusetts Institute of Technology.

HUMPEL, C. 2011. Identifying and validating biomarkers for Alzheimer's disease. *Trends Biotechnol,* 29**,** 26-32.

IQBAL, K. & GRUNDKE-IQBAL, I. 2006. Discoveries of tau, abnormally hyperphosphorylated tau and others of neurofibrillary degeneration: a personal historical perspective. *J Alzheimers Dis,* 9**,** 219-42.

IQBAL, K., LIU, F., GONG, C. X. & GRUNDKE-IQBAL, I. 2010. Tau in Alzheimer disease and related tauopathies. *Curr Alzheimer Res,* 7**,** 656-64.

IRWIN, D. J. 2016. Tauopathies as clinicopathological entities. *Parkinsonism & related disorders,* 22 Suppl 1**,** S29-S33.

JAEKEN, J. 2016. Glycosylation and its Disorders: General Overview☆. *Reference Module in Biomedical Sciences.* Elsevier.

JAZAYERI, M. H., AMANI, H., POURFATOLLAH, A. A., PAZOKI-TOROUDI, H. & SEDIGHIMOGHADDAM, B. 2016. Various methods of gold nanoparticles (GNPs) conjugation to antibodies. *Sensing and Bio-Sensing Research,* 9**,** 17-22.

JEROMIN, A. & BOWSER, R. 2017. Biomarkers in Neurodegenerative Diseases. *Adv Neurobiol,* 15**,** 491-528.

JOHANN, C., PODZIMEK, S. & LEBEDA, P. 2009. Asymmetric Flow Field Flow Fractionation: A Powerful Method for Polymer Characterization. *LCGC North America,* 27**,** 62-69.

JOHNSON, G. V. & STOOTHOFF, W. H. 2004. Tau phosphorylation in neuronal cell function and dysfunction. *J Cell Sci,* 117**,** 5721-9.

JOSEPHS, K. A. 2017. Current Understanding of Neurodegenerative Diseases Associated With the Protein Tau. *Mayo Clinic Proceedings,* 92**,** 1291-1303.

JU, H., LAI, G. & YAN, F. 2017a. 2 - Signal amplification for immunosensing. *In:* JU, H., LAI, G. & YAN, F. (eds.) *Immunosensing for Detection of Protein Biomarkers.* Elsevier.

JU, H., LAI, G. & YAN, F. 2017b. 3 - Electrochemical immunosensing. *In:* JU, H., LAI, G. & YAN, F. (eds.) *Immunosensing for Detection of Protein Biomarkers*. Elsevier.

KARUNAKARAN, C., PANDIARAJ, M. & SANTHARAMAN, P. 2015a. Chapter 4 - Immunosensors. *In:* KARUNAKARAN, C., BHARGAVA, K. & BENJAMIN, R. (eds.) *Biosensors and Bioelectronics.* Elsevier.

KARUNAKARAN, C., RAJKUMAR, R. & BHARGAVA, K. 2015b. Chapter 1 - Introduction to Biosensors. *In:* KARUNAKARAN, C., BHARGAVA, K. & BENJAMIN, R. (eds.) *Biosensors and Bioelectronics.* Elsevier.

KHAN, I., SAEED, K. & KHAN, I. 2017. Nanoparticles: Properties, applications and toxicities. *Arabian Journal of Chemistry*.

KIDD, M. 1963. Paired Helical Filaments in Electron Microscopy of Alzheimer's Disease. *Nature,* 197**,** 192-193.

KIM, A. C., LIM, S. & KIM, Y. K. 2018. Metal Ion Effects on Aβ and Tau Aggregation. *International Journal of Molecular Sciences,* 19**,** 128.

KIMURA, T., TSUTSUMI, K., TAOKA, M., SAITO, T., MASUDA-SUZUKAKE, M., ISHIGURO, K., PLATTNER, F., UCHIDA, T., ISOBE, T., HASEGAWA, M. & HISANAGA, S.-I. 2013. Isomerase Pin1 stimulates dephosphorylation of tau protein at cyclin-dependent kinase (Cdk5)-dependent Alzheimer phosphorylation sites. *The Journal of biological chemistry,* 288**,** 7968-7977.

KOCH, W., HOLTHAUSEN, M. C. & HOLTHAUSEN, M. C. 2001. *A chemist's guide to density functional theory,* Wiley Online Library.

KOSIK, K. S. 1990. Tau Protein and Neurodegeneration. *Molecular Neurobiology,* 4**,** 171–179.

KOVACECH, B. & NOVAK, M. 2010. Tau truncation is a productive posttranslational modification of neurofibrillary degeneration in Alzheimer's disease. *Curr Alzheimer Res,* 7**,** 708-16.

KOVACS, G. & BUDKA, H. 2010. *Current concepts of neuropathological diagnostics in practice: Neurodegenerative diseases*.

KOVACS, G. G. 2015. Invited review: Neuropathology of tauopathies: principles and practice. *Neuropathol Appl Neurobiol,* 41**,** 3-23.

KOVACS, G. G. 2017. Tauopathies. *Handb Clin Neurol,* 145**,** 355-368.

KOVACS, G. G. 2018. Chapter 21 - Concepts and classification of neurodegenerative diseases. *In:* KOVACS, G. G. & ALAFUZOFF, I. (eds.) *Handbook of Clinical Neurology*. Elsevier.

KUMAR, A. & DIXIT, C. K. 2017. 3 - Methods for characterization of nanoparticles. *In:* NIMESH, S., CHANDRA, R. & GUPTA, N. (eds.) *Advances in Nanomedicine for the Delivery of Therapeutic Nucleic Acids.* Woodhead Publishing.

LEBOUVIER, T., PASQUIER, F. & BUÉE, L. 2017. Update on tauopathies. *Current Opinion in Neurology,* 30**,** 589-598.

LEE, J., KIM, J., KIM, S. & MIN, D.-H. 2016. Biosensors based on graphene oxide and its biomedical application. *Advanced Drug Delivery Reviews,* 105**,** 275-287.

LEE, S. H. & JUN, B. H. 2019. Silver Nanoparticles: Synthesis and Application for Nanomedicine. *Int J Mol Sci,* 20.

LEWARS, E. G. 2011. Computational Chemistry. *Introduction to the Theory and Applications of Molecular and Quantum Mechanics.* second ed.: Springer.

LIM, S. A. & AHMED, M. U. 2016. Electrochemical immunosensors and their recent nanomaterial-based signal amplification strategies: a review. *RSC Advances,* 6**,** 24995-25014.

LINERT, W. & KOZLOWSKI, H. 2011. Metals in the brain. *Monatshefte für Chemie - Chemical Monthly,* 142**,** 321-321.

LISOWSKA, E. & JASKIEWICZ, E. 2012. Protein Glycosylation, an overview.

LIU, F., ZAIDI, T., IQBAL, K., GRUNDKE-IQBAL, I., MERKLE, R. K. & GONG, C. X. 2002. Role of glycosylation in hyperphosphorylation of tau in Alzheimer's disease. *FEBS Lett,* 512**,** 101-6.

LIU, K., LIU, Y., LI, L., QIN, P., IQBAL, J., DENG, Y. & QING, H. 2016. Glycation alter the process of Tau phosphorylation to change Tau isoforms aggregation property. *Biochimica et Biophysica Acta (BBA) - Molecular Basis of Disease,* 1862**,** 192-201.

LJUNGBLAD, J. 2009. Antibody-conjugated Gold Nanoparticles integrated in a Fluorescence based Biochip.

LUPPA, P. B., SOKOLL, L. J. & CHAN, D. W. 2001. Immunosensors—principles and applications to clinical chemistry. *Clinica Chimica Acta,* 314**,** 1-26.

MA, H. & O'KENNEDY, R. 2017. Recombinant antibody fragment production. *Methods,* 116**,** 23-33.

MAKAROV, V. V., LOVE, A. J., SINITSYNA, O. V., MAKAROVA, S. S., YAMINSKY, I. V., TALIANSKY, M. E. & KALININA, N. O. 2014. "Green" nanotechnologies: synthesis of metal nanoparticles using plants. *Acta naturae,* 6**,** 35-44.

MARTIC, S., BEHESHTI, S., RAINS, M. K. & KRAATZ, H. B. 2012. Electrochemical investigations into Tau protein phosphorylations. *Analyst,* 137**,** 2042-6.

MARTIC, S., RAINS, M. K. & KRAATZ, H. B. 2013. Probing copper/tau protein interactions electrochemically. *Anal Biochem,* 442**,** 130-7.

MARTIN, L., LATYPOVA, X. & TERRO, F. 2011. Post-translational modifications of tau protein: implications for Alzheimer's disease. *Neurochem Int,* 58**,** 458-71.

MATTSSON, N. 2011. CSF biomarkers in neurodegenerative diseases. *Clinical Chemistry and Laboratory Medicine.*

MEIER, F. & HEINZMANN, G. 2017. Field-Flow Fractionation: A powerful technology for the separation and advanced characterization of proteins, antibodies, viruses, polymers and nano-/microparticles. *www.chemie.de*.

MILATOVIC, D., ZAJA-MILATOVIC, S., BREYER, R. M., ASCHNER, M. & MONTINE, T. J. 2017. Chapter 55 - Neuroinflammation and Oxidative Injury in Developmental Neurotoxicity. *In:* GUPTA, R. C. (ed.) *Reproductive and Developmental Toxicology (Second Edition).* Academic Press.

MORRIS, G. M., HUEY, R., LINDSTROM, W., SANNER, M. F., BELEW, R. K., GOODSELL, D. S. & OLSON, A. J. 2009. AutoDock4 and AutoDockTools4: Automated docking with selective receptor flexibility. *J Comput Chem,* 30**,** 2785-91.

MORRIS, R. & FILLENZ, M. 2003. *Neuroscience: Science of the Brain,* The British Neuroscience Association.

MOURDIKOUDIS, S., PALLARES, R. M. & THANH, N. T. K. 2018. Characterization techniques for nanoparticles: comparison and complementarity upon studying nanoparticle properties. *Nanoscale,* 10**,** 12871-12934.

MUKRASCH, M. D., BIERNAT, J., VON BERGEN, M., GRIESINGER, C., MANDELKOW, E. & ZWECKSTETTER, M. 2005. Sites of tau important for aggregation populate {beta}-structure and bind to microtubules and polyanions. *J Biol Chem,* 280**,** 24978-86.

NEUDERT, G. & KLEBE, G. 2011. DSX: a knowledge-based scoring function for the assessment of protein-ligand complexes. *J Chem Inf Model,* 51**,** 2731-45.

NOBLE, W., HANGER, D. P., MILLER, C. C. J. & LOVESTONE, S. 2013. The importance of tau phosphorylation for neurodegenerative diseases. *Frontiers in neurology,* 4**,** 83-83.

OOSTENBRINK, C., VILLA, A., MARK, A. E. & VAN GUNSTEREN, W. F. 2004. A biomolecular force field based on the free enthalpy of hydration and solvation: the GROMOS force-field parameter sets 53A5 and 53A6. *J Comput Chem,* 25**,** 1656-76.

PARVEEN, K., BANSE, V. & LEDWANI, L. 2016. *Green synthesis of nanoparticles: Their advantages and disadvantages*.

PEÑA-BAHAMONDE, J., NGUYEN, H. N., FANOURAKIS, S. K. & RODRIGUES, D. F. 2018. Recent advances in graphene-based biosensor technology with applications in life sciences. *Journal of nanobiotechnology,* 16**,** 75-75.

PICHAIMUTHU, K., KEERTHI, M., CHEN, S.-M., CHEN, T.-W. & SU, C. 2018. Silver Nanoparticles Decorated on Graphene Oxide Sheets for Electrochemical Detection of Ascorbic Acid(AA) in Human Urine Sample. *International Journal of Electrochemical Science,* 13**,** 7859 – 7869.

POOJA, A. K. P. N. J. & BAJAPI, P. R. 2016. Synthesis and Application of Graphene Oxide (GO): A Review.

PRONK, S., PALL, S., SCHULZ, R., LARSSON, P., BJELKMAR, P., APOSTOLOV, R., SHIRTS, M. R., SMITH, J. C., KASSON, P. M., VAN DER SPOEL, D., HESS, B. & LINDAHL, E. 2013. GROMACS 4.5: a high-throughput and highly parallel open source molecular simulation toolkit. *Bioinformatics,* 29**,** 845-54.

RACHAKONDA, V., PAN, T. H. & LE, W. D. 2004. Biomarkers of neurodegenerative disorders: how good are they? *Cell Res,* 14**,** 347-58.

RAINS, M. K., MARTIC, S., FREEMAN, D. & KRAATZ, H. B. 2013. Electrochemical investigations into kinase-catalyzed transformations of tau protein. *ACS Chem Neurosci,* 4**,** 1194-203.

RAUWEL, P., #XFC, #XFC, NAL, S., FERDOV, S. & RAUWEL, E. 2015. A Review on the Green Synthesis of Silver Nanoparticles and Their Morphologies Studied via TEM. *Advances in Materials Science and Engineering,* 2015**,** 9.

ROBERT, M. & MATHURANATH, P. 2007. Tau and Tauopathies. *Neurology India,* 55**,** 11-16.

ROBERTSON, L. A., MOYA, K. L. & BREEN, K. C. 2004. The potential role of tau protein O-glycosylation in Alzheimer's disease. *J Alzheimers Dis,* 6**,** 489-95.

RONKAINEN, N. J., HALSALL, H. B. & HEINEMAN, W. R. 2010. Electrochemical biosensors. *Chemical Society Reviews,* 39**,** 1747-1763.

ROY, K., SARKAR, C. K. & GHOSH, C. K. 2015. Single-step novel biosynthesis of silver nanoparticles using cucumis sativus fruit extract and study of its photcatalytic and antibacterial activity. *Digest Journal of Nanomaterials and Biostructures,* 1**,** 107-115.

SCHAMING, D. & REMITA, H. 2015. *Nanotechnology: from the ancient time to nowadays*.

SCHMIDPETER, P. A. M. & SCHMID, F. X. 2015. Prolyl Isomerization and Its Catalysis in Protein Folding and Protein Function. *Journal of Molecular Biology*, 427**,** 1609-1631.

SCHUTTELKOPF, A. W. & VAN AALTEN, D. M. 2004. PRODRG: a tool for high-throughput crystallography of protein-ligand complexes. *Acta Crystallogr D Biol Crystallogr,* 60**,** 1355-63.

SIDDIQI, K. S., HUSEN, A. & RAO, R. A. K. 2018. A review on biosynthesis of silver nanoparticles and their biocidal properties. *Journal of nanobiotechnology,* 16**,** 14-14.

SNEHA, P. & GEORGE PRIYA DOSS, C. 2016. Chapter Seven - Molecular Dynamics: New Frontier in Personalized Medicine. *In:* DONEV, R. (ed.) *Advances in Protein Chemistry and Structural Biology*. Academic Press.

SQUIRE, L., BERG, D., BLOOM, F. E., LAC, S. D., GHOSH, A., SPITZER, N. C., SQUIRE, L. R., BERG, D., BLOOM, F., LAC, S. D., GHOSH, A. & SPITZER, N. 2008. *Fundamental Neuroscience* Elsevier.

STANLEY, S. 2014. Biological nanoparticles and their influence on organisms. *Current Opinion in Biotechnology,* 28**,** 69-74.

SUN, L. 2019. Structure and Synthesis of graphene oxide.

SWEET, M. J. & SINGLETON, I. 2011. Chapter 5 - Silver Nanoparticles: A Microbial Perspective. *In:* LASKIN, A. I., SARIASLANI, S. & GADD, G. M. (eds.) *Advances in Applied Microbiology*. Academic Press.

SYAFIUDDIN, A., SALMIATI, SALIM, M. R., BENG HONG KUEH, A., HADIBARATA, T. & NUR, H. 2017. A Review of Silver Nanoparticles: Research Trends, Global Consumption, Synthesis, Properties, and Future Challenges. *Journal of the Chinese Chemical Society,* 64**,** 732-756.

TAGARELLI, A., PIRO, A., TAGARELLI, G., LAGONIA, P. & QUATTRONE, A. 2006. Alois Alzheimer: a hundred years after the discovery of the eponymous disorder. *International journal of biomedical science : IJBS,* 2**,** 196-204.

THAMILSELVI, V. & RADHA, K. V. 2017. A Review On The Diverse Application Of Silver Nanoparticles. *IOSR Journal Of Pharmacy* 7**,** 21-27.

TOMAR, A. & GARG, G. 2013. Short Review on Application of Gold Nanoparticles. *Global Journal of Pharmacology,* 1**,** 34-38.

TRZECIAKIEWICZ, H., ESTEVES-VILLANUEVA, J. O., CARLIN, N. & MARTIĆ, S. 2015. Electrochemistry of heparin binding to tau protein on Au surfaces. *Electrochimica Acta,* 162**,** 24-30.

USDA. 2019. U.S. DEPARTMENT OF AGRICULTURE. Available: https://fdc.nal.usda.gov/fdc-app.html#/food-details/170487/nutrients [Accessed 30 May 2019].

VESTERGAARD, M., KERMAN, K., KIM, D. K., HA, M. H. & TAMIYA, E. 2008. Detection of Alzheimer's tau protein using localised surface plasmon resonance-based immunochip. *Talanta,* 74**,** 1038-42.

VON BERNHARDI, R., HEREDIA, F., SALGADO, N. & MUNOZ, P. 2016. Microglia Function in the Normal Brain. *Adv Exp Med Biol,* 949**,** 67-92.

WANG, B., AKIBA, U. & ANZAI, J.-I. 2017a. Recent Progress in Nanomaterial-Based Electrochemical Biosensors for Cancer Biomarkers: A Review. *Molecules (Basel, Switzerland),* 22**,** 1048.

WANG, J.-Z., GRUNDKE-IQBAL, I. & IQBAL, K. 1996. Glycosylation of microtubule–associated protein tau: An abnormal posttranslational modification in Alzheimer's disease. *Nature Medicine,* 2**,** 871-875.

WANG, J. Z., XIA, Y. Y., GRUNDKE-IQBAL, I. & IQBAL, K. 2013. Abnormal hyperphosphorylation of tau: sites, regulation, and molecular mechanism of neurofibrillary degeneration. *J Alzheimers Dis,* 33 Suppl 1**,** S123-39.

WANG, S. X., ACHA, D., SHAH, A. J., HILLS, F., ROITT, I., DEMOSTHENOUS, A. & BAYFORD, R. H. 2017b. Detection of the tau protein in human serum by a sensitive four-electrode electrochemical biosensor. *Biosens Bioelectron,* 92**,** 482-488.

WANG, X., WANG, W., LI, L., PERRY, G., LEE, H.-G. & ZHU, X. 2014. Oxidative stress and mitochondrial dysfunction in Alzheimer's disease. *Biochimica et Biophysica Acta (BBA) - Molecular Basis of Disease,* 1842**,** 1240-1247.

WEINGARTEN, M. D., LOCKWOOD, A. H., HWO, S.-Y. & KIRSCHNER, M. W. 1975. A Protein Factor Essential for Microtubule Assembly. *Proc. Nat. Acad. Sci. USA* 72**,** 1858-1862.

WEN, W., YAN, X., ZHU, C., DU, D. & LIN, Y. 2017. Recent Advances in Electrochemical Immunosensors. *Analytical Chemistry,* 89**,** 138-156.

YACOUBIAN, T. A. 2017. Chapter 1 - Neurodegenerative Disorders: Why Do We Need New Therapies? *In:* ADEJARE, A. (ed.) *Drug Discovery Approaches for the Treatment of Neurodegenerative Disorders.* Academic Press.

YAN, S. D., CHEN, X., SCHMIDT, A. M., BRETT, J., GODMAN, G., ZOU, Y. S., SCOTT, C. W., CAPUTO, C., FRAPPIER, T. & SMITH, M. A. 1994. Glycated tau protein in Alzheimer disease: a mechanism for induction of oxidant stress. *Proceedings of the National Academy of Sciences,* 91**,** 7787.

YANAMANDRA, K., JIANG, H., MAHAN, T. E., MALONEY, S. E., WOZNIAK, D. F., DIAMOND, M. I. & HOLTZMAN, D. M. 2015. Anti-tau antibody reduces insoluble tau and decreases brain atrophy. *Annals of clinical and translational neurology,* 2**,** 278-288.

YANG, S.-Y., CHIU, M.-J., CHEN, T.-F., LIN, C.-H., JENG, J.-S., TANG, S.-C., LEE, Y.-F., YANG, C.-C., LIU, B.-H., CHEN, H.-H. & WU, C.-C. 2017. Analytical performance of reagent for assaying tau protein in human plasma and feasibility study screening neurodegenerative diseases. *Scientific Reports,* 7**,** 9304.

YEH, Y.-C., CRERAN, B. & ROTELLO, V. M. 2012. Gold nanoparticles: preparation, properties, and applications in bionanotechnology. *Nanoscale,* 4**,** 1871-1880.

YOUNG, D. C. 2001. Computational Chemistry: A Practical Guide for Applying Techniques to Real-World Problems.: John Wiley & Sons, Inc.

YU, Q., WANG, Q., LI, B., LIN, Q. & DUAN, Y. 2014. Technological Development of Antibody Immobilization for Optical Immunoassays: Progress and Prospects. *Critical Reviews in Analytical Chemistry,* 45**,** 62-75.

ZENG, X., SHEN, Z. & MERNAUGH, R. 2012. Recombinant antibodies and their use in biosensors. *Analytical and bioanalytical chemistry,* 402**,** 3027-3038.

ZHANG, H. & LYDEN, D. 2019. Asymmetric-flow field-flow fractionation technology for exomere and small extracellular vesicle separation and characterization. *Nature Protocols,* 14**,** 1027-1053.

ZHANG, X.-F., LIU, Z.-G., SHEN, W. & GURUNATHAN, S. 2016. Silver Nanoparticles: Synthesis, Characterization, Properties, Applications, and Therapeutic Approaches. *International journal of molecular sciences,* 17**,** 1534.

ZHOU, X. Z., KOPS, O., WERNER, A., LU, P. J., SHEN, M., STOLLER, G., KULLERTZ, G., STARK, M., FISCHER, G. & LU, K. P. 2000. Pin1-dependent prolyl isomerization regulates dephosphorylation of Cdc25C and tau proteins. *Mol Cell,* 6**,** 873-83.

ZHOU, Y., SHI, J., CHU, D., HU, W., GUAN, Z., GONG, C.-X., IQBAL, K. & LIU, F. 2018. Relevance of Phosphorylation and Truncation of Tau to the Etiopathogenesis of Alzheimer's Disease. *Frontiers in aging neuroscience,* 10**,** 27-27.

ZIELKIEWICZ, J. 2005. Structural properties of water: comparison of the SPC, SPCE, TIP4P, and TIP5P models of water. *J Chem Phys,* 123**,** 104501.